Charles University
Second Faculty of Medicine

Doctoral study programme: Neurosciences


Mgr. Denisa Kirdajová

NG2-glia proliferation and differentiation following CNS injuries
NG2-glia proliferace a diferenciace po poškození CNS

Dissertation Thesis

Supervisor: Ing. Miroslava Anděrová, CSc.

Prague, 2022

Prohlášení

Prohlašuji, že jsem disertační práci zpracovala samostatně a že jsem řádně uvedla a citovala všechny použité prameny a literaturu. Současně prohlašuji, že práce nebyla využita k získání jiného nebo stejného titulu.

Souhlasím s trvalým uložením elektronické verze mé práce v databázi systému meziuniverzitního projektu Theses.cz za účelem soustavné kontroly podobnosti kvalifikačních prací.

V Praze, 14. 03. 2022

Denisa Kirdajová

……

Acknowledgements

I would like to express my gratitude to my supervisor, Dr. Miroslava Anděrová, for her advice and patient guidance from the very early beginning of my research experience. I would also like to thank my colleagues and the technicians in the laboratory who participated in experiments described in my thesis.

NG2-glia proliferace a diferenciace po poškození CNS

Abstrakt

NG2 glie mají velký proliferační a diferenciační potenciál za fyziologických i patologických podmínek. Jsou velmi dobře známé jako prekurzory oligodendrocytů, avšak po poškození centrálního nervového systému (CNS) hrají důležitou roli v regeneraci. Z tohoto důvodu jsme zkoumali jejich vlastnosti po různých typech mozkových poškození jako je fokální cerebrální ischemie (FCI), kortikální bodná rána (SW) a demyelinizace (DEMY) u mladých (tříměsíčních) myší, u kterých jsou NG2 glie značené pomocí tdTomato pod promotorem Cspg4. V případě FCI jsme se také věnovali faktoru věku s využitím osmnáctiměsíčních myší. Abychom chování NG2 glií prozkoumali, provedli jsme mnoho technik na různých úrovních, jako je RT-qPCR na úrovni jedné buňky, RNA sekvenování a sekvenování na úrovni jedné buňky, imunohistochemie a technika patch-clamp. Tento přístup nám umožnil rozlišit dvě hlavní populace (NG2 glie, oligodendrocyty), z nichž každá obsahuje čtyři odlišné subpopulace. Profilování exprese dále odhalilo, že subpopulace NG2 glií exprimující GFAP (marker reaktivních astrocytů) je přítomna pouze přechodně po FCI. Po méně závažném poranění, konkrétně SW a DEMY však výrazně převažují subpopulace odrážející různá stádia zrání oligodendrocytů. Rozdílná genová exprese napříč ischemií a věkem odhalila sníženou expresi genů zodpovědných za údržbu/stabilitu axonů a synapsí a zvýšenou aktivaci interferonu typu I (IFN-I) u starých myší. Tyto výsledky vykreslují obraz komplexní heterogenity NG2 glií – jejich multipotentního fenotypu po poranění CNS a poukazují na ischemii jako na komplexní onemocnění související s věkem.

Klíčová slova

astrocyty, bodná rána, demyelinizace, fokální mozková ischemie, oligodendrocyty, stárnutí

NG2-glia proliferation and differentiation following CNS injuries

Abstract

NG2 glia display wide proliferation and differentiation potential under physiological and pathological conditions. They are very well known as precursors of oligodendrocytes, however, following central nervous system (CNS) injury they play an important role in regeneration. For this reason, we examined these features following different types of brain disorders such as focal cerebral ischemia (FCI), cortical stab wound (SW), and demyelination (DEMY) in young (3-month-old) mice, in which NG2 glia are labeled by tdTomato under the Cspg4 promoter. In the case of FCI, the factor of age was also studied using 18-month-old mice. To address these issues, we employed many techniques on tissue/cellular levels, such as single-cell RT-qPCR, single-cell/bulk RNA-sequencing, immunohistochemistry, and the patch-clamp technique in situ. First, such approach enabled us to distinguish two main populations (NG2 glia, oligodendrocytes), each of them comprising four distinct subpopulations. Next, the expression profiling revealed that a subpopulation of NG2 glia expressing GFAP, a marker of reactive astrocytes, appears transiently after FCI. However, following less severe injury, namely the cortical SW and DEMY, subpopulations mirroring different stages of oligodendrocyte maturation markedly prevail. Additionally, differential gene expression across ischemia and age uncovered downregulation of axonal and synaptic maintenance genetic program and increased activation of type I interferon (IFN-I) in aged mice. These results paint a picture of the complex heterogeneity of NG2 glia-their multipotent phenotype following CNS injuries and point to ischemia as a complex age-related disease.

Keywords

aging, astrocytes, demyelination, focal cerebral ischemia, oligodendrocytes, stab wound

List of abbreviations

aCSF	artificial cerebrospinal fluid
AD	Alzheimer's disease
ALDH1L1	aldehyde dehydrogenase 1 family member L1 (ALDH1L1
ALS	Amyotrophic lateral sclerosis
AMPA	α-amino-3-hydroxy-5-methyl-4-isoxazolepropionic acid
A-NG2 cells	astrocyte-like NG2 glia
Apc	gene encoding adenomatous polyposis coli
ATP	adenosine triphosphate
BBB	blood brain barrier
BF-NG2 cells	bona fide NG2 glia
BMDMs	bone marrow-derived macrophages
BrdU	bromodeoxyuridine
CC	corpus callosum
CD11b	microglial marker
CD31	endothelial cell marker
C_m	membrane capacitance
CNS	central nervous system
CPZ	cuprizone
CTRL	control
CTX	cortex
Dcx	doublecortin
DE	differential expression
DEMY	demyelination
E	embryonic
EAE	experimental autoimmune encephalomyelitis
EdU	5′-ethynyl-2′-deoxyuridine
EGFP	enhanced green fluorescent protein
EGTA	ethylene glycol-bis(β-aminoethyl ether)-*N*,*N*,*N*′,*N*′-tetraacetic acid
FACS	fluorescent activated cell sorting
FCI	focal cerebral ischemia
FDR	false discovery rate
GABA	γ-aminobutyric acid
GC	galactocerebroside

GCI	global cerebral ischemia
GFAP	glial fibrillary acidic protein
GLAST	glutamate-aspartate transporter
GLT	glutamate transporter
GO	gene ontology
GOBP	gene ontology biological process
GOCC	gene ontology cellular component
GS	glutamine synthetase
GSEA	gene set enrichment analysis
Hcn	gene encoding hyperpolarization-activated cyclic nucleotide-gated
HEPES	4-(2-hydroxyethyl)-1-piperazineethanesulfonic acid
HIV	human immunodeficiency virus
IEA	inferred from electronic annotation
IFN-I	type I interferon
IL	interleukin
IR	input resistance
ISG	interferon-stimulated gene
K_A	inactivating outwardly rectifying K^+
KA	kainite
K_{DR}	delayed outwardly rectifying K^+
K_{IR}	inwardly rectifying potassium K^+
KV	potassium voltage-gated channels
LC/MS	liquid chromatography /mass spectrometry
LPS	lipopolysaccharide
Mbp	gene encoding myelin basic protein
MBP	myelin basic protein
MCAO3/18	middle cerebral artery occlusion (=FCI) in 3- or 18-month-old mice
mGlur	metabotropic glutamate receptors
MGP	marker gene profile
MMPs	matrix metallopeptidases
MOG	myelin oligodendrocyte protein
Mosp	gene encoding myelin-oligodendrocyte-specific protein
MS	multiple sclerosis
NaV	sodium voltage-gated channels

Nes	nestin
NG2 glia (S1)	subpopulation 1 of NG2 glia
NG2 glia (S2)	subpopulation 2 of NG2 glia
Ng2	gene encoding nerve/glia antigen
NG2	nerve/glia antigen
NMDA	N-methyl-D-aspartate
O4	gene encoding oligodendrocyte marker
OL	oligodendrocyte (for Figure 27)
Olig2	gene oligodendrocyte transcription factor
OL-NG2 cells	oligodendrocyte-like NG2 glia
OPC	oligodendrocyte precursor cells (NG2 glia)
OR	odds ratio
P	postnatal
p_{adj}	adjusted p-value
PB	phosphate buffer
PCA	principal component analysis
Pdgfrb	gene encoding platelet-derived growth factor beta receptor
Pdgfrα	gene encoding platelet-derived growth factor alpha receptor
PFA	paraformaldehyde
PLP	proteolipid protein
P-NG2 cells	proliferating NG2 glia
PTB	pentobarbital
PV	parvalbumin
RNA-seq	RNA-Sequencing
ROS	reactive oxygen species
RT	room temperature
SEM	standard error of the mean
Shh	Sonic Hedgehog
Slc1a2/3	gene encoding Na^+-dependent glutamate transporters
SOD	superoxide dismutase
Sox10	gene encoding sex determining region Y-box 10
SW	stab wound
Trpv4	transient receptor potential cation channel subfamily V member 4
TX	tamoxifen

UMAP	uniform manifold approximation and projection
UMI	unique molecular identifier
Vim	vimentin
V_m	membrane potential
WB	western blot

TABLE OF CONTENTS

1 INTRODUCTION

Injuries of central nervous system (CNS), including ischemic stroke, are major promoters of death and disability worldwide (Corps et al., 2015, Benjamin et al., 2018). The medical costs of strokes are forecasted to increase from $71.6 billion in 2012 to $184.1 billion by 2030 (USA). Despite the immeasurable burden on patients and families, there are no effective treatments to protect the CNS and promote functional recovery after acute injuries (Kim et al., 2019). A major roadblock to developing effective therapies is the lack of understanding of the cellular and molecular mechanisms that promote secondary neuronal damage and functional deficits after injury.

Despite the different etiology of brain damage, strikingly similar consequent events are triggered (Bramlett and Dietrich, 2004, Amani et al., 2019), which could possibly lead to the development of a common treatment for a number of disorders in the CNS. Under physiological conditions, neuronal cells heavily depend on glia. However, during ischemia, they fail to carry out these functions and become a threat to the adjacent neurons. Thus, glial cells can act as defenders of the CNS as well as initiators and propagators of injury (Takano et al., 2009).

To promote recovery, could be the utilization of naturally residing precursor brain cells - NG2 glia, which are capable differentiate to other cell types, regulating the metabolic environment, and directly modulating neuronal functions (Galichet et al., 2021). A better understanding of this enigmatic cell type will shed light on the pathogenesis and potential treatment strategies for numerous CNS disorders, such as ischemia or neurodegeneration.

The goal of the thesis was to analyze the NG2 glia proliferation and differentiation potential following different types of CNS injuries. Considering the natural stem cell features of NG2 glia that could perfectly serve target for therapeutic purposes as part of regenerative medicine.

1.1 NG2 glia

NG2 (neuron/glia antigen 2) glia represent a fourth resident glial cell population in the mammalian CNS that is distinct from astrocytes, mature oligodendrocytes, and microglia. They are defined as non-neuronal, non-vascular glial cells in the CNS parenchyma that express the NG2 antigen and the alpha receptor for a platelet-derived growth factor (*Pdgfrα*) (Nishiyama et al., 2016, Nishiyama et al., 2009). NG2 glia are equally distributed in both gray and white matter and they represent 5-10 % of the total brain cells and the most active cycling population with enormous proliferative capacity within the adult brain (Kirdajova and Anderova, 2020). They have small cell bodies with multiple branched processes in all directions (Fig. 1A)(Hermann et al., 2010).

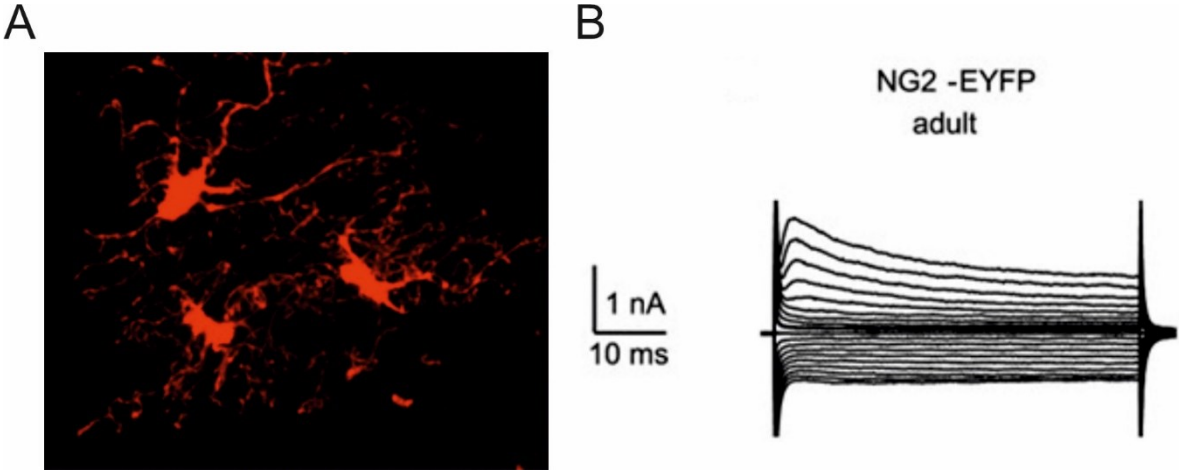

Figure 1: A) Cortical NG2 glia morphology in intact brain of transgenic Cspg4/tdTomato mouse. B) Typical current pattern of NG2 glia in situ from NG2-EYFP mice after de- and hyperpolarization of the membrane between −160 and +20 mV (10 mV increments; holding potential was −70 mV). The adult NG2 glia had resting potentials of −86 mV (Moshrefi-Ravasdjani et al., 2017).

NG2 glia are generated in the ventral germinal zones of the medial and lateral ganglionic eminences during embryogenesis. Another subpopulation of NG2 glia arises from the dorsal and ventral ventricular zone perinatally. In the postnatal life they are generated in the subventricular zone of the lateral ventricles, from the neurogenic niche (Kessaris et al., 2006, Menn et al., 2006). NG2 glia originates from oligodendrocyte transcription factor (*Olig2*)$^{+}$ progenitor cells, which first give rise to motor neurons at embryonic day (E)9-10 and subsequently switch to produce oligodendrocyte lineage cells after E12 (Kessaris et al., 2001). During neuronal differentiation, (*Olig2*) expression is downregulated while the expression of neurogenic transcription factors persists. On the contrary, in the NG2^{+} cells committed to the oligodendrocyte lineage, expression of *Olig2* while neuronal genes are repressed (Novitch et al., 2001, Petryniak et al., 2007) (Fig. 2).

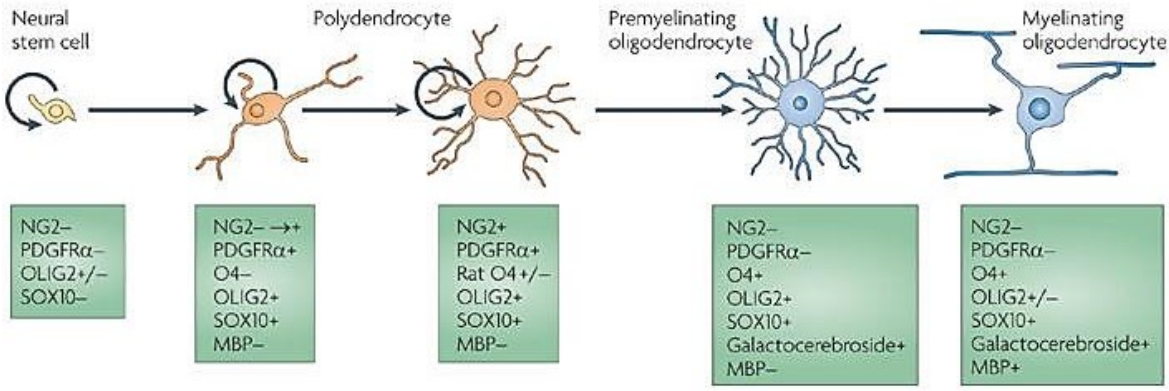

Figure 2: Maturation of oligodendrocyte from nerve/glial antigen (*Ng2*) glia. Neural stem cells do not express platelet-derived growth factor alpha receptor (*Pdgfrα*) and *Ng2*. NG2 glia are able to self-renew (circular arrows) and increase their ramification during maturation. Oligodendrocyte-committed precursors start to express *O4* (oligodendrocyte marker) and downregulate *Ng2* and *Pdgfrα*. Finally, mature oligodendrocytes upregulate expression of oligodendroglial markers, such as galactocerebroside (*GC*) and myelin basic protein (*Mbp*). *Olig2*, oligodendrocyte transcription factor 2; *Sox10*, sex determining region Y-box 10)(Nishiyama et al., 2009).

Currently, one of the most known functions of NG2 glia is their role in gliogenesis. NG2 glia represent the majority of proliferating cells in the intact CNS. Under physiological conditions, 70-75% of bromodeoxyuridine positive ($BrdU^+$) cells are NG2 glia (Dawson et al., 2003). Their proliferation potential remains throughout life and their cell cycle time lengthens significantly with age (Young et al., 2013, Psachoulia et al., 2009). The rate of NG2 glia proliferation is greater in white matter than in gray matter (Young et al., 2013, Hill et al., 2013). Similarly, the cell cycle duration in the corpus callosum in postnatal day (P)21 mice is 2.7 days and 18.6 days in the neocortex (Psachoulia et al., 2009, Young et al., 2013).

Another important function is their differentiation into oligodendrocytes during CNS development and entire postnatal life. Thus, they have often been equated with oligodendrocyte precursor cells (OPCs) and the studies suggested that their unique function is the generation and maintenance of oligodendrocytes in the CNS (Bernhardi et al., 2016). Thanks to the Cre studies we know that the oligodendrogenesis is probably triggered by asymmetric division of NG2 glia, which loses the expression of *Ng2* and *Pdgfrα* and conversely, increases the expression of oligodendroglial markers, such as *Mbp*, myelin-oligodendrocyte-specific protein (*Mosp*) or adematous polyposis coli (*Apc*, also called CC1)(Zhu et al., 2008) (Fig. 2). Not all oligodendrocytes are derived from NG2 glia, because the mutual distribution is not parallel (Dawson et al., 2000, Zhu et al., 2008). However, the fate of NG2 glia is not only restricted to oligodendrocytes. It has been demonstrated that NG2 glia can give rise to astrocytes *in vitro* (Stallcup and Beasley, 1987), and *in vivo,* they

can generate the subpopulation of protoplasmic astrocytes in the ventral forebrain only during embryogenesis (Zhu et al., 2008). Currently, the most discussed topic is the ability of NG2 glia to generate neurons or neuronal precursors (Huang et al., 2014). Findings appear inconsistent because some studies observed neurons differentiated from NG2 glia (Aguirre et al., 2004, Robins et al., 2013, Tsoa et al., 2014, Guo et al., 2009, Guo et al., 2010, Rivers et al., 2008), but on the other hand, some other studies showed no evidence for neurogenic potential of NG2 glia (Clarke 2012, Kang et al., 2010; Zhu et al., 2008, Zhu 2011, Huang 2014, Huang 2018, Tognatta 2017). Despite the shared origin of neurons and NG2 glia from *Olig2*$^{+}$ cells, there are more samples of evidence to show that during development and also in adulthood, NG2 glia do not generate neurons (Zhu et al., 2008, Zhu et al., 2011, Huang et al., 2018, Huang et al., 2019, Huang et al., 2014, Kang et al., 2010, Clarke et al., 2012)(Fig. 3).

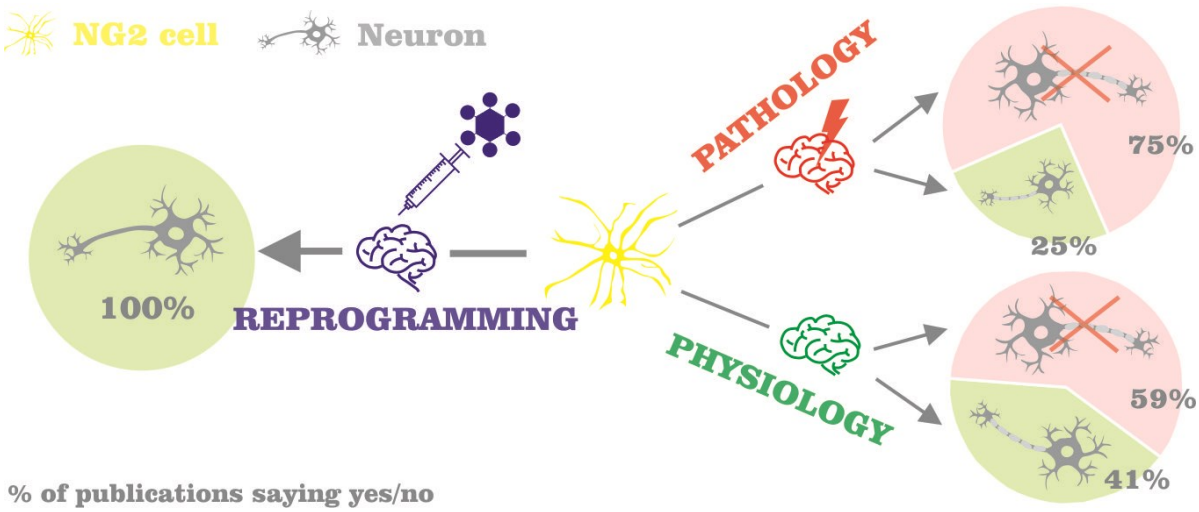

Figure 3: Neurogenic potential of NG2 glia. (Right part) Percentage of publications showing if NG2 glia (yellow cell) is capable to give rise to neurons (green) or not (red). (Left part) Percentage of publications showing the success of reprogramming NG2 glia (yellow cell) to neurons (green)(Kirdajova and Anderova, 2020).

The precursor role of NG2 glia is not their only function in the adult CNS. Electrophysiological studies indicated that NG2 glia express a complex set of voltage-gated channels, including tetrodotoxin-sensitive NA^+ channels and several types of K^+ channels (Bergles et al., 2000, Chittajallu et al., 2004, Kukley et al., 2008, De Biase et al., 2010, Káradóttir et al., 2008) (Fig.4) with typical current pattern (Fig. 1B). Furthermore, NG2 glia in gray and white matter areas of the brain express α-amino-3-hydroxyl-5-methyl-4-isoxazole-propionate (AMPA)/KA and/or γ-aminobutyric acid (GABAA) receptors, and receive glutamatergic and/or GABAergic synaptic input from neurons (Bergles et al., 2000, Ziskin et al., 2007, Lin and Bergles, 2004, Káradóttir et al., 2005, Kukley et al., 2007). These channels and receptors, which are essential for NG2 glia to sense neuronal activity, are differentially expressed in NG2 glia in an age- and region-dependent manner. Notably, when NG2 glia first appear, they lack all ion channels, but then gradually acquire voltage-gated K^+ channels, voltage-gated NA^+ channels, AMPA/KA, and NMDA receptors at different rates and differentially between and within CNS regions (Spitzer et al., 2019, Jia et al., 2019) (Fig. 4).

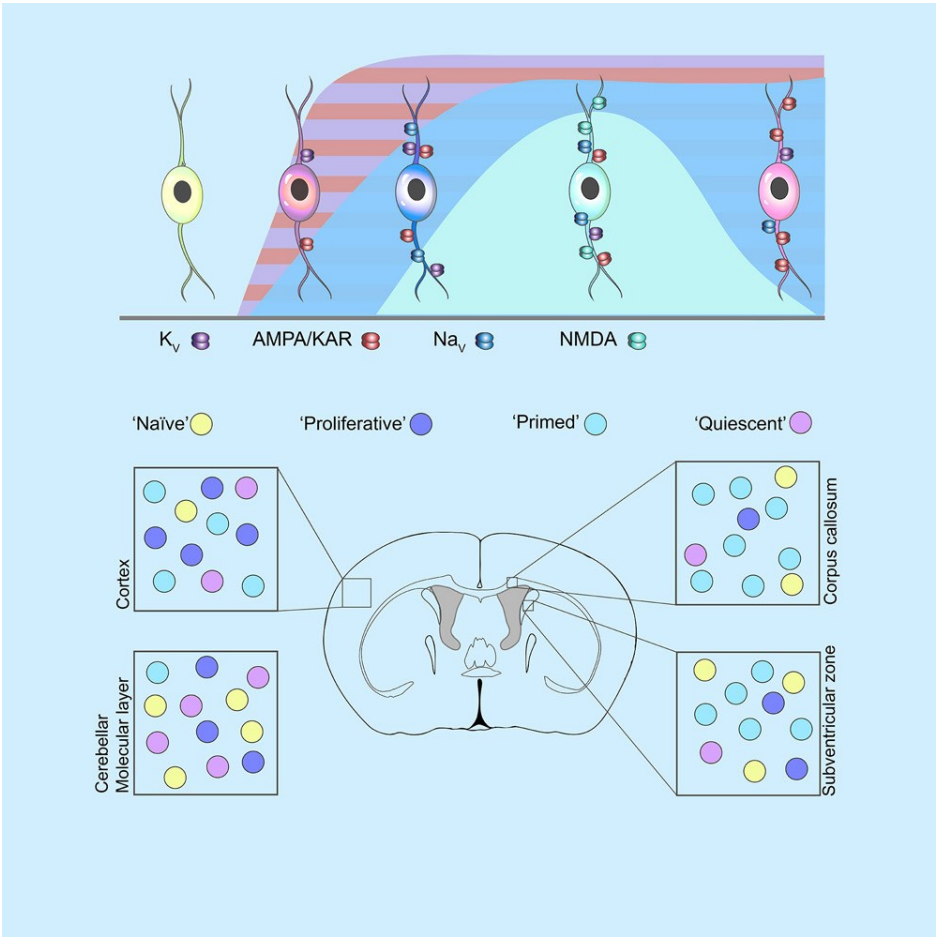

Figure 4: Distribution of different NG2 glia subpopulations in several regions of the brain. KV, voltage-gated potassium channel; NaV, voltage-gated sodium channels; AMPA, α-amino-3-hydroxy-5-methyl-4-

isoxazolepropionic acid receptors; KARs, kainate receptors; NMDAR, N-methyl-D-aspartate receptors (Spitzer et al., 2019).

Unlike neurons, NG2 glia are not able to propagate action potentials, but are integrated into the neuronal circuits. The synaptic inputs from neurons regulate proliferation and differentiation of NG2 glia and vice versa (Spitzer et al., 2016, Kukley et al., 2007, Kukley et al., 2008, De Biase et al., 2010, McTigue and Tripathi, 2008). However, the neuron-NG2 glia synaptic activities are reduced apparently after the initiation of myelination and intense formation of the myelin sheath (Kukley et al., 2010, Vélez-Fort et al., 2010)(Fig. 5).

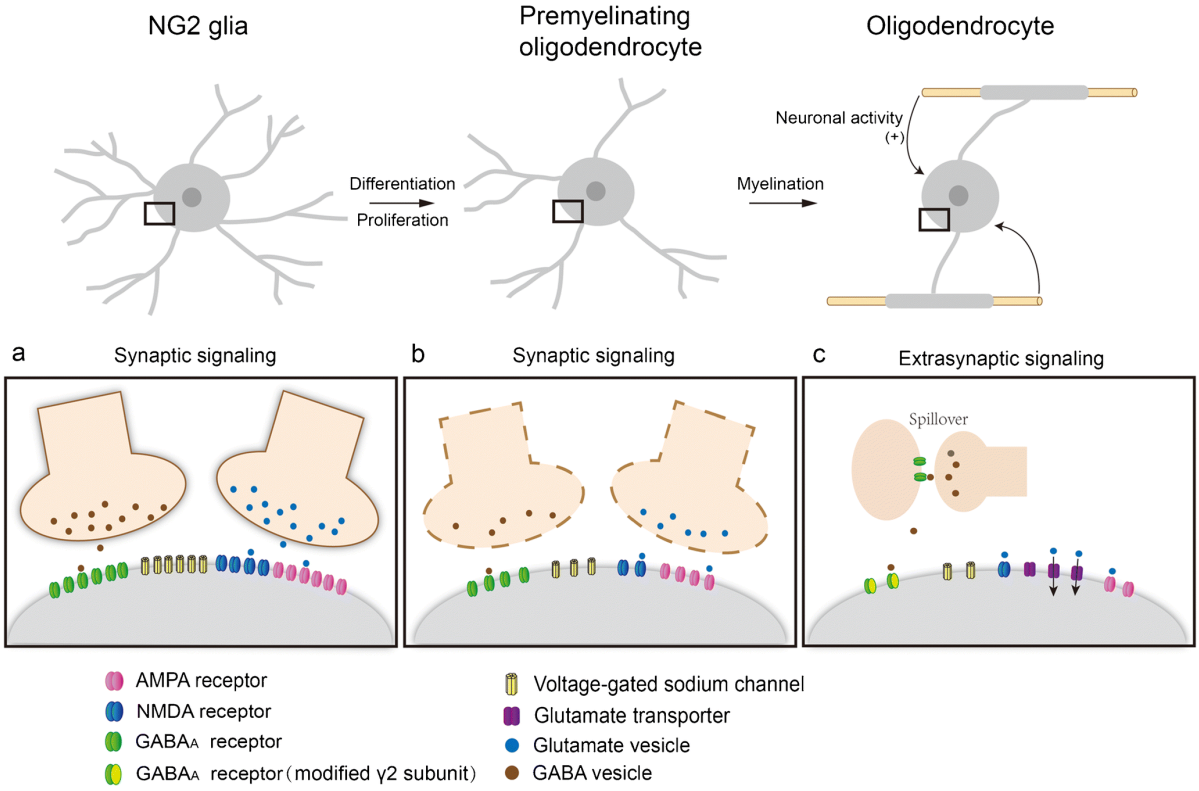

Figure 5: A) Functional α-amino-3-hydroxy-5-methyl-4-isoxazolepropionic acid (AMPA), N-methyl-D-aspartate (NMDA), and γ-aminobutyric acid (GABA)A receptors express NG2 glia. Expression of voltage-gated Na^+ channels on NG2 glia and Na^+ spikes can be elicited. B) Numbers of AMPA, NMDA, and GABAA receptors and voltage-gated Na^+ channels decrease when NG2 glia differentiate into premyelinating oligodendrocytes C) Small fractions of AMPA, NMDA, and GABAA receptors and voltage-gated Na^+ channels are preserved on mature oligodendrocytes, accompanied with an increasing number of glutamate transporters. Neuronal and extrasynaptic activities can enhance myelination (Li et al., 2020).

1.2 NG2 glia and CNS pathology

NG2 glia represent a very flexible glial cell type, which react to the different pathologies in the brain and spinal cord. After activation, they change their morphology, proliferation rate,

and differentiation. The type of NG2 glia response to injury is strongly dependent on the insult and the developmental stage (Song et al., 2017).

NG2 glia respond to traumatic injuries, including stab wound lesions (Dimou et al., 2008, Buffo et al., 2005) spinal cord injury (McTigue et al., 2001), and ischemia (Zhang et al., 2013). The number of NG2 glia decreases significantly in the infarct core area, whereas they increase in the peri-infarct area, termed penumbra after focal cerebral ischemia (FCI) (Tanaka et al., 2001). NG2 glia are the first cells to react and this rapid, reaction resembles the time-course of microglia reactivity. The number of proliferating NG2 glia increases greatly at three days after injury and further increases to seven days after injury. This proportion remains constant until 14 days after injury and then declines (Simon et al., 2011). It was shown that the accumulation of NG2 glia near the injury could have opposite effects. The physical barrier of NG2 proteoglycan participates in the growth-inhibitory environment (Tan et al., 2005) or NG2 glia provide an adhesive substrate for axonal growth cones and promote their growth in the glial scar (Yang et al., 2006). Besides the proliferation, it was shown that activated NG2 glia are able to differentiate into reactive astrocytes or even neurons after ischemia in the brain (Honsa et al., 2016, Komitova et al., 2011, Kirdajova et al., 2021)(Fig. 6) or in the spinal cord injury (Hackett et al., 2018, Huang et al., 2018).

Besides acute brain injury, NG2 glia can respond also to progressive neurodegenerative diseases, such as Alzheimer`s disease (AD) and Amyotrophic lateral sclerosis (ALS). An increased proliferation and differentiation rate of NG2 glia was shown in superoxide dismutase (SOD) mouse model of ALS. Due to that, no changes in the number of oligodendrocytes were observed. However, newly derived oligodendrocytes are dysfunctional, in terms of myelination and metabolic/trophic support of axons (Kang et al., 2013, Philips et al., 2013). Similarly, in the mouse model of AD (amyloid precursor protein/presenilin-1) increased proliferation and differentiation of NG2 glia was found. However, such increases in NG2 glia proliferation/differentiation are much lower in both types of neurodegenerative diseases than those observed after the acute injury mentioned above (Behrendt et al., 2013).

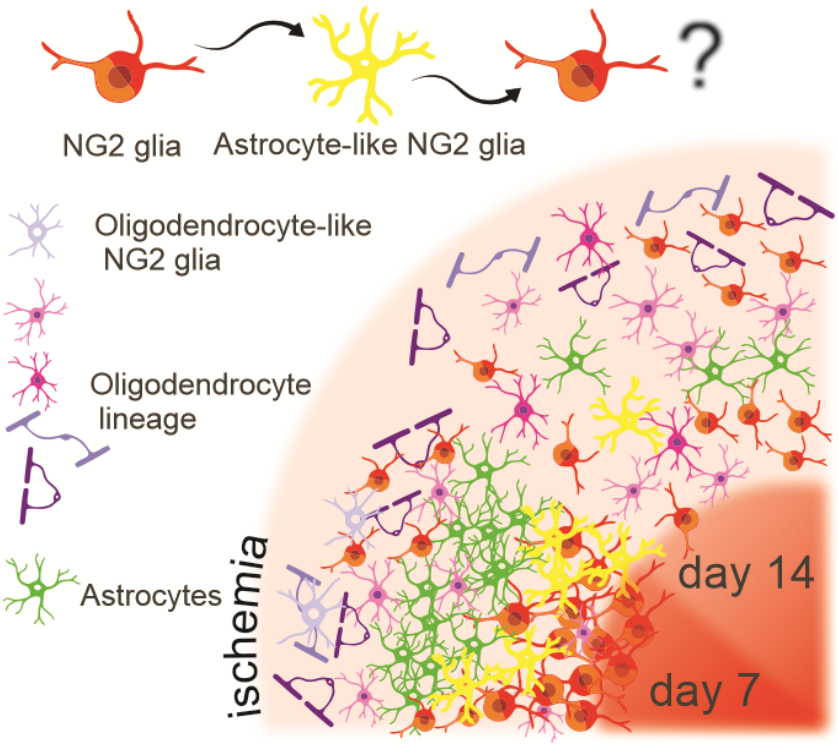

Figure 6: Scheme of cell types after focal cerebral ischemia seven and 14 days after injury. Formation of compact glial scar occurs along borders to infarct zone and includes astrocytes (green cells), NG2 glia (yellow cells) and cells derived therefrom such as astrocyte-like NG2 glia, oligodendrocyte-like NG2 glia, and oligodendrocytes (Kirdajova et al., 2021).

As was mentioned above NG2 glia rapidly react to neurodegeneration but it seems that the response of NG2 glia observed in ALS and AD is rather due to demyelination than due to neurodegeneration (Cruz et al., 2003, Sirko et al., 2013). Since NG2 glia are mainly precursors of oligodendrocytes, they are the perfect candidate to respond to demyelination. In fact, adult NG2 glia differentiate into oligodendrocytes capable of remyelinating axons (Zawadzka et al., 2010) and restoring nearly normal nerve conduction (Fig. 7). The problem arises when the demyelination in multiple sclerosis (MS) progresses and NG2 glia lose the ability to respond to myelin damage limiting their remyelination capacity (Kipp et al., 2012). It was previously thought that NG2 glia depletion is the limiting factor of remyelination, but it turns out that it is rather the inhibition of NG2 glia recruitment and differentiation into myelinating oligodendrocytes (Boyd et al., 2013).

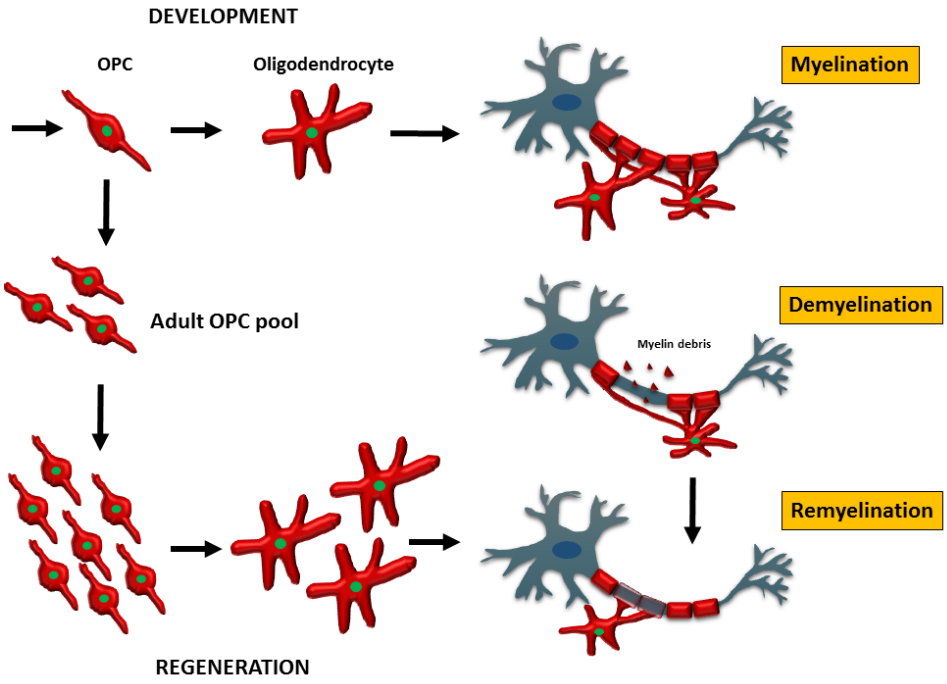

Figure 7: NG2 glia (=OPC) and oligodendrocytes in the process of myelination, demyelination, and remyelination. Oligodendrocytes myelinate axons in the development of the central nervous system. Oligodendrocytes are vulnerable to insults such as trauma, immune-mediated attacks or ischemia lead to oligodendrocyte death - demyelination. An adult OPC pool can give rise to new oligodendrocytes and replace deceased oligodendrocytes – remyelination (Kuhn et al., 2019).

1.3 Ischemia and stab wound

Ischemic injury is one of the leading causes of death and disability worldwide. Brain ischemia stems from cardiac arrest or stroke, in which poor blood flow to the tissue causes glucose and oxygen deprivation in the brain parenchyma. Glucose and oxygen deficiency disrupts oxidative phosphorylation, which results in energy depletion and ionic disbalance, followed by cell membrane depolarization, calcium overload, and extracellular accumulation of excitatory amino acid glutamate (Belov Kirdajova et al., 2020)(Fig. 8). Therewith is associated with the death of neurons, because they are extremely sensitive to ischemia due to their high energetic demands (Dirnagl et al., 1999). Morphological changes, such as activation of microglia and astrocytes, or higher proliferation of NG2 glia, microglia, and astrocytes are all hallmarks of ischemia (Dávalos, 2005, Pforte et al., 2005, Anderova et al., 2011, Burns et al., 2009). According to the location and extent of the injury, we recognize two types of ischemia: focal and global cerebral ischemia (Yao et al., 2018).

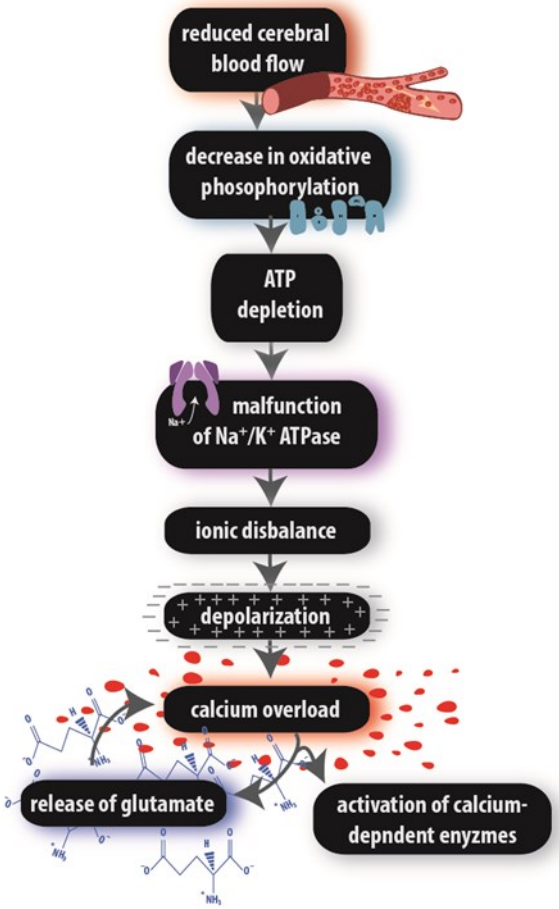

Figure 8: Ischemic cascade. The relay of extracellular and intracellular processes leads to pathogenic states and eventually to cell death (Belov Kirdajova et al., 2020).

Global cerebral ischemia (GCI) stems from an overall decrease in blood flow due to cardiac arrest or near-drowning. Disruption of blood supply results in loss of consciousness and leads to irreversible damage of the brain parenchyma. Global cerebral ischemia is characterized by delayed neuronal death (Guo et al., 2019) and by the proliferation and activation of glial cells (Anderova et al., 2011) and formation of reactive gliosis (Pekny and Nilsson, 2005). The restoration of cerebral blood flow is crucial for the protection of damaged brain tissue (Duran-Laforet et al., 2019, Durán-Laforet et al., 2019), but reperfusion may also result in additional increases in intracellular Ca^{2+}, causing further damage (Harukuni and Bhardwaj, 2006, Kauppinen and Swanson, 2007, Unal-Cevik et al., 2004).

As the name suggests, focal cerebral ischemia (FCI) is due to the occlusion of specific arteries of the brain, caused by thrombosis or embolism (VanGilder et al., 2012a). A cortical stab wound (SW) can be considered also as a type of FCI since in this type of injury arteries are also damaged (Anderová et al., 2004, Komitova et al., 2011). Close to the occluded/damaged vessel, two distinct zones can be distinguished: infarction core (a zone of severe ischemia) and penumbra (a zone of moderate ischemia, with partially maintained blood supply) (Rossi et al., 2007). The infarction core is characterized by a lack of adenosine triphosphate (ATP), pathological concentrations of ions, high concentrations of extracellular glutamate, and tissue acidosis (Fig. 9). On the contrary, in the penumbra due to the presence of residual blood flow, there are only lowered concentrations of ATP and maintained some ionic concentrations (Hinzman et al., 2015, Oliveira-Ferreira et al., 2019). However, in general, cells of the penumbra near the infarct core undergo apoptosis, whereas cells in the distal part exhibit only mild damage (Nedergaard and Dirnagl, 2005). Moreover, astrocytes and NG2 glia, on the edge of the penumbra form a glial scar that prevents detrimental compounds from entering the spared nervous tissue (Adams and Gallo, 2018).

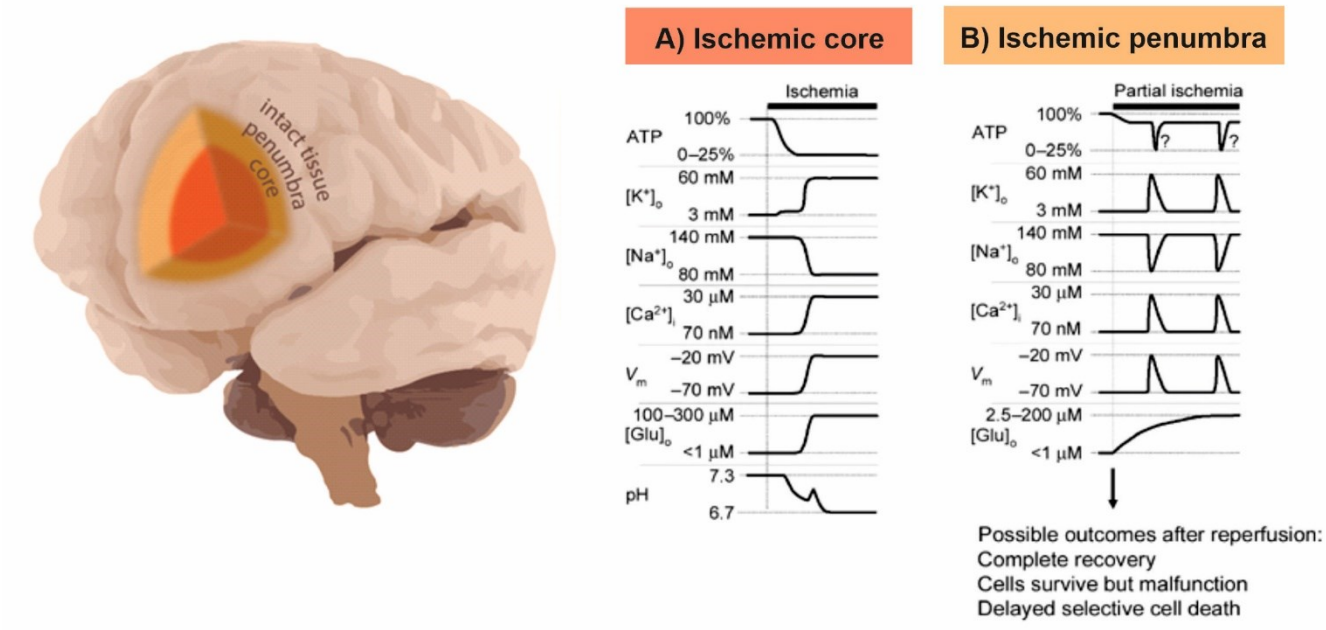

Figure 9: Nervous tissue in focal cerebral ischemia. The affected tissue is divided into the infarction zone and the penumbra. A) Schematic illustration of events that in the core of focal cerebral ischemia. Interruption of ATP production leads to inhibition of the Na^+-K^+ ATPase and to a consequent decrease of the transmembrane ion gradients. The disruption of ion homeostasis depolarizes cells and causes a large release of glutamate into the extracellular space. Ischemia also leads to extracellular acidification. B) Events in the penumbra of focal cerebral ischemia. Initially, the drop in ATP is less severe, but triggers repeated transient depolarizations and associated ion shifts, while $[Glu]_o$ rises slowly but steadily. If reperfusion is initiated soon enough, complete recovery or selective damage may occur (bottom). With increasing duration of ischemia and proximity to the

core, the transient ischemic depolarizations may evolve into terminal depolarization and ionic disruption, which leads to pan-necrosis and expansion of the infarct. Adapted from (Rossi et al., 2007).

In the tissue affected by ischemia, the process called the ischemic pathway takes place. It is a biochemical cascade caused as a consequence of a low supply of oxygen and glucose, which completely disrupts mitochondrial oxidative phosphorylation (Erecińska and Silver, 2001). The primary consequence of oxygen and glucose absence, which are crucial for glycolysis and oxidative phosphorylation, is the depletion of ATP (Rama and García, 2016). The loss of ATP results in the subsequent failure of ATP-dependent mechanisms - Na^+/K^+-ATPase and other ATP-dependent ionic transporters. The cells fail to maintain electrochemical gradients, which results in disruption of ionic gradients (Na^+, K^+) and depolarization of membranes. The elevated extracellular concentration of K^+ causes the opening of L-type voltage-gated Ca^{2+} channels (Luoma et al., 2011). The high level of Ca^{2+} triggers the release of glutamate and other neurotransmitters into the extracellular space (Papazian et al., 2018, Verma et al., 2018) (Fig. 8). The release of glutamate triggers a positive feedback loop by activation of AMPA/NMDA receptors, which leads to additional Ca^{2+} increase and further glutamate release. This process is known as glutamate-induced excitotoxicity (Won et al., 2002, Onteniente et al., 2003) (Fig. 10).

This complex process involves activation of Ca^{2+}-dependent proteins that are responsible for the initiation of a series of cytoplasmatic and nuclear events, such as activation of proteolytic enzymes that degrade cytoskeletal proteins (calpains, phospholipases, and endonucleases); activation of phospholipase A2 and cyclooxygenase, which generates free-radicals producing lipid peroxidation and membrane damage (Dirnagl et al., 1999) (Fig. 10). Also, mitochondria function is impaired due to presence of free radicals and becomes leaky. Once the membrane is disrupted, cytochrome C is released from mitochondria and provides a trigger for apoptotic signals. Moreover, when the intracellular Ca^{2+} concentration is elevated, Ca^{2+}-dependent nitric oxide synthase produces a mixture of superoxide anions and nitric oxide called reactive oxygen species (ROS) (Iadecola and Ross, 1997). These signals from mitochondria together with ROS provide a trigger for apoptosis and necrosis which lead to cell death (Dugan and Choi, 1994, Kristián and Siesjö, 1998)(Fig. 10).

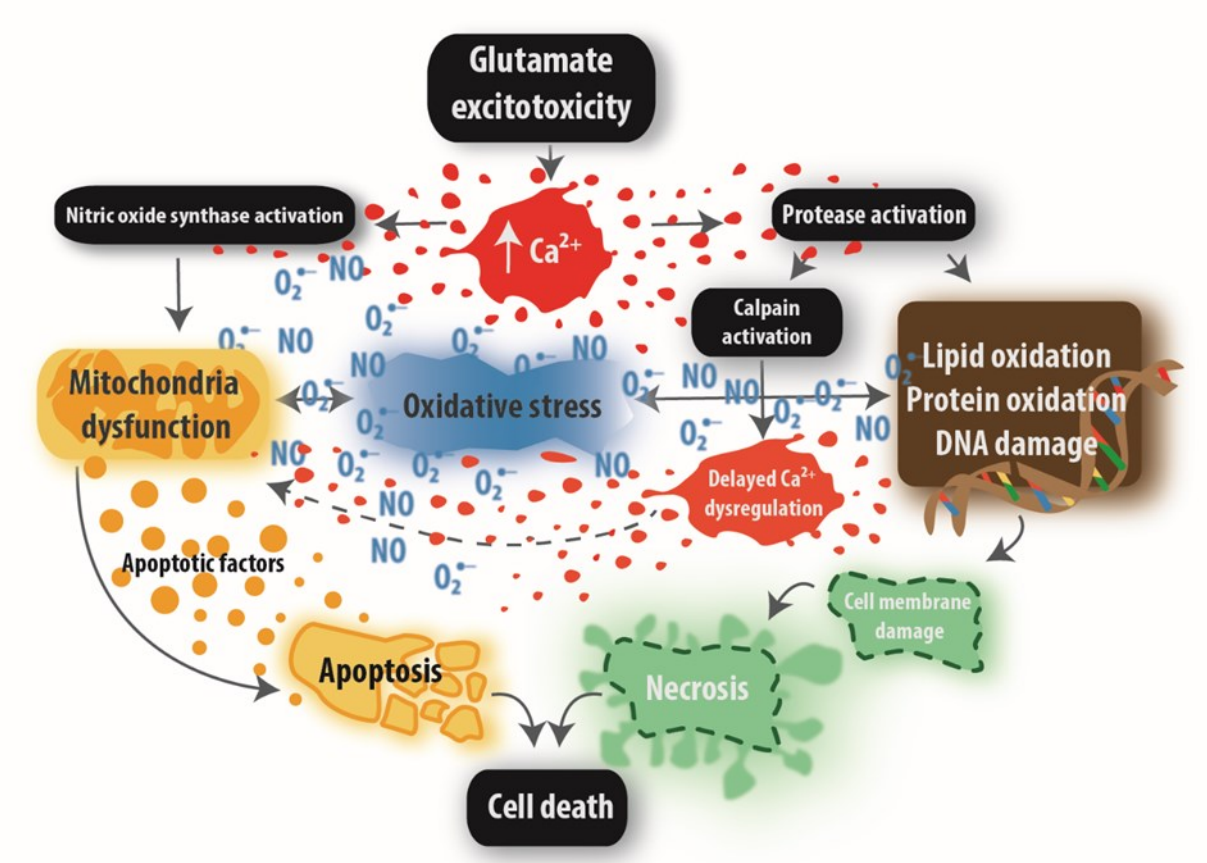

Figure 10: Schematic overview of excitotoxic events during ischemia. Glutamate excitotoxicity causes an excessive increase in calcium concentration in the cytosol. Disruption of intracellular calcium homeostasis leads to protease, and nitric oxide synthase activation. This leads to mitochondrial dysfunction, oxidative stress, and oxidation of essential molecules. Activation of these mechanisms initiates the chain of apoptotic or necrotic events causing cell death (Belov Kirdajova et al., 2020).

1.4 Demyelinating diseases

Demyelinating diseases of the CNS comprise a group of neurological disorders characterized by progressive loss of oligodendrocytes and myelin sheaths in the white matter tracts (Vega-Riquer et al., 2019). Myelin disorders were once thought to be confined to leukodystrophies (Waldman, 2018), inflammatory diseases such as MS (Plemel et al., 2017), and injury such as periventricular leukomalacia (Back and Rivkees, 2005). Recently, more diverse neurological diseases, such as human immunodeficiency virus (HIV) and HIV-associated neurocognitive deficits (Zhou et al., 2015a, Solomon et al., 2019), ALS (Kang et al., 2013, Ferraiuolo et al., 2016, Nasrabady et al., 2018), AD (Nasrabady et al., 2018, Liddelow et al., 2017), schizophrenia (Raabe et al., 2019), and autism (Graciarena et al., 2018) were included into the myelin pathology. During demyelinating diseases such as MS, myelin is destroyed and along with it, also the oligodendrocytes that produce the myelin. Thus, recovery is

limited because of interruptions in neuronal transmission as well as a lack of support for neurons. Although NG2 glia remain abundant in the CNS, they are unable to mature and form new functional myelin in the diseased CNS (Grinspan, 2020).

The most prevalent and the best-studied primary demyelinating disease in the adult brain is MS (Goldschmidt et al., 2009). It is an inflammatory disease characterized by large inflammatory plaques of white matter demyelination. Such lesions are associated with oligodendrocyte destruction, reactive gliosis, and axonal degeneration. The inflammatory plaques beside the neuronal and glial cells include T-lymphocytes and macrophages (Kipp et al., 2016)(Fig. 11). Furthermore, reactive astrocytes and microglia participate in the inflammatory plaques development, progression, and resolution of MS by the secretion of cytokines and other inflammatory mediators. The white matter plaques can arise anywhere in the brain, but some predilection sites, such as the periventricular white matter, exist (Comi, 2009). Besides the very-well known focal lesions also gray matter demyelination and diffuse white matter injury were described (Vrenken et al., 2007) (Fig. 11).

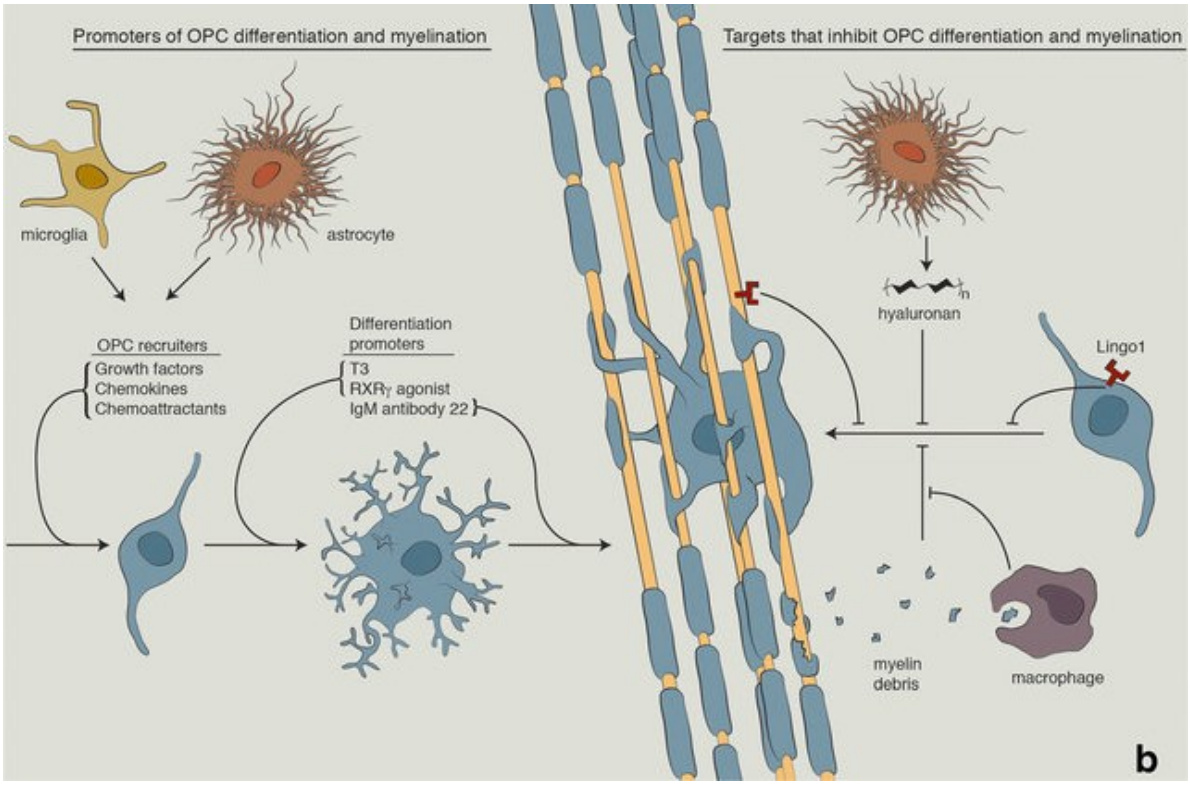

Figure 11: NG2 glia (=OPC) differentiation in development and disease. A demyelinated lesion in multiple sclerosis contains many cell types and molecular factors involved in both promoting (left) and inhibiting (right) NG2 glia differentiation and myelination (Hartley et al., 2014).

On the clinical level, distinct phases of disease can be distinguished: at the beginning most patients suffer from new neurological symptoms, which usually disappear after several

weeks (Kipp et al., 2017). This initial phase is called relapsing-remitting MS, which means that symptoms appear (i.e., a relapse) and then fade away, either partially or completely (i.e., remitting). After several years (10–15 years), the frequency of relapses decreases. This so-called second phase of MS is characterized by chronically progressive clinical worsening over time (Zhan et al., 2020). On the pathological level, the relapsing-remitting phase of MS is characterized by recurrent episodes of inflammatory white matter demyelination. These inflammatory events are probably driven by peripheral, autoreactive immune cells, which invade the CNS via the blood-brain barrier (BBB). From pre-clinical and post-mortem studies, there is large evidence that focal inflammatory demyelination induces neurodegeneration, such as axonal transection or neuronal apoptosis (Trapp et al., 1998). In the early relapsing phases, episodes of demyelination are usually followed by remyelination (Huang et al., 2011), however, in the progress of the disease it is mostly insufficient and the majority of chronic MS plaques remain demyelinated (Trapp et al., 1998). The reason for the failure of remyelination could be caused by a combination of decreased regenerative factors and the presence of inhibitory factors (Huang et al., 2011). Also, the disease is heterogeneous, and the failure might vary in different brain regions (Mi et al., 2013, Chari, 2007).

To date, the etiology of the MS is not well understood and it is necessary to have appropriate animal models that closely resemble the pathophysiology and clinical signs of these diseases. Experimental autoimmune encephalomyelitis (EAE) is the most commonly used animal model to study inflammation and autoimmune-mediated in MS. Mice are immunized with a CNS-related antigen (myelin oligodendrocyte protein (MOG), proteolipid protein (PLP)…) administered in a strong adjuvant. The combination of the peptide used and the mouse strain determine the specific phase of the MS, such as the relapsing or chronic phase (Al-Izki et al., 2012, Star et al., 2012). The EAE model is an excellent tool to study mechanisms associated with T-cell infiltration which is central to the development of acute monophasic EAE and relapsing-remitting disease. This model was useful in developing new drugs for MS, such as natalizumab (Bauer et al., 2009) and fingolimod (Choi et al., 2011). However, while these current therapies for MS reduce the frequency of relapses by modulating adaptive immune responses they fail to limit the irreversible damage of myelin and neurodegeneration (Kipp et al., 2016). This problem, in turn, tries to explain the model of cuprizone (CPZ)-induced demyelination (Gudi et al., 2014, Praet et al., 2014). The model of toxic demyelination induced by CPZ, a copper chelator that reduces the cytochrome and monoamine oxidase activity into the brain, produces mitochondrial stress, and triggers the

local immune response (Vega-Riquer et al., 2019). This intoxication results in loss of oligodendrocytes (Fig. 12) and microglia and astrocytes activation, finally leading to demyelination of distinct white and grey matter brain areas (Zhan et al., 2020)(Fig. 12). This model reflects the progressive phase of MS and could be used to investigate: first, immune cell-driven myelin and axonal degeneration, and second, remyelination of the demyelinated axon (Zhan et al., 2020).

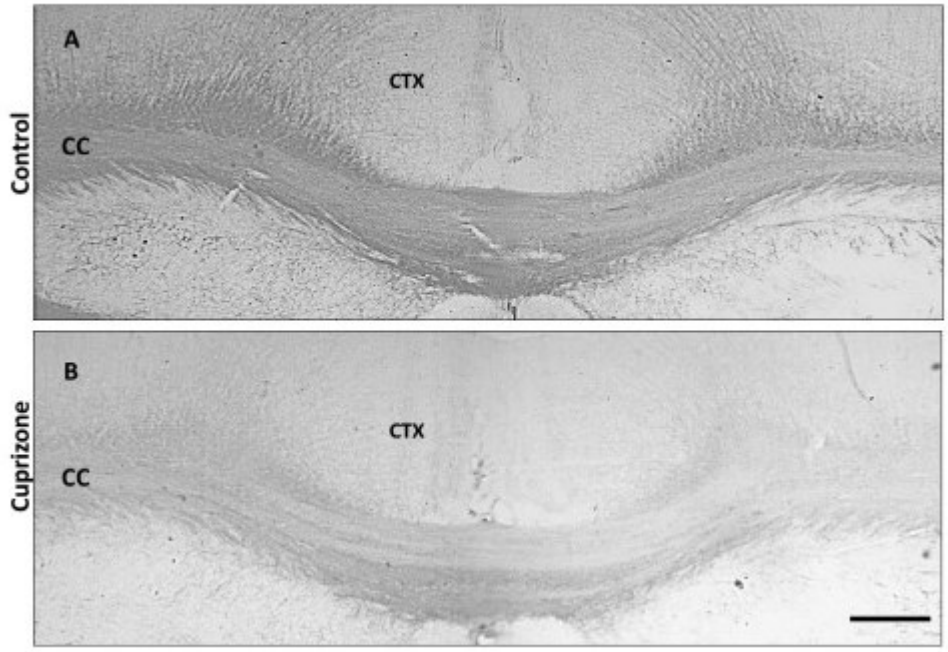

Figure 12: Cuprizone effects in the mouse brain. The mice received 0.2% cuprizone for 6 weeks. Coronal sections stained with anti-myelin basic protein (MBP). The control animal (A) shows a strong expression of MBP in the corpus callosum (CC), whereas the cuprizone-treated mouse (B) expresses low levels of MBP. CTX: cortex. Bar = 5µm, (Vega-Riquer et al., 2019).

1.5 Aging of CNS

CNS is sensitive to age with increasing deficits in neuronal functions including cognitive decline, motor, and sensory abnormalities during aging (Sousounis et al., 2014, Damoiseaux, 2017, Jeromin and Bowser, 2017). It is a complex and irreversible process accompanied by morphological, biochemical, and physiological changes and increased susceptibility to neurodegenerative diseases (Pan et al., 2020). Initial studies extensively tested neuron-loss hypothesis; however, the neuron loss is not the only contributor to the functional decline. There is no loss of neurons in most regions of the brain (Morrison and Hof, 1997, Pakkenberg and Gundersen, 1997, Ihara et al., 2018), but the cognitive deficit could be due to changes in branching or density of dendritic spikes (Burke and Barnes, 2006). Furthermore, reduction of adult neurogenesis in the subgranular zone of the dentate gyrus of the hippocampus and

the subventricular zone of the lateral ventricles was described (Seib and Martin-Villalba, 2015). In addition to morphological changes of neurons, white matter abnormalities were identified that increased with age starting from middle age in humans (Kohama et al., 2012). The reduction in white matter volume was shown by as much as 28% during aging (Liu et al., 2017), which might explain connectivity failure and the decline of information processing within neural circuits (Tripathi, 2012, Young et al., 2013). Besides the altered myelination, the aged brain exhibits an increased number of two main glial cell types: astrocytes and oligodendrocytes (Peters and Sethares, 2002)(Fig. 13). Moreover, aging is characterized by chronic low-grade inflammation and increased microglial reactivity, compared to the young brain. The microglia release proinflammatory cytokines, such as interleukin (IL)-1β, IL-6, and tumor necrosis factor (Maher et al., 2004, Godbout et al., 2005), while anti-inflammatory cytokines, such as IL-10 and IL-4, are reduced (Maher et al., 2005, Ye and Johnson, 2001).

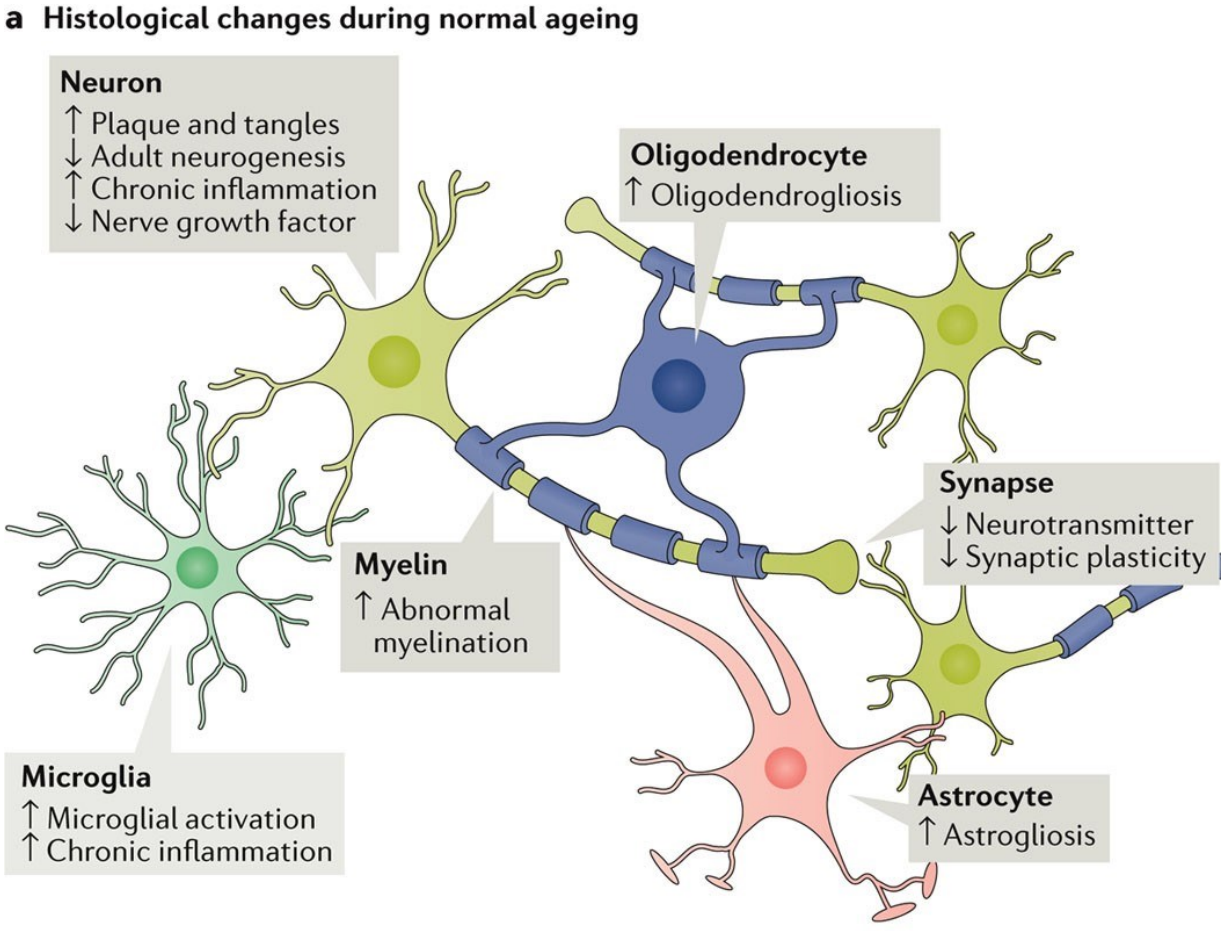

Figure 13: During the aging process, amyloid plaques and neurofibrillary tangles are generated inside and outside of neurons, adult neurogenesis and nerve growth factor concentration decline, and chronic low-grade inflammation persists as a result of microglial activation. In addition, neurotransmitter production and synaptic plasticity are significantly reduced with age. Correct myelination of neurons can also become disrupted with age along with increased brain gliosis (Satoh et al., 2017).

1.6 Ischemic brain injury impaired by aging and influenced by sex

Age was found to be one of the most important risk factors for brain infarction and its mortality (Hoyer, 1987). Older mice exhibit a differential response to stroke and have worse outcomes than adult mice (Chauhan et al., 2018). Abnormalities in glycolytic flux, lactate production, cessation of oxidation, and energy production were found to be more pronounced with advancing age, which indicates reduced plasticity of the brain to the pathological conditions (Hoyer, 1987). In response to cerebral injury, microglia are some of the first responders. However, microglia in aged mice acquire a dysfunctional phenotype and exaggerated response to injury (Niraula et al., 2017). They produce higher levels of ROS and have a greater inflammatory response after ischemic stroke compared to young animals (Ritzel et al., 2018). Aging also alters the proliferation of reactive astrocytes and this results in accelerated glial scar formation in aged animals (Badan et al., 2003). Along with an accelerated astrocytic response, the number of glial fibrillary acidic protein (GFAP) positive cells was increased in the aged brain compared to the adult brain, still persisting 30 days after ischemia (Manwani et al., 2011). On the contrary, the number of neural stem/progenitor cells near the infarct area or subventricular zone in the aged brain is lower than in the adult brain (Liang et al., 2016). Similarly, numbers of NG2 glia in the corpus callosum are higher (Liang et al., 2016) and their bodies are enlarged and highly branched in the adult brain compared to the aged brain (Ohta et al., 2003). This suggests that aging decreases post-stroke compensatory responses towards neurogenesis and oligodendrogenesis, and it can partially explain poor behavioral outcomes following ischemic injury in this period of life (Liang et al., 2016).

In addition to aging, sex was identified as an important variable for stroke outcome as well as in animal models as in humans (Chisholm and Sohrabji, 2016). A recent study found that even though acute stroke care is similar for males and females, women have poorer functional outcomes (Gattringer et al., 2014). In particular, adult females have smaller infarcts and better cerebral blood flow than adult males (Alkayed et al., 1998, Selvamani et al., 2014), however aged females have larger infarct volumes than aged males (Manwani et al., 2013) while adult and aged males did not differ (Selvamani et al., 2014). The mechanism underlying the advantage of the adult female is not well understood, although estrogen and progesterone are believed to play a role in neuroprotection (Simpkins et al., 1997). A recent preclinical study proved this, concluding that progesterone administration results in reduced lesion size following ischemia (Wong et al., 2013). Besides the infarct volume size, sex-specific differences are seen throughout the lifespan in inflammation, BBB permeability (Liu

et al., 2009, Manwani et al., 2013), and glial cell reactivity (Chisholm and Sohrabji, 2016, Sohrabji et al., 2013).

2 AIMS OF THE STUDY

Hypothesis 1.: NG2 glia were shown to have multipotent capacity in the development and following injury, generating, beside oligodendrocytes, also astrocytes and even neural precursor cells (Kirdajova and Anderova, 2020). Since such observations were based on the expression of only few cell-type-specific markers, we hypothesize that multiple subpopulations exist within $NG2^+$ cells, especially after severe CNS injury, and they are characterized by distinct combination of genes. Therefore, the more precise analysis based on the expression of larger battery of genes is necessary to get better insight into multipotency of NG2 glia.

Aim 1.: To characterize the proliferation and differentiation potential of NG2 glia following FCI using genetic fate-mapping in combination with gene expression profiling.

Hypothesis 2.: Several studies suggested that astrocytes can originate from embryonic rather than postnatal or adult NG2 glia, in the intact CNS (Huang et al., 2019, Huang et al., 2014). In reaction to CNS pathology, some studies reported that a small fraction of NG2 glia can differentiate into astrocytes after spinal cord injury (Hackett et al., 2018) and after brain injury (Dimou et al., 2008, Honsa et al., 2016, Valny et al., 2018), while others showed that fewer NG2 glia, if any, become astrocytes (Kang et al., 2010, Zawadzka et al., 2010). We hypothesize that using the same transgenic mice, same method of astrocyte identification and protocol for tamoxifen administration in different CNS injuries confirm generation of astrocytes from NG2 glia in adult brain.

Aim 2.: To compare the fate of NG2 glia-derived astrocytes, between different types of CNS disorders in tamoxifen-inducible BAC transgenic mice.

Hypothesis 3.: Previous global gene expression studies of experimental stroke using microarrays (Mitsios et al., 2007, Roth et al., 2003) and more recently RNA-Seq (Dergunova et al., 2018) have provided useful insights into the pathophysiology of ischemic stroke and uncovered many altered molecular pathways (VanGilder et al., 2012b). However, only few studies included aged animals. We assume that aging alterations on its own could be risk factor and reason for worse outcome after ischemia. Therefore, the profound comparation of transcriptional profile between young and aged brain after ischemia is needed.

Aim 3.: To dissect the interaction between stroke and aging at the genome-wide level using FCI on young adult (3-month-old) and aged (18-month-old) female mice.

3 MATERIALS AND METHODS

3.1 Material and methods common for aims: 1, 2 and 3

3.1.1 Animals

All procedures involving the use of laboratory animals were performed in accordance with the European Communities Council Directive 24 November 1986 (86/609/EEC) and animal care guidelines approved by the Institute of Experimental Medicine, Academy of Sciences of the Czech Republic (Animal Care Committee on March 15, 2017; approval number 2/2017, 77/2015,51/2014, 2/2013). All efforts were made to minimize both the suffering and the number of animals used.

For purpose of characterization of the proliferation and differentiation potential of NG2 glia following CNS injuries we used 3-month old transgenic mice, which were derived by crossing the mouse strain B6.Cg-Tg(Cspg4-cre-Esr1∗)BAkik/J and B6;129S6-Gt(ROSA)26Sortm14 (CAG-tdTomato)Hze/J (further termed Cspg4/tdTomato mouse; Fig. 14A), (Jackson Laboratory, Bar Harbor, ME, USA), in which the expression of tamoxifen(TX)-inducible Cre recombinase is controlled by the Cspg4 promoter (Zhu et al., 2011). After TX administration, tdTomato red fluorescent protein is expressed in Cspg4-positive ($Cspg4^{+}$) cells – predominantly in NG2 glia and cells derived therein. Tamoxifen was administered intraperitoneally for two days (100 mg/kg, Sigma–Aldrich, St. Louis, MO, USA; Valny et al. (2016) and CNS injuries were induced 14 days after the last TX injection (Fig. 14C). In addition, to follow NG2-glia derived astrocytes, the Cspg4/tdTomato mice were cross-bred with constitutive Gfap/EGFP mice, in which the visualization of astrocytes is feasible because of the enhanced green fluorescent protein (EGFP) under the control of the human promoter for GFAP, (Nolte et al., 2001)(Fig. 14B). This approach enabled the identification of NG2 glia that differentiated into astrocyte-like NG2 glia based on their co-expression of tdTomato and EGFP.

Finally, to dissect the interaction between stroke and aging, we performed experiments on 3- and 18-month-old C57Black/6 mice.

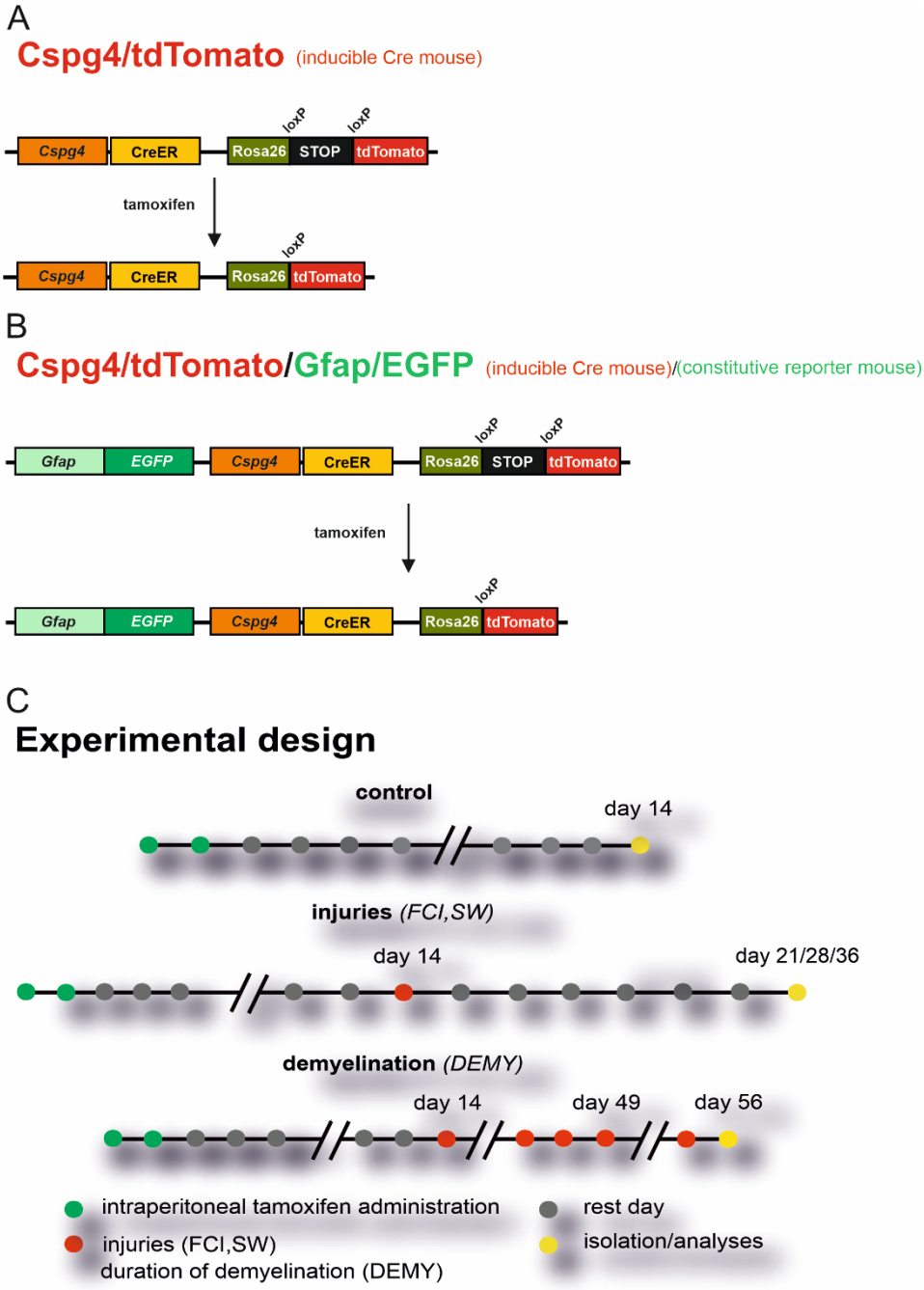

Figure 14: Scheme summarizing genetically modified mouse strains used in the experiments, and tamoxifen applications. (A) Cspg4/tdTomato mouse in which red fluorescent protein (tdTomato) is expressed in NG2 glia and cells derived therefrom. (B) Cspg4/tdTomato/Gfap/EGFP mouse in which, in addition to red NG2 glia, enhanced green fluorescent protein (EGFP) is constitutively expressed under the control of glial fibrillary acidic protein (GFAP) promoter, an astrocytic marker. (C) Scheme of administration of tamoxifen. FCI, focal cerebral ischemia; SW, stab wound; DEMY, demyelination (Kirdajova et al., 2021).

3.1.2 Induction of focal cerebral ischemia

Mice were anesthetized with 3% isoflurane (Abbot, Illinois, USA) and maintained in 2% isoflurane using a vaporizer (Tec-3, Cyprane Ltd., Keighley, UK). A skin incision between

the orbit and the external auditory meatus was made and a 1-2 mm hole was drilled through the frontal bone, 1 mm rostral to the fusion of the zygoma and the squamosal bone and about 3.5 mm ventrally to the dorsal surface of the brain. The middle cerebral artery was exposed after the dura was opened and removed. The middle cerebral artery was occluded by short coagulation with bipolar tweezers (SMT, Czech Republic) at a proximal location, followed by transection of the vessel to ensure permanent occlusion. During the surgery, the body temperature was maintained at 37±1°C using a heat pad. The sham-operated animals (CTRL) were subjected to the same surgery procedure, but without dura opening and vessel occlusion. This middle cerebral artery occlusion model yields small infarct lesions in the parietal cortical region (Fig. 15).

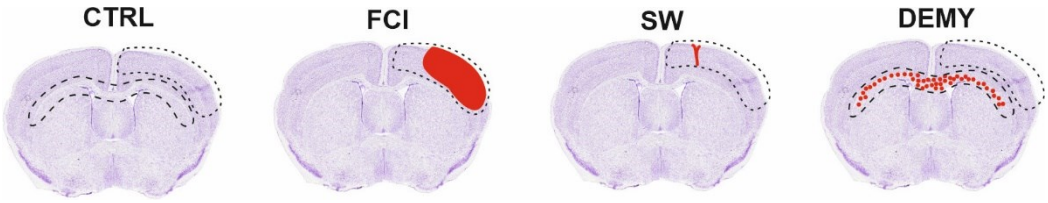

Figure 15: Scheme depicting brain regions (dashed lines), which were used for tdTomato$^+$ cell isolation (Kirdajova 2021).

3.1.3 Preparation of single cell suspension

The mice were deeply anesthetized with pentobarbital (PTB) (100 mg/kg, i.p.), and perfused transcardially with a cold (4–8°C) isolation buffer containing (in mM): NaCl 136.0, KCl 5.4, HEPES 10.0, glucose 5.5, osmolality 290±3 mOsmol/kg. To isolate the cerebral cortex (CTX) or corpus callosum (CC), the brain was sliced into 600 µm coronal sections using a vibrating microtome HM650V (MICROM International GmbH, Germany). Sections were dissected from different regions depending on the type of CNS injury; FCI (+1.5 to -2 mm from bregma) of CTX, SW (-1.3 to -2.5 mm from bregma) of CTX and demyelination (DEMY) (1.5 to -2.5 mm from bregma) of CTX and CC (Fig. 15). The collected tissue was incubated with continuous shaking at 37°C for 45 min in 1 ml of papain solution (20 U/ml) and 0.2 ml DNase (both from Worthington, NJ, USA) prepared in isolation buffer. After papain treatment, the tissue was mechanically dissociated by gentle trituration using a 1 ml pipette. The dissociated cells were layered on top of 5 ml of ovomucoid inhibitor solution (Worthington, NJ, USA,) and harvested by centrifugation (70 x g for 6 min). This method routinely yielded ~2 x 10^6 cells per mouse brain. Cell aggregates were removed by filtering with 70 µm cell strainers (Becton Dickinson, NJ, USA). In case of Cspg4/tdTomato and GFAP/EGFP mice there is no need of additional labeling. But in case of C57Black/6 mice, the cell suspension was then labeled for oligodendrocyte marker 1:50 anti-O4-PE (Miltenyi

Biotec), endothelial cell marker 1:50 anti-CD31-PE (Miltenyi Biotec) and microglial marker 1:50 anti-CD11b-APC (Miltenyi Biotec), according to the standard manufacturer´s protocol. The cells were kept on ice until sorting.

3.1.4 Collection of single cells

Single cells were sorted using fluorescent activated cell sorting (FACS; BD Influx, San Jose, CA, USA). The flow cytometer was manually calibrated to deposit a single cell in the center of each collection tube. Hoechst 33258 (Life Technologies, Carlsbad, CA, USA) was added to the suspension of cells to check viability. Single cells were collected into 96-well plates (Life Technologies, Carlsbad, CA, USA) containing 5 µl nuclease-free water with bovine serum albumin (1 mg/µl, Fermentas, Rockford, IL, USA) and RNaseOut 20 U (Life Technologies, Carlsbad, CA, USA). The plates were placed on a pre-cooled rack and stored at -80°C until analyzed.

3.1.5 Immunohistochemistry and cell counting

The mice were anesthetized with PTB (100 mg/kg, i.p.; Sigma-Aldrich) and transcardially perfused with 20 ml of saline with heparin (2500 IU/100ml; Zentiva) followed by 20 ml of 4% parafromaldehyde (PFA) in 0.1M phosphate buffer (PB). The brains were dissected, post-fixed in 4% PFA overnight and placed in sucrose (Sigma-Aldrich) with gradually increasing concentrations (10%, 20%, 30%) for cryoprotection. Coronal slices (30 µm) were prepared using Hyrax C50 cryostat (Zeiss). The slices were incubated in a blocking solution containing 5% ChemiBLOCKER (EMD Millipore) and 0.5% Triton X-100 (Sigma-Aldrich) in PB saline for 1 hour. They were then incubated overnight at 4°C with primary antibodies diluted in a blocking solution followed by two-hour incubation with secondary antibodies at room temperature (RT). Following primary antibodies were used: see Table 1. Respective secondary antibodies were used: goat anti-rabbit IgG or goat anti-mouse, conjugated with Alexa-Fluor 488, 594 or 660 (1:200, Thermofisher Scientific). Proliferating cells were labeled with 5′-ethynyl-2′-deoxyuridine (EdU) (Sigma–Aldrich, St. Louis, MO, USA) dissolved in the drinking water at 0.2 mg/mL (Young et al., 2013). Mice were exposed to EdU immediately after FCI induction for seven days. EdU was visualized using the AlexaFluor-647 Click-iT EdU Cell Proliferation Assay Kit (Sigma–Aldrich, St. Louis, MO, USA) prior to immunohistochemistry when co-immunostained with GFAP antibody. Floating sections were incubated at 20°C–23°C for 15 min in PBS/0.2 % (v/v) Triton X-100 and then transferred to the EdU developing cocktail, incubated in the dark at 20°C–23°C for

40 min, and washed in PBS. Cell nuclei were visualized by DAPI staining (Sigma-Aldrich). Following staining, slices were mounted and imaged on a Zeiss 510DUO LSM or a Zeiss LSM 880 Airyscan confocal microscope equipped with Ar/HeNe lasers. Stacks of consecutive confocal images taken at intervals of 3 µm were acquired sequentially with the two lasers to avoid cross-talk between fluorescent labels. The background noise of each confocal image was reduced by averaging four image inputs.

Table 1: Primary antibody used for immunohistochemistry

Cell type marker	Antibody	Species	Dilution	Company
Astrocytes	**GFAP coupled Alexa 488**	mouse	1:300	Ebioscience
	ALDH1l1	rabbit	1:500	Abcam
	VIM	mouse	1:1000	Abcam
	AQP4	rabbit	1:500	Millipore
Oligodendrocytes	**APC**	mouse	1:200	Merck
Pericytes	**PDGFRbeta**	rabbit	1:200	Santa Cruz
Proliferation	**KI-67**	rabbit	1:1000	Abcam
	KI-67 coupled FITC	mouse	1:200	ThermoFisher Scientific
	PCNA	mouse	1:800	Abcam
Interneurons	**PARVALBUMIN**	rabbit	1:500	Synaptic system
Neurons	**NeuN**	rabbit	1:100	Chemicon
Newly formated neurons	**Doublecortin**	rabbit	1:1000	Abcam

To determine the number/percentage of cells confocal images (315 x 315 x 20 µm; aim 1), (318µm x 318 µm x 15 µm; aim 2), (212 × 212 × 18 µm,aim 3) covering the studied regions were taken from brain coronal slices prepared from ischemic animals (three animals from each group, three brain slices and at least five regions from each slice). Co-localization images and maximum *z* projection images were made using Zeiss LSM Image Browser (Zeiss, Oberkochen, Germany), ZEN black edition (Zeiss, Oberkochen, Germany) or Fiji (ImageJ).

3.2 Material and methods common for aims: 1, 2

3.2.1 Single-cell RT-qPCR analysis

The single-cell RT-qPCR analysis was used to profile individual cells. The single-cell RT-qPCR analysis was performed using the protocol described previously (Rusnakova et al., 2013). Briefly, samples were reverse transcribed into cDNA using SuperScript III (ThermoFisher Scientific, Waltham, MA, USA). Non-diluted cDNA was pre-amplified using a mix of 95 primers. The primers were designed using Primer-BLAST (Ye et al.,

2012). When possible, each primer pair was designed to span introns to avoid the amplification of genomic DNA. For each assay, the specificity was tested by the melt curve analysis and gel electrophoresis; the efficiency was determined using a standard dilution series spanning six orders of magnitude. Pre-amplified cDNA was 4-times diluted and analyzed in BioMark platform (Fluidigm, San Francisco, CA, USA), measuring the expression of 95 genes. The data was pre-processed in Fluidigm Real-Time Analysis software (Fludigm, San Francisco, CA, USA) and further analyzed by GenEx 6 software (MultiD, Gothenburg, Sweden).

3.2.2 Self-organizing Kohonen maps

Kohonen self-organizing maps (SOM) of size 4/8x1, dividing the cells into four groups, were trained using GenEx 6 (MultiD, Gothenburg, Sweden) software with the following parameters: 0.60 learning rate, 4/8 neighbors and 5000 iterations. The SOM analysis was repeated eight times with identical classification of the cells in each of the repeats. This classification of cells into groups was substantiated with the principal component analysis (PCA).

3.2.3 Statistics

The results are expressed as the mean ± standard error of the mean (SEM). Statistical analyses of the differences among groups were performed using ANOVA and Student's t-test when appropriate. Values of $p < 0.05$ were considered significant, $p < 0.01$ very significant and $p < 0.001$ extremely significant.

3.3 Material and methods specific for aim 2:

3.3.1 Induction of cortical stab wound

Prior to SW, mice were anesthetized with 3% isoflurane and maintained in 2% isoflurane using a vaporizer (Tec-3, Cyprane Ltd., Keighley, UK). The cranium was thinned in 1.5-mm^2 area to pass the sharp knife, 2 mm caudal to the bregma, 1 mm lateral to the midline. Then, a 1.1-mm sterile sharp knife was inserted vertically into the right cerebral hemisphere 1 mm deep to the dura surface (Fig. 15). The skin incision was closed with sutures. CTRL mice were subjected to the same surgical procedure, but without dura opening and SW (Buffo et al., 2005).

3.3.2 Induction of demyelination (DEMY)

Demyelination (DEMY) was induced by administration of 0.3% cuprizone (Sigma-Aldrich, Inc., St. Louis, MO) to mice *ad libitum* in chow (Ssniff Spezialdiäten GmbH, Soest, Germany; Fig. 15). The treated mice received cuprizone chow for 5 weeks to cause DEMY and, after this period, they were returned to a regular diet and allowed to recover for seven days. CTRL mice received regular mice chow, without cuprizone, for the entire period.

3.3.3 Single cell RNA-sequencing

The single-cell RNA-Sequencing (RNA-Seq) analysis was employed to analyze the transcriptome of NG2 glia and astrocytes in 3-month-old male CTRL and ischemic mice using the Cspg4/tdTomato mouse strain. The preparation of cell suspension followed the standard protocol described above, apart from two modifications. First, transcriptional inhibitor actinomycin D (Sigma-Aldrich, St. Louis, MO, USA) was added into media (30 µM during enzymatic dissociation, 3 µM in follow-up steps) to prevent activation of immediate-early genes (Wu et al., 2017). Second, the final cell suspension was labeled by ACSA-2 antibodies (4°C, 10 min; Miltenyi-Biotec, Germany) to allow for the enrichment of astrocytes (Kantzer et al., 2017). The cells were enriched using flow cytometry (FACS; BD Influx) calibrated to sort tdTomato$^+$, ACSA-2$^+$ and tdTomato$^+$/ACSA-2$^+$ cells. Hoechst 33258 (ThermoFisher Scientific, Waltham, MA, USA) was used to check viability. The cells were collected into 200 µl Advanced Dulbecco's Modified Eagle Medium, supplemented with 10 % of fetal bovine serum (ThermoFisher Scientific Waltham, MA, USA). Three animals per condition were pooled for the preparation of cell suspension. After FACS, cell suspension was spun down, concentrated, and used for library preparation using 10x Chromium Next GEM Single Cell 3′ Reagent Kits v3.1 (10x Genomics; Pleasanton, CA, USA). The prepared libraries were sequenced on NovaSeq 6000 using SP flow cell, 100 cycles (Illumina, San Diego, CA, USA).

Raw sequencing data consisted of 951M reads were de-multiplexed, aligned to the mouse GRCm38 reference genome and unique molecular identifier (UMI)-collapsed using STAR aligner (Dobin et al., 2013). EmptyDrops function from the DropletUtils R package was used to identify cell-containing droplets (Lun et al., 2019), resulting in 1656 cells in the CTRL sample and 2978 cells in the ischemic sample. The mapping statistics showed mean values of 107 495 reads, 8 316 UMIs and 2 882 genes per cell. The total number of genes detected was 23 194. Both samples were combined and normalized using the SCTransform function in Seurat v3 (Stuart et al., 2019). To visualize cell clusters, we generated a uniform manifold

approximation and projection (UMAP) plot using the first 15 principal components and resolution parameter, set to 0.5. Cell clusters were annotated using scCATCH (Shao et al., 2020), as well as using a manual curation based on a referenced database (Zeisel et al., 2018). As we only identified seven NG2 glia in the CTRL sample, we limited our further analysis to just the ischemic dataset. In the ischemic sample, we removed all the other cell types, keeping only the cells that had the characteristics of NG2 glia, astrocytes or both. The resulting expression matrix contained 666 cells, expressing 10635 genes in total; each gene was expressed in at least 5 % of cells. For the final analysis, the matrix was uploaded and analyzed using the updated version of ASAP software (David et al., 2020). Briefly, the cells were quality controlled, excluding 117 cells from the analysis (less than 1000 genes detected and/or more than 20 % of mitochondrial reads). The expression matrix was further reduced to 2249 highly variable genes, and normalized using Seurat implementation. The cells were visualized on a UMAP plot and clustered using the hierarchical clustering method. The Wilcoxon test was employed for differential expression (DE) analysis. Sets of DE genes (FDR<0.05, FC>2) were analyzed using Fisher's exact test against gene ontology collections.

3.3.4 Preparation of acute brain slices

Mice were anesthetized with an intraperitoneal injection of a lethal dose (100 mg/kg) of 1% PTB diluted in saline (Sigma-Aldrich, St. Louis, MO, USA), transcardially perfused with an ice-cold isolation solution, and then decapitated. The brains were dissected and placed into a cold isolation solution (4–8 °C), bubbled with carbogen. Coronal slices (200 μm) were cut using an HM650 V vibratome (MICROM International GmbH, Waldorf, Germany). The brain slices were then incubated for 40 minutes at 34 °C in the isolation solution. After the incubation period, the slices were kept at RT (23–25 °C) in an artificial cerebrospinal fluid (aCSF) containing (in mM): 122 NaCl, 3 KCl, 1.5 CaCl2, 1.3 MgCl2, 1.25 Na2HPO4, 28 NaHCO3, and 10 D-glucose (osmolality 300 mmol/kg).

3.3.5 Patch-clamp technique

Cell membrane currents were recorded *in situ* seven days after FCI, using the patch-clamp technique in the whole-cell configuration. Recording pipettes with a tip resistance of 8–12 MΩ were made from borosilicate capillaries (Sutter Instruments, Novato, CA, USA,) using a P-97 Brown-Flaming micropipette puller (Sutter Instruments, Novato, CA, USA). The recording pipettes were filled with an intracellular solution containing (in mM): 130 KCl,

0.5 $CaCl_2$, 2 $MgCl_2$, 5.0 EGTA, 10 HEPES (pH 7.2). All the recordings were made in aCSF. The solution was continuously gassed with 5% CO_2, to maintain a final pH of 7.4. The electrophysiological data were measured with a 10 kHz sample frequency, using an EPC9 or EPC10 amplifier, controlled by PatchMaster software (HEKA Elektronik, Lambrecht/ Pfalz, Germany), and filtered using a Bessel filter. The slices were transferred to the recording chamber of an upright Axioscop microscope (Zeiss, Gottingen, Germany), equipped with electronic micromanipulators (Luigs & Neumann, Ratingen, Germany) and a high-resolution AxioCam HR digital camera (Zeiss, Gottingen, Germany). The resting membrane potential was measured by switching the EPC9 or EPC10 amplifier to the current-clamp mode. With the use of FitMaster software (HEKA Elektronik, Lambrecht/Pfalz, Germany), input resistance (IR) was calculated from the current value at 40 ms after the onset of the depolarizing 10 mV pulse, from the holding potential of -70 mV to -60 mV. Membrane capacitance (C_m) was determined automatically from the Lock-in protocol by PatchMaster. The current patterns were obtained by hyper- and depolarizing the cell membrane from the holding potential of -70 mV to the values ranging from -160 to +40 mV, at 10 mV intervals. The pulse duration was 50 ms. In order to isolate the delayed outwardly rectifying K^+ (K_{DR}) current components, a voltage step from -70 to -60 mV was used to subtract the time- and voltage-independent currents, as previously described (Anderová et al., 2006, Neprasova et al., 2007). To activate the K_{DR} currents only, the cells were held at -50 mV, and the amplitude of the K_{DR} currents was measured at 40 mV, 40 ms after the onset of the pulse. The inwardly rectifying potassium K^+ (K_{IR}) currents were determined analogously at -140 mV, also 40 ms after the onset of the pulse, while the cells were held at -70 mV. The fast activating and inactivating outwardly rectifying K^+ (K_A) currents were isolated by subtracting the current traces clamped at -110 mV from those clamped at -50 mV, and its amplitude was measured at the peak value. The current densities were calculated by dividing the maximum current amplitudes by the corresponding C_m values for each individual cell.

3.4 Material and methods specific for aim 3:

3.4.1 Magnetic resonance imaging

For measurement of the mouse brains three days after FCI-induced lesion (Fig. 16), animals were scanned on a 4.7 T magnetic resonance scanner (ParaVision 4, Bruker BioSpec) equipped with a home-made surface coil and using 2D Rapid Acquisition with a Relaxation Enhancement multi-spin echo sequence acquiring T2-weighted coronal and axial images.

The basic sequence parameters were: repetition of time = 3300 ms, effective echo time = 36 ms, excitation and refocusing pulses = hermite pulses, number of acquisitions = 4, acquisition time = 5 min 16 s, slice thickness = 0.6 mm, turbo factor = 8 and spatial resolution = 137 × 137 µm. During scanning, the animals were anesthetized with 1.5% Isoflurane mixed with air.

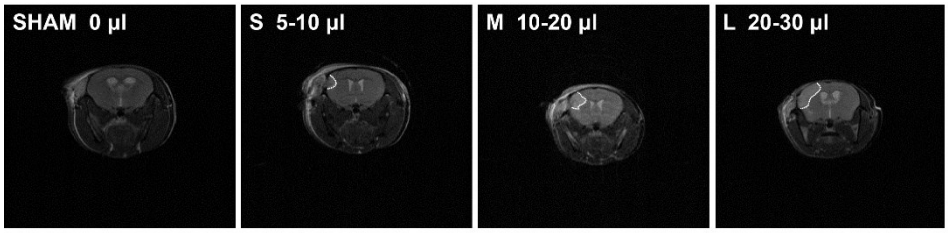

Figure 16: Representative magnetic resonance images of focal cerebral ischemia-induced lesion size. The lesion size classified by experienced operator during sample collection (S – small, M – medium, L – large) (Androvic et al., 2020).

3.4.2 RNA isolation, library preparation and sequencing

Brain tissue samples were homogenized using the TissueLyser (Qiagen). Total RNA was extracted with TRI Reagent (Sigma-Aldrich) according to the manufacturer´s protocol and treated with TURBO DNA-free kit (Thermo Fisher). RNA quantity and purity was assessed using the NanoDrop 2000 spectrophotometer (Thermo Fisher) and RNA integrity was assessed using the Fragment Analyzer (Agilent). All samples had RQN > 8. Libraries were prepared from 400 ng total RNA with QuantSeq 3' Library Prep Kit FWD (Lexogen) according to manufacturer's protocol. 1 µl of ERCC spike-in (c = 0.01x; Thermo Fisher) per library was included. This library preparation method generates stranded libraries predominantly covering the 3' end of the transcript, thus producing gene-centric expression values. Libraries were quantified on the Qubit 2 fluorometer (Thermo Fisher) and Fragment Analyzer (Agilent) and sequenced on the NextSeq 500 high-output (Illumina) with 85 bp single-end reads. 11.5 – 38 million reads were obtained per library with a median of 16 million reads.

3.4.3 RNA-Seq data processing, mapping and counting

Adaptor sequences and low quality reads were removed using TrimmomaticSE v0.36 (Bolger et al., 2014). Reads mapping to mtDNA and rRNA were filtered out using SortMeRNA v2.1 with default parameters (Kopylova et al., 2012). The remaining reads were aligned to GRCm38 and ERCC reference using STAR v2.5.2b with default parameters (Dobin et al., 2013). Mapped reads were counted over Gencode vM8 gene annotation using htseq-count with union mode for handling of overlapping reads (Anders et al., 2015).

3.4.4 Differential expression (DE) analysis

Several comparisons of DE were generated using DESeq2 v1.16.1(Love et al., 2014). For pairwise comparisons, we compared aged CTRL to young CTRL, young stroke group to young CTRLs, aged stroke group to aged CTRLs and aged stroke group to young stroke group ($p_{adj} < 0.05$, $\log_2FC > 1$ for upregulation and < -0.65 for downregulation). We also generated two-factor comparisons using injury (CTRL/MCAO=FCI) and age (3-month-old/18-month-old) and their interaction as predictor variables. During the initial analysis of the dataset, we noted that there was a relatively large number of genes induced or repressed exclusively, or with a greater fold-change in aged animals, although only a subset of them reached statistically significant interaction term as outputted by DESeq2 analysis. In order to identify all of the genes that are likely subject to age-stroke interaction, we have prepared four additional sets of genes with age-dependent differential response to stroke containing genes that are significantly influenced by stroke in one age group and at the same time their fold-change (vs CTRL) is at least doubled compared to second age group. That is, the set "more up MCAO18" is comprised of genes significantly upregulated in aged animals after stroke (compared to aged CTRLs; $p_{adj} < 0.01$, $\log_2FC_{aged} > 1$), and at the same time having significant interaction term ($p_{adj} < 0.1$) and/or having at least double the fold change of young strokes (compared to young CTRLs; $\log_2FC_{aged} - \log_2FC_{young} > 1$). The same rationale was applied for more highly upregulated genes in the young stroke group ("more up MCAO3") and for downregulated genes in both age groups ("more down MCAO18", "more down MCAO3"), with an exception that the $\log_2FC$ threshold was < -0.65 for downregulation. Only genes with average expression ≥ 5 normalized counts in at least one experimental condition were considered for further analysis.

3.4.5 Gene set enrichment analysis (GSEA)

GSEA (Subramanian et al., 2005) was performed for pairwise DE comparisons. First, a gene score was calculated for every gene using DESeq2 output as $-\log_{10}(p_{adj})$ and assigned a positive or negative sign based on direction of regulation. Genes were ranked by their gene-scores and GSEA was run in a weighted pre-ranked mode with 1000 permutations. Gene sets were downloaded from http://download.baderlab.org/EM_Genesets/, and GSEA was run separately for two gene ontology (GO) categories (biological process – GOBP, cellular component – GOCC). Only gene sets containing between 15 and 1000 (for GOBP) or 5 to 1000 (for GOCC) genes were considered. Annotations with IEA (inferred from electronic

annotation) evidence codes were excluded. For pathway enrichment, a gene set file integrating several pathway databases was used. Significantly overrepresented gene sets were visualized as a network using Enrichment Map (Merico et al., 2010). In the network, each node represents gene set and highly overlapping gene sets are connected with edges, resulting in a tight clustering of highly redundant gene sets. For functional annotation of discrete sets of genes we used Cytoscape plugin ClueGO(Bindea et al., 2009) with the following parameters: no IEA codes, right-sided hypergeometric test with Benjamini-Hochberg correction for statistical testing and all genes after filtering (16048 genes) as the background set.

3.4.6 Cell-specific gene sets and cell type proportion estimation

Marker genes for major cell types specifically in the mouse CTX region were taken as an initial reference (Mancarci et al., 2017). Unlike other marker databases that rely on a single data source, this marker set represents a consensus from several published studies and accounts for brain regional heterogeneity. The microglial marker genes in the reference marker set were already devoid of genes differentially expressed in activated microglia (Holtman et al., 2015). In order to acquire marker genes with stable expression regardless of activation states, we have further removed the genes previously found to be differentially expressed in microglia after transient MCAO (Arumugam et al., 2017); in aged cortical microglia (Grabert et al., 2016), and aged whole-brain microglia (Holtman et al., 2015) compared to young microglia; and genes enriched in bone marrow-derived macrophages compared to microglia (Bruttger et al., 2015). We have also removed genes that were differentially expressed in astrocytes after transient MCAO (Zamanian et al., 2012) and aged cortical astrocytes (Boisvert et al., 2018, Clarke et al., 2018). Because peripheral immune cells may infiltrate the brain following stroke, we have also excluded genes enriched in the major leukocyte populations obtained from ImmGen database (www.immgen.org).

DESeq2-normalized gene expression data and the cell-specific gene lists were used as an input into the *markerGeneProfile* R package v1.0.3 (Mancarci et al., 2017) for the estimation of marker gene profiles (MGPs), which serve as a proxy for relative cell type proportion changes. We used a more stringent expression cutoff (average ≥ 5 normalized counts across all samples) to reduce the transcriptional noise. Since it still may be possible that some marker genes are transcriptionally regulated under our experimental conditions, genes with reduced correlation (potentially regulated) to the majority of marker genes (assumed to reflect primarily cell type proportion change) were excluded from final estimates as

described in (Mancarci et al., 2017). Resulting MGP estimates were flagged if a high proportion of marker genes was removed in the previous step (> 40 %) and/or proportion of variance explained by the first principal component was low (< 50 %). Differences in expression of final marker gene sets were analyzed by linear mixed model in R project v3.6.0 using *lmerTest* package v3.1 (Kuznetsova et al., 2017) on $\log_2$ transformed, DESeq2-normalized expression values. We used two-factor design (age, injury) with interaction as fixed effects and gene intercept as random effect. Significance was tested by Satterthwaite's method. Post-hoc t-tests were performed using *emmeans* package v1.3.5 and p-values were adjusted by Holm method.

To validate the first estimations, we employed CIBERSORT, a transcriptome deconvolution algorithm that uses gene expression matrix of individual cell types as a reference, and deconvolutes the cellular composition of mixed sample by linear support vector regression (Newman et al., 2015). We used published single-cell RNA-Seq dataset of adult mouse CTX as a reference gene expression signature (Tasic et al., 2016). From the normalized gene-expression matrix, we excluded all intermediate cells as defined by authors and used the remaining 1424 core cells assigned to the major CNS cell types. CIBERSORT was run in the relative mode with 1000 permutations, quantile normalization was disabled as recommended for RNA-Seq data and q-value cutoff was lowered to 0.15. The results were correlated to the corresponding cellular MGPs.

3.4.7 Protein-protein interaction network

Known interactions (minimal interaction score 0.4) between genes in the “more up MCAO18” DE gene set were downloaded from STRING database v10.5 (Szklarczyk et al., 2015). Remaining unconnected genes from “more up MCAO18” gene set were then added to the network based on their correlation with any of the genes already present in the network requiring Pearson $r \geq 0.96$. The resulting interaction network was then visualized and analyzed in Cytoscape v3.5.1. Spectral partition-based network clustering algorithm (Newman, 2006) via Cytoscape ReactomeFI plugin v6.1.0 (Wu et al., 2010) was used for network clustering.

3.4.8 Custom gene set enrichment

Gene sets of interest were collected directly from relevant publications. R package *GeneOverlap* v1.20 was used to calculate the odds ratio (OR) and the significance of the overlap of the gene sets of interest with the Fisher’s exact test.

3.4.9 High-throughput RT-qPCR

Samples were reverse transcribed in a reaction volume of 10 µl containing: 5 µl template (either 125 ng total tissue RNA or 100 sorted cells after direct lysis), 0.5 µl spike-in RNA (Tataa Biocenter; c = 0.1x for tissues or 0.01x for sorted cells), 0.5 µl equimolar mixture of random hexamers with oligo(dT) (c = 50 µM), 0.5 µl dNTPs (c = 10 mM), 2 µl 5× RT buffer, 0.5 µl RNaseOUT, 0.5 µl Maxima H- Reverse Transcriptase (all Thermo Fisher) and 0.5 µl nuclease-free water. After the pre-incubation step at 65°C (t = 5 min), followed by the immediate cooling on ice, the main incubation was performed at 25°C (t = 10 min), 50°C (t = 30 min), 85°C (t = 5 min), after which the samples were immediately cooled on ice. cDNA from tissue samples was diluted 4x in nuclease-free water; sorted cell-cDNA was left undiluted. All cDNA samples were pre-amplified immediately after reverse transcription in 40 µl total reaction volume containing 4 µl cDNA, 20 µl IQ Supermix buffer (Bio-Rad), 4 µl primer mix of 96 assays (c = 250 nM each), and 12 µl of nuclease-free water. Reactions were incubated at 95°C (t = 3 min) following by 18 cycles of 95°C (t = 20 s), 57°C (t = 4 min) and 72°C (t = 20 s). After thermal cycling, reactions were immediately cooled on ice and diluted in nuclease-free water (sorted cells 4x, tissue 50x). High-throughput qPCR was then performed on a 96.96 microfluidic platform BioMark (Fluidigm. Cycling program consisted of activation at 95°C (t = 3 min), followed by 40 cycles of 95°C (t = 5 s), 60°C (t = 15 s) and 72°C (t = 20 s) and melting curve analysis. The same protocol, excluding the pre-amplification step and using CFX384 instrument (Bio-rad), was applied to evaluate the impact of sham surgery on gene expression of FCI-responsive genes.

3.4.10 RT-qPCR data analysis

Raw data were pre-processed with the Real-Time PCR analysis software v4.1.3 (Fluidigm); unspecific values were deleted based on melting-curve analysis. Further processing was done in GenEx v6.0.1 (MultiD Analyses AB): Cq value cutoff of 28 was applied; gDNA background was substracted using ValidPrime (Laurell et al., 2012) (Tataa Biocenter); data were normalized to the mean expression of 5 reference genes (*Actb, Gapdh, Ppia, Ywhaz, Tubb5*); outliers were deleted (within group Grubbs test, $p < 0.05$) and a gene was considered undetected for given group if more than 75 % values per group were missing; technical replicates (RT and FACS) were averaged; if appropriate, missing data were inputed on a within-group basis and remaining missing data were replaced with Cq_{max} +2 for tissue samples or Cq_{max}+0.5 for sorted cells. Of note, the RT-qPCR and RNA-Seq data showed high correlation (Pearson $r \geq 0.942$).

Temporal expression of individual genes was first analyzed with two-way ANOVA in R project v3.6.0 using time-point and age as predictor variables, then differences between time-points were tested separately for each age by one-way ANOVA and post-hoc t-tests using *emmeans* package v1.3.5. P-values were adjusted with Benjamini-Hochberg method. Temporal expression of groups of cellular marker genes was first analyzed using linear mixed model in R project v3.6.0 (*lmerTest* package v3.1) (Kuznetsova et al., 2017) with random gene intercept using two-factor design (time-point including CTRL, age) with interaction, then differences between time-points were tested separately for each age. Significance was tested by Satterthwaite's method. Post-hoc pairwise t-tests were performed using *emmeans* package v1.3.5 and p-values were adjusted by Holm method. Temporal expression of type I interferon (IFN-I) pathway was analyzed in similar steps using random slope and random intercept mixed model with 23 interferon-stimulated genes (ISG) as response variables. IFN-I pathway expression in sorted cells was analyzed in the same way with two-factor design (age, injury) with interaction, using only detected ISGs per each cell type. Differential expression of individual genes (relative to age-matched CTRL) in sorted cells was tested in GenEx v6.0.1 (MultiD Analyses AB) using ANOVA with Bonferroni's post-hoc test for selected pairwise comparisons and p-values were corrected using Benjamini-Hochberg method.

3.4.11 Western blot analysis (WB)

Proteins were isolated using RIPA extraction procedure with addition of protease and phosphatase inhibitors (Thermo Fisher) and concentration determined by bicinchoninic acid protein assay kit (Thermo Fisher). 70 µg of protein was separated on 8 % and 12.5 % polyacrylamide gel and transferred to nitrocellulose membrane. Primary antibodies used (all from Cell Signaling Technology) were specific for STAT1 (1:1000), phosphorylated STAT1 (Tyr701) (1:1000), IRF-9 (1:1000) or ISG15 (1:200). Protein detection was performed using secondary antibodies specific for Anti-Rabbit IgG (whole molecule)–Peroxidase (Sigma-Aldrich, 1:10000). Membrane Fraction WB Cocktail (Abcam, 1:250 for primary antibodies and 1:2500 for secondary antibodies) was used for the normalization. Clarity Western ECL Substrate (Bio-Rad) or SuperSignal West Femto Maximum Sensitivity Substrate (Thermo Fisher) were applied on the nitrocellulose membrane to detect the chemiluminescent signal. The signal was quantified using ImageJ software. Images were preprocessed using the Subtract Background function. The density of the bands was normalized to the density of

the bands for the Membrane Fraction WB Cocktail by using the profile plot of each lane. The area under the curve was used to calculate the relative amount of the protein.

3.4.12 Liquid chromatography (LC)–mass spectrometry (MS) sample preparation

Tissues were homogenised and lysed by boiling at 95°C for 10 min in 100 mM TEAB containing 2 % SDC, 40 mM chloroacetamide, 10 mM TCEP and further sonicated (Bandelin Sonoplus Mini 20, MS 1.5). Protein concentration was determined using BCA protein assay kit (Thermo Fisher) and 30 µg of protein per sample was used for MS sample preparation. Samples were further processed using SP3 beads according to (Hughes et al., 2019). Briefly, 5 µl of SP3 beads was added to 30 µg of protein in lysis buffer and filled to 50 µl with 100 mM TEAB. Protein binding was induced by addition of ethanol to 60 % (vol./vol.) final concentration. Samples were mixed and incubated for 5 min at room temperature. After binding, the tubes were placed into magnetic rack and the unbound superntatant was discarded. Beads were subsequently washed two times with 180 µl of 80% ethanol. After washing, samples were digested with trypsine (trypsin/protein ration 1/30) reconstituted in 100 mM TEAB at 37°C overnight. After digestion samples were acidified with TFA to 1% final concentration and peptides were desalted using in-house made stage tips packed with C18 disks (Empore) according to (Rappsilber et al., 2007).

3.4.13 MS data analysis

All data were analyzed and quantified with the MaxQuant software (version 1.6.3.4)(Cox and Mann, 2008). The false discovery rate (FDR) was set to 1 % for both proteins and peptides and we specified a minimum peptide length of seven amino acids. The Andromeda search engine was used for the MS/MS spectra search against the *Mus musculus* dabase (downloaded from Uniprot on July 2019, containing 22 267 entries). Enzyme specificity was set as C-terminal to Arg and Lys, also allowing cleavage at proline bonds and a maximum of two missed cleavages. Dithiomethylation of cysteine was selected as fixed modification and N-terminal protein acetylation and methionine oxidation as variable modifications. The "match between runs" feature of MaxQuant was used to transfer identifications to other LC-MS/MS runs based on their masses and retention time (maximum deviation 0.7 min) and this was also used in quantification experiments. Quantifications were performed with the label-free algorithm in MaxQuant (Cox and Mann, 2008). Data analysis was performed using Perseus 1.6.1.3 software (Tyanova et al., 2016) and R project v3.6.0. Identifications mapping to more than one protein ID were discarded. Remaining identifications were

mapped to gene names based on their ID using Uniprot database and only uniquely mapping genes were kept for further analysis. Matrix was then further filtered to remove genes with less than 7 positive values and remaining missing data were imputed according to Wei et al., 2018.

4 RESULTS

4.1 Proliferation and differentiation potential of NG2 glia following FCI

To disclose the changes in the expression profiles of NG2 glia and those derived from NG2 glia after FCI we analyzed their mRNA transcripts of 93 genes using single-cell RT-qPCR. We used Cspg4/tdTomato transgenic mice expressing TX-inducible cre recombinase under the control of the Cspg4 promoter, which triggers the expression of red fluorescent protein tdTomato in NG2 glia. TdTomato$^+$ cells were isolated from uninjured and post-ischemic CTX 3, 7 and 14 days after FCI (Fig. 17A). To further verify our observations, we used immunohistochemistry to detect proteins and proliferation via cumulative EdU labeling in fixed brain slices.

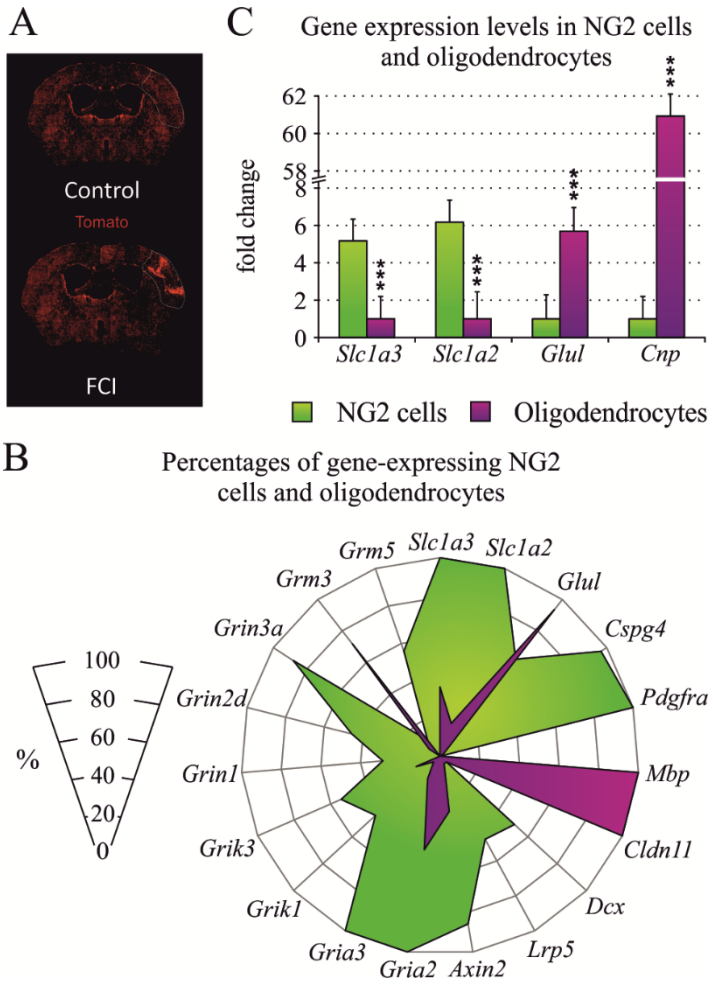

Figure 17: (A) Scheme depicting tdTomato$^+$ cells distribution and the brain regions (dashed lines), which were used for tdTomato$^+$ cells isolations. Note that ischemic lesion is bordered by a high density of tdTomato$^+$ cells. (B, C) NG2 glia and oligodendrocytes isolated from uninjured mice differ in: percentage of cells expressing several genes (B) and levels of expression of several genes (C). Statistics were calculated using t-test. ***, $p < 0.001$. In the case of B, only statistically significant differences with $p < 0.05$ are showed.

4.1.1 tdTomato$^+$ cells expression pattern in uninjured cortex

Using PCA we identified three populations of tdTomato$^+$ cells in the uninjured CTX (Fig. 18). First small population of tdTomato$^+$ cells was characterized by the strong expression of *Pdgfrb*, the well-known marker of pericytes (Zehendner et al., 2015). Since we focused only on NG2 glia and their progeny in this study (e.g. oligodendroglial lineage cells), *Pdgfrb*$^+$ pericytes were excluded from further analyses. The second and third populations of tdTomato$^+$ cells were identified as oligodendrocytes (n = 46 cells/8 mice) and NG2 glia (n = 21 cells/6 mice) based on DE of respective cell-type specific *markers Mbp, Cldn11, Glul, Cspg4,* and *Pdgfra* (Fig.17B, Fig. 18).

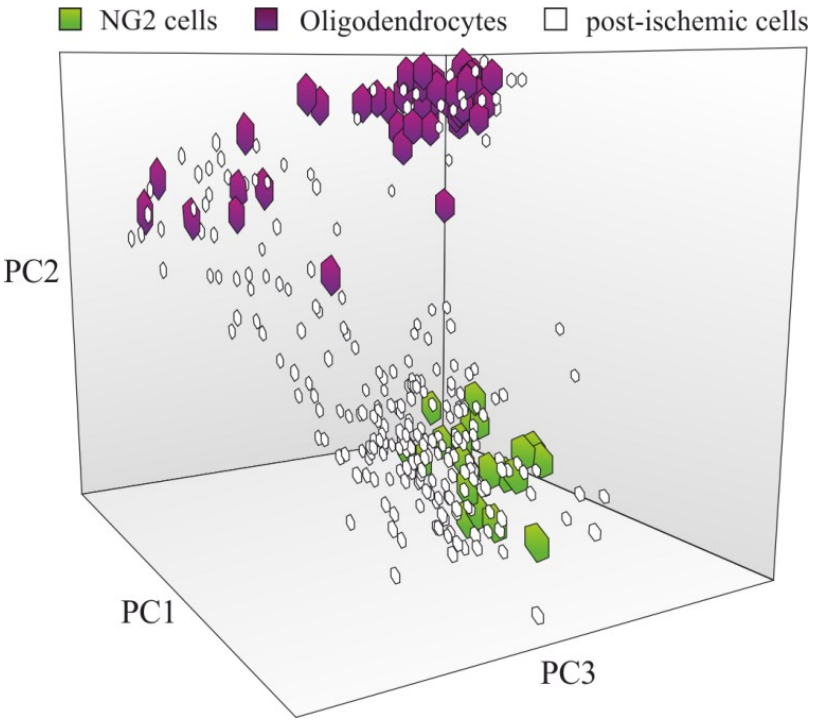

Figure 18: PCA showing two well-separated clusters of tdTomato$^+$ oligodendroglial lineage cells from uninjured cortex, identified as NG2 glia and oligodendrocytes.

Besides the marker genes, we detected DE of *Slc1a2* and *Slc1a3* in NG2 glia, encoding glial glutamate transporter (GLT) and glutamate-aspartate transporter (GLAST), that are generally considered as astroglial markers (Jungblut et al., 2012, Azami Tameh et al., 2013). Moreover, we detected DE of genes encoding metabotropic glutamate receptors (mGlur) 3 and 5, *Grm3* and *Grm5,* between NG2 glia and oligodendrocytes. Whereas *Grm3* was expressed by 10.9 ± 3.7 % of NG2 glia and 71.8 ± 10.7 % of oligodendrocytes, *Grm5* was detected in 55.9 ± 9.9 % of NG2 glia and no oligodendrocyte expressed mRNA encoding this gene (Fig. 17B).

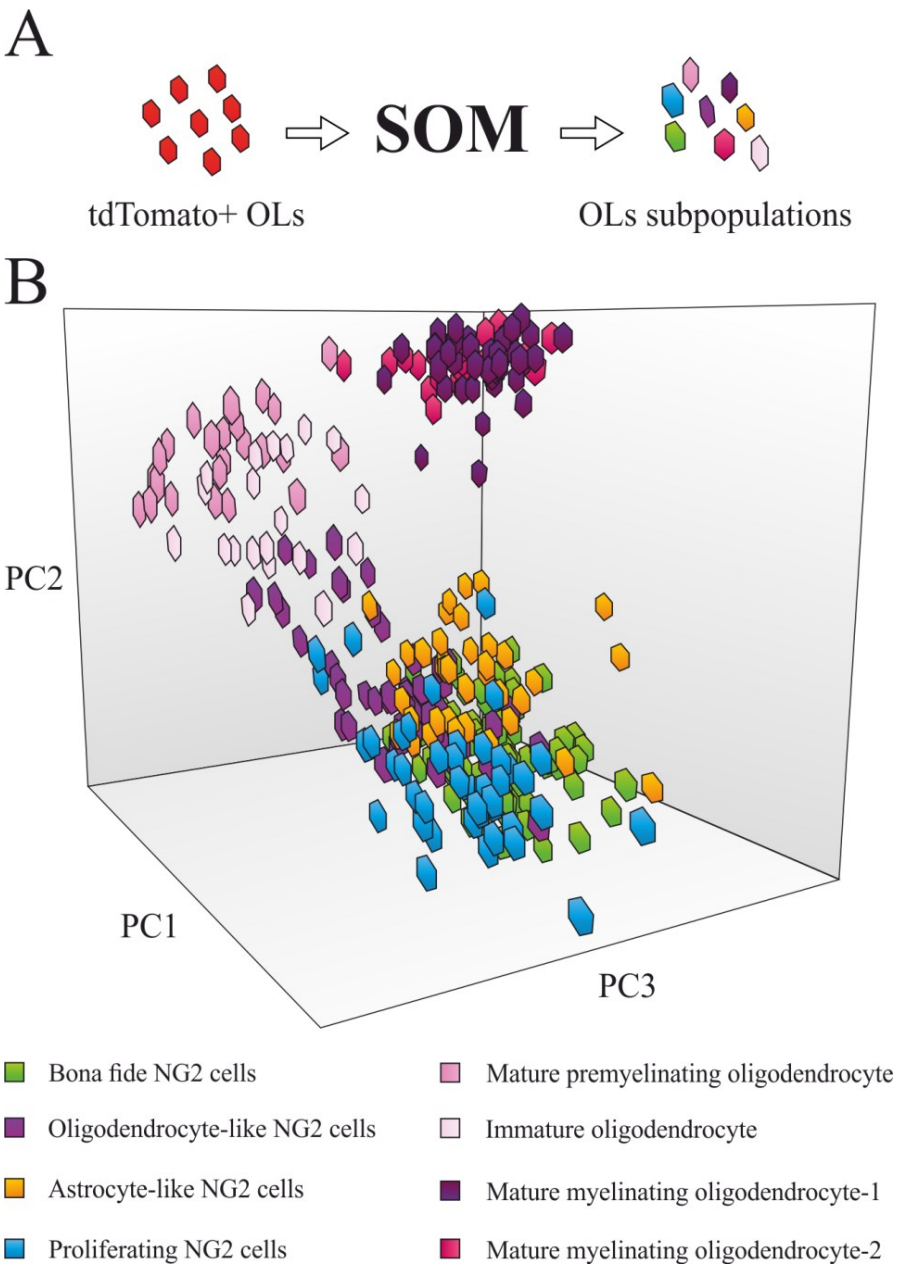

Figure 19: (A) Scheme depicting principle of SOM analysis. (B) PCA showing distribution of SOM-defined subpopulations of oligodendroglial lineage cells. Note the gradual transition from Bona fide NG2 glia through Oligodendrocyte-like NG2 to glia immature and mature stages of oligodendrocytes. SOM, self-organizing Kohonen maps; PCA, principal component analysis.

4.1.2 Multipotency of NG2 glia contributes to glial scar formation

After FCI, NG2 glia (n = 199 cells/8 mice) and oligodendroglial (n = 62 cells/8 mice) clusters became less well separated in PCA (Fig. 19); however, we were still able to distinguish between NG2 glia- and oligodendroglial population based on the cell-type specific markers enrichment.

Following ischemia, beside the NG2 glia from uninjured animals (Bona fide NG2 glia; BF-NG2 cells) we identified three other NG2 glia subpopulations (Fig. 20, 21). The first

subpopulation characterized by a high percentage of cells expressing oligodendrocyte marker genes, such as *Mbp* (42.3 ± 9.5 %), *Cldn11* (84.6 ± 6.3 %) and Tcf7l2 (94.2 ± 4.9 %) and the Wnt signaling effectors critical for oligodendrocyte maturation (Guo et al., 2015), was termed oligodendrocyte-like NG2 glia (OL-NG2 cells)(Fig. 20). This subpopulation had an increased level of expression of *Cldn11* and *Cnp* and a decreased expression of *Pdgfra* compared to BF-NG2 cells, which further confirms shift of OL-NG2 cells (Fig. 21A). Moreover, 38.5 ± 7.2 % of OL-NG2 cells started to express transient receptor potential cation channel subfamily V member 4 (*Trpv4*) (Fig. 20), which was shown to be expressed by committed oligodendrocyte precursors (Marques et al., 2016).

The second subpopulation, astrocyte-like NG2 glia (A-NG2 cells), was characterized by the highest number of cells expressing astroglial markers, such as *Gfap* (43.2 ± 6.0 %) and *Aqp4* (51.6 ± 9.9 %) (Fig. 20) and had also the highest *Gfap* expression level among all NG2 glia subpopulations (Fig. 21A). On the contrary, only 9.5 ± 5.7 % A-NG2 cell expressed *Mbp* (Fig. 20) and the expression levels of *Cnp* and *Cldn11* were significantly lower compared to OL-NG2 cells (Fig. 21A).

Both subpopulations (OL-NG2 cells, A-NG2 cells) downregulated expression of *Pdgfra* (Fig. 21A) and displayed a lower incidence of cells expressing *Grm5* (50.0 ± 3.5 % of OL-NG2 cells; 30.5 ± 6.8 % of A-NG2 cells) (Fig. 20), which is not expressed by oligodendrocytes (Fig. 21B) neither by astrocytes (Sun et al., 2013). The last subpopulation of ischemic NG2 glia was characterized by the highest percentage of cells expressing proliferation marker *Mki67* (84.1 ± 8.3 %) and marker of newly derived cells Nestin (*Nes*) (86.4 ± 8.7 %) (Fig. 20)(Anderova et al., 2011, Honsa et al., 2012). We named this subpopulation as proliferating NG2 glia (P-NG2 cells), also because of the highest expression level of another proliferation marker *Pcna* (Fig. 21A). P-NG2 glia had the highest expression of *Nes* and vimentin (*Vim)* (Fig. 21A), which is intermediate filament characteristic for reactive glia. Sonic Hedgehog (*Shh*) receptors PATCHED 1 and SMOOTHENED, encoded by *Ptch1* and *Smo* genes, had the significantly highest incidence in P-NG2 cells (*Ptch1*, 81.8 ± 10.3 %; *Smo*, 40.9 ± 4.0 %) when compared to all other NG2 glia subpopulations (Fig. 20). Apart from *Grm5*, we observed DE of other metabotropic glutamate receptors subunits such as *Grm7*, encoding mGlur7, among NG2 glial subpopulation (Fig. 20). Finally, the number of cells, which expressed ionotropic NMDA receptors subunits *Grin1* and *Grin2d,* was decreased in all ischemic subpopulations when compared to BF-NG2 cells (Fig. 20).

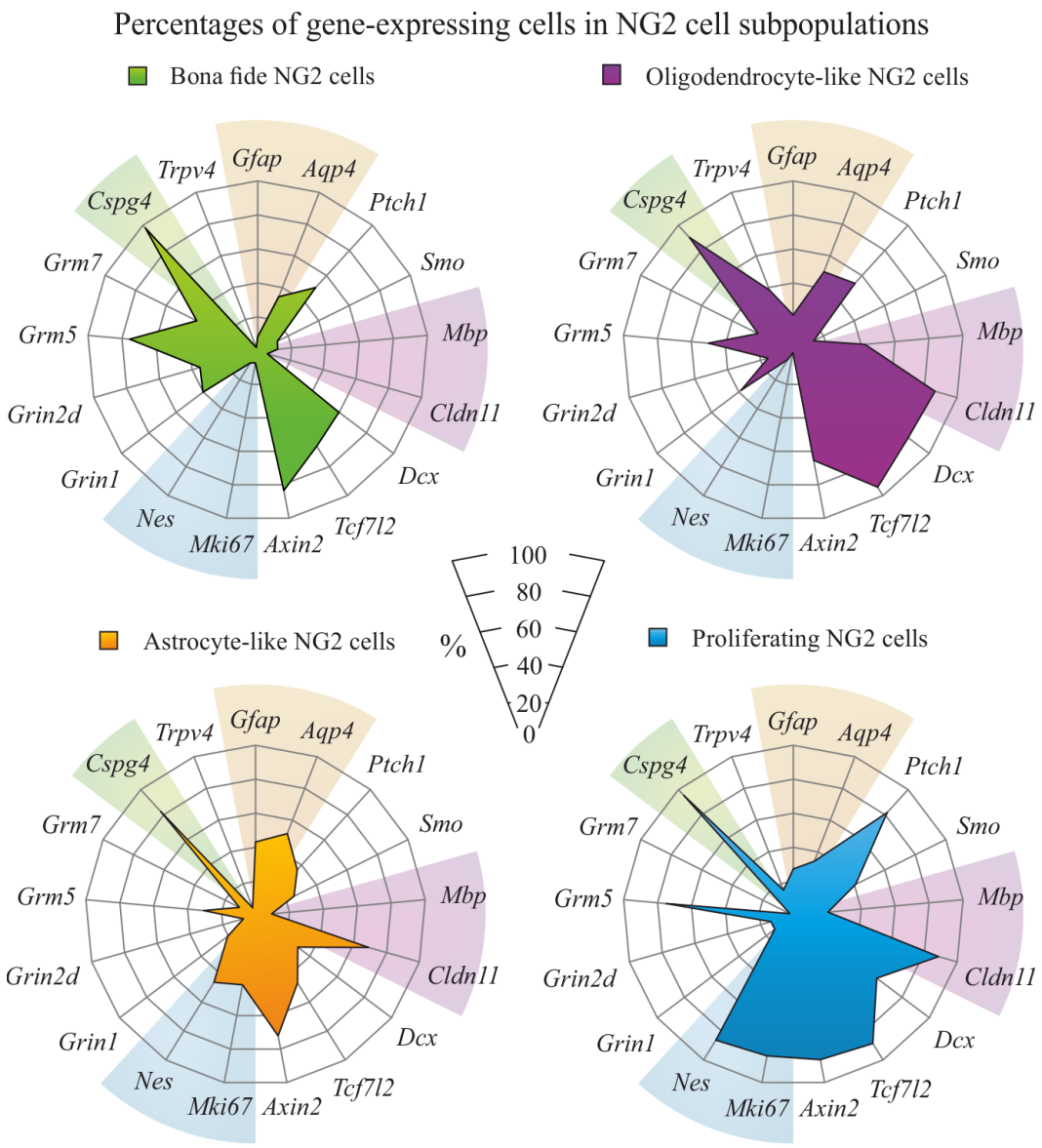

Figure 20: Four NG2 glia subpopulations were identified after FCI using SOM analysis. Subpopulations differ in percentage of cells expressing several genes; only genes, expression of which was changed significantly ($p < 0.05$) are depicted; the background colors indicate genes characteristic for particular subpopulation; statistics were calculated using two-way ANOVA test comparing each subpopulation with every other.

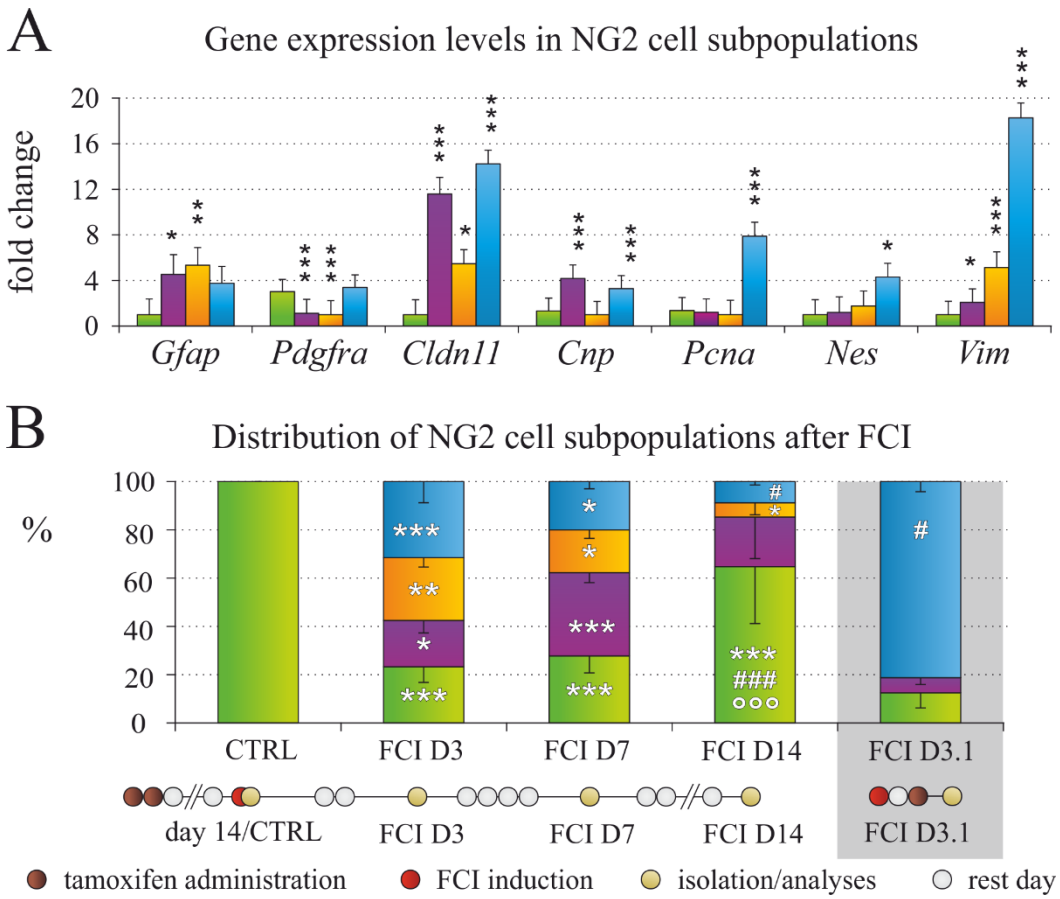

Figure 21: Four NG2 glia subpopulations were identified after FCI using SOM analysis. Subpopulations differ in (A) levels of expression of several genes (significances are expressed relative to "Bona fide NG2 glia" subpopulation). (B) Oligodendrocyte-, astrocyte-like and proliferating NG2 glia subpopulations emerged after FCI and are distributed unequally within the period of 14 days after FCI. The scheme of tamoxifen administration is depicted under the graph. In case of **A** statistics were calculated using one-way ANOVA test relative to "Bona fide NG2 glia" group . In case of **C** statistics were calculated using two-way ANOVA with Bonferroni post-test comparing incidences of particular subpopulation among time-points and t-test to compare distribution of subpopulations between same time-points when different tamoxifen administration scheme was used; asterisks show significances compared to control (CTRL) group, hashtags show significances relative to FCI D3 group and circles show significances relative to FCI D7 group. *, #, $p < 0.05$; **,##, $p < 0.01$; ***, ###, °°° $p < 0.001$. FCI, focal cerebral ischemia; SOM, self-organizing Kohonen maps

While NG2 glia isolated from uninjured mice were classified as BF-NG2 cells, all NG2 glia subpopulations were distributed unequally following ischemia (Fig. 21B). The maximal changes were observed three and seven days after FCI. The highest incidences of P- and A-NG2 cells were observed three days after FCI, unlike the OL-NG2, which culminated at day 7 after FCI. At day 14 after FCI the distribution of NG2 glial subpopulations became similar to that observed in CTRL (Fig. 21B). When we postponed TX administration two days after FCI induction and analyzed oligodendrocytes at day 3 after FCI (post-ischemic TX scheme) the distribution of NG2 glial subpopulations was significantly different compared to that

with TX administration prior to FCI (Fig. 21B). The incidence of P-NG2 cells was significantly increased, while A-NG2 cells completely disappeared. This result suggests that P-NG2 cells retain, to some extent, the phenotype of BF-NG2 cells, which was confirmed by no difference in *Pdgfra* expression levels between P-NG2- and BF-NG2 cells (Fig. 21A).

4.1.3 Astrocyte-like NG2 glia are derived directly from NG2 glia

To further verify the differences between NG2 glia subpopulations, we double-stained brains seven days after FCI against specific markers such as GFAP (reactive astrocytes), Ki67 (proliferating cells) and CC1 (also called APC), the cell-body marker of oligodendrocytes (Fig. 22A, B, C). We detected the expression of markers in oligodendrocytes at the ischemic border. The little overlap of signals from each marker confirmed the heterogeneity of reactive oligodendrocytes. It is known that oligodendrocytes are generated by direct differentiation of NG2 glia, however asymmetric division of NG2 glia also exists in the adult brain (Hughes et al., 2013, Boda et al., 2015). To shed some light into the origin of A-NG2 cells we utilized cumulative EdU labeling (Fig. 22D, E). We found that 73.1 ± 4.9 % of $GFAP^+$/$tdTomato^+$ stain positively for EdU. This suggests that 26.9 ± 4.9 % of EdU^-/$tdTomato^+$/$GFAP^+$ A-NG2 cells probably differentiated directly from NG2 glia. However, we also observed only EdU^+/$tdTomato^+$ pairs of recently divided sister cells (classified according to (Boda et al., 2015), of which some expressed GFAP symmetrically (Fig. 22E) and some asymmetrically (Fig. 22D). This suggests that A-NG2 cells might be generated also by asymmetric division of NG2 glia and that subpopulation of A-NG2 cells retain the ability to proliferate as documented also by expression of *Mki67* in 41.6 ± 10.0 % of A-NG2 cells (Fig. 20). Collectively, these results confirmed that FCI induces the multipotency of NG2 glia, which give rise, beside oligodendrocytes, also to a population of reactive astrocytes.

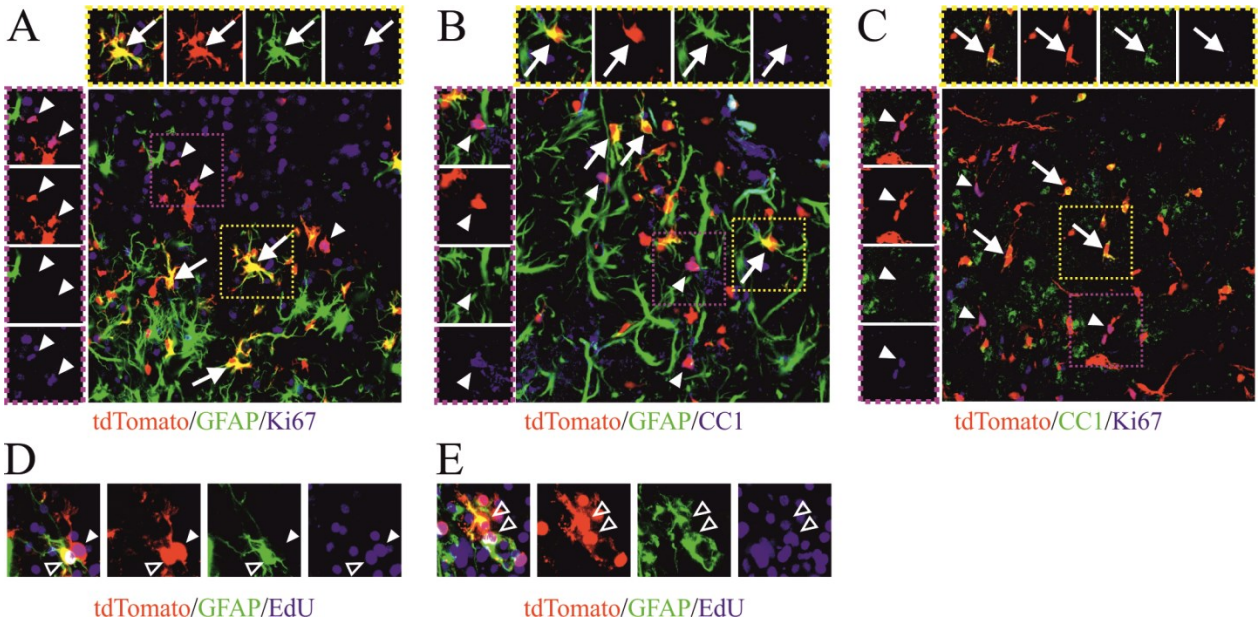

Figure 22: Representative images depicting the heterogeneity of NG2 glia seven days after FCI at the ischemic border. (A) Image showing tdTomato$^+$ NG2 glia expressing astroglial marker GFAP and marker of proliferating cells Ki67. (B) Image showing tdTomato$^+$ NG2 glia expressing astroglial marker GFAP and oligodendroglial marker CC1 (APC). (C) Image showing tdTomato$^+$ NG2 glia expressing oligodendroglial marker CC1 and marker of proliferating cells Ki67. (D) Image showing asymmetric division of tdTomato$^+$/Edu$^+$ cells giving rise to one GFAP$^+$/tdTomato$^+$/EdU$^+$ and one GFAP$^-$/tdTomato$^+$/Edu$^+$. (E) Image showing symmetric division of two GFAP$^+$/tdTomato+/EdU$^+$ cells. (A-C) arrows indicate the colocalization of green and red signal; arrowheads indicate the colocalization of red and blue channels. (D, E) Full arrowheads indicate GFAP$^-$/tdTomato$^+$/EdU$^+$ cells; empty arrowheads indicate GFAP$^+$/tdTomato$^+$/EdU$^+$ cells.

4.2 Appearance of NG2 glia-derived astrocytes between different types of CNS disorders

Since we detected NG2 glia-derived astrocytes following FCI, the next question was whether this subpopulation also appears in other types of brain disorders such as SW or DEMY. We performed single-cell RT-qPCR, in which we analyzed the expression of 95 genes. To achieve this, we used Cspg4/tdTomato mice, in which the TX-application triggers the expression of the red fluorescent protein in NG2 glia and the cells derived therefrom (Fig. 14A). In all experiments, we administrated the TX 14 days before the analysis/disorder induction in the 3-month-old mice (Fig. 14C). In order to disclose changes in the gene expression of NG2 glia in glial scar formation (Wanner et al., 2013) and remyelination (Skripuletz et al., 2011), we isolated two different regions of the brain (CC and CTX) from the CTRLs and mice seven days after the induction of FCI/SW or withdrawal of the CPZ diet (DEMY) (Fig. 15).

4.2.1 NG2 glia and oligodendrocytes in the uninjured brain

Primarily, we sorted all the cells based on their marker genes as NG2 glia (*Cspg4, Pdgfrα*) (n=75 cells/10 mice) and oligodendrocytes, derived from the NG2 glia (*Mbp, Cldn11*) (n=80 cells/11 mice) (Fig. 23A) Despite the fact that these cells were isolated from different regions of the brain (CTX, CC) they displayed a similar expression pattern within the populations. Besides the well-known cell-type-specific genes of NG2 glia and oligodendrocytes, we detected a high percentage (92.0±2.5 %) of oligodendrocytes that expressed the gene for glutamine synthetase (GS, *Glul* gene) (Fig. 23A). Even though this gene is considered as a marker for astrocytes our data are in accordance with the latest findings, confirming that oligodendrocytes express both mRNA for GS as well as the protein (Xin et al., 2019, Zhang et al., 2014, Marques et al., 2016). The metabolic coupling between oligodendrocytes and axons has been generally accepted (Simons and Nave, 2015, Saab et al., 2016), but it has now been shown, from the studies of oligodendrocyte-GS knock-outs, that oligodendrocytes do not require GS for survival and myelination; however the loss of oligodendrocyte GS disrupts neuronal glutamate signaling and glutamate-dependent behavior (Xin et al., 2019). Recently, glutamate signaling has been shown to play a role in the regulation of oligodendrocyte maturation and differentiation (Suárez-Pozos et al., 2020). Further genes previously considered as astrocytic markers - *Slc1a2* and *Slc1a3*, were also detected in NG2 glia (75.0±6.8 % and 73.5±9.8 %; Fig. 23A) which accords well with the previous findings (DeSilva et al., 2009), supporting a developmentally regulated expression pattern of *Slc1a2* and *Slc1a3*. Their highest expressions were found in the earlier stages of oligodendrocytes development, prior to robust myelination (DeSilva et al., 2009, Zhang et al., 2014, Marques et al., 2016, Chamling et al., 2020). Martinez-Lozada et al. suggested that the activation of Na^+-dependent glutamate transporters (*Slc1a2*, *Slc1a3)* promotes a transient increase in intracellular Ca^{2+} levels, which leads to changes in the actin-cytoskeleton and leads to oligodendrocyte maturation (Martinez-Lozada et al., 2014). In line with other studies, we hardly observed any oligodendrocytes (3.4±0.9 %) expressing doublecortin (*Dcx),* while its expression was detected in NG2 glia (33.8±6.5 %; Fig. 23A). This indicates that *Dcx* is not only associated with the immature neuronal phenotype and our findings are in agreement with those of Boulanger et al., who found that almost all OPCs express *Dcx* but also the levels of expression appear to be much lower than those found in the neural precursor. *Dcx* is downregulated when NG2 glia start expressing mature oligodendrocyte markers, and is absent in myelinating oligodendrocytes. Their study also proposed that *Dcx* could either be involved in cell migration, or that it may represent another marker of progenitor cells, which

also accords well with our previous studies (Tamura et al., 2007, Zhang et al., 2014, Honsa et al., 2016, Marques et al., 2016, Boulanger and Messier, 2017). The transcription factors of the Sox family have been widely studied in the context of oligodendrocyte development. We observed 74.3±6.5 % of NG2 glia expressed *Sox2*, compared to only 42.5±9.4 % of oligodendrocytes (Fig. 23A). This is in agreement with the findings that *Sox2* maintains cells in a proliferative state and prepares NG2 glia for myelination (Zhang et al., 2018, Zhao et al., 2015). We also analyzed all subunits of ionotropic and metabotropic glutamate receptors, as these may play important roles in CNS disorders. NG2 glia had a higher percentage of cells which expressed AMPA (*Gria2, Gria3, Gria4*) and kainate receptor subunits (*Grik3, Grik4, Grik5*), compared to oligodendrocytes (Fig. 23A). The presence of glutamate receptors in NG2 glia suggests that they are well equipped to sense neuronal activity, as already suggested (Kukley et al., 2008, Káradóttir et al., 2008). NG2 glia show the highest density of ionotropic glutamate receptors compared to later lineage stages (De Biase et al., 2010), which is very well reviewed by (Spitzer et al., 2016, Song et al., 2017, Ceprian and Fulton, 2019). We also confirmed our previous results about subunits of metabotropic glutamate receptors (Valny et al., 2018); *Grm5* was predominantly expressed by NG2 glia (70.2±7.3 %) and *Grm3* by oligodendrocytes (75.5±5.6 %) (Fig. 23A). Interestingly, in the optic nerve these two types of metabotropic receptors were shown to be protective for oligodendrocytes in neuropathologies involving excitotoxicity and ischemia (Butt et al., 2017); therefore, we hypothesize that such increased levels of *Grm5* in NG2 glia and *Grm3* in oligodendrocytes might be protective. Hyperpolarization-activated cyclic nucleotide-gated (*Hcn*) channel subunit 2 was highly expressed in a large number of oligodendrocytes. Notomi and Shigemoto found HCN2-immunopositivity in a type of perineuronal oligodendrocytes that are in the gray matter close to the neuronal perikarya (Notomi and Shigemoto, 2004). However, to the best of our knowledge, there are no reports on HCN2 functioning in mature oligodendrocytes. Nevertheless, they might participate in setting the V_m to more positive values, like in NG2 glia or astrocytes (Battefeld et al., 2016, Honsa et al., 2012).

Since we isolated the gray matter (CTX) and the white matter (CC) of the brain, we compared NG2 glia and oligodendrocytes in these two regions. Based on our single-cell RT-qPCR analyses, which comprised 95 genes, we found only subtle differences between CTX and CC - neither in the case of NG2 glia nor in the case of oligodendrocytes. In cortical NG2 glia, the expression of two genes of the Wnt signaling pathway (*Fzd8, Axin2*) and AMPA receptor subunit *Gria2,* was up-regulated (Fig. 23B) when compared to the white matter

NG2 glia. The cortical oligodendrocyte expression of *Grm6* and *Hcn2* were up-regulated (Fig. 23B) compared to the white matter oligodendrocyte. Similarly, within the two adult brain regions, Marques et al. were unable to identify specific subpopulations of oligodendrocytes, but some oligodendrocyte populations were present throughout the brain and other oligodendrocytes were enriched in certain regions (Marques et al., 2016).

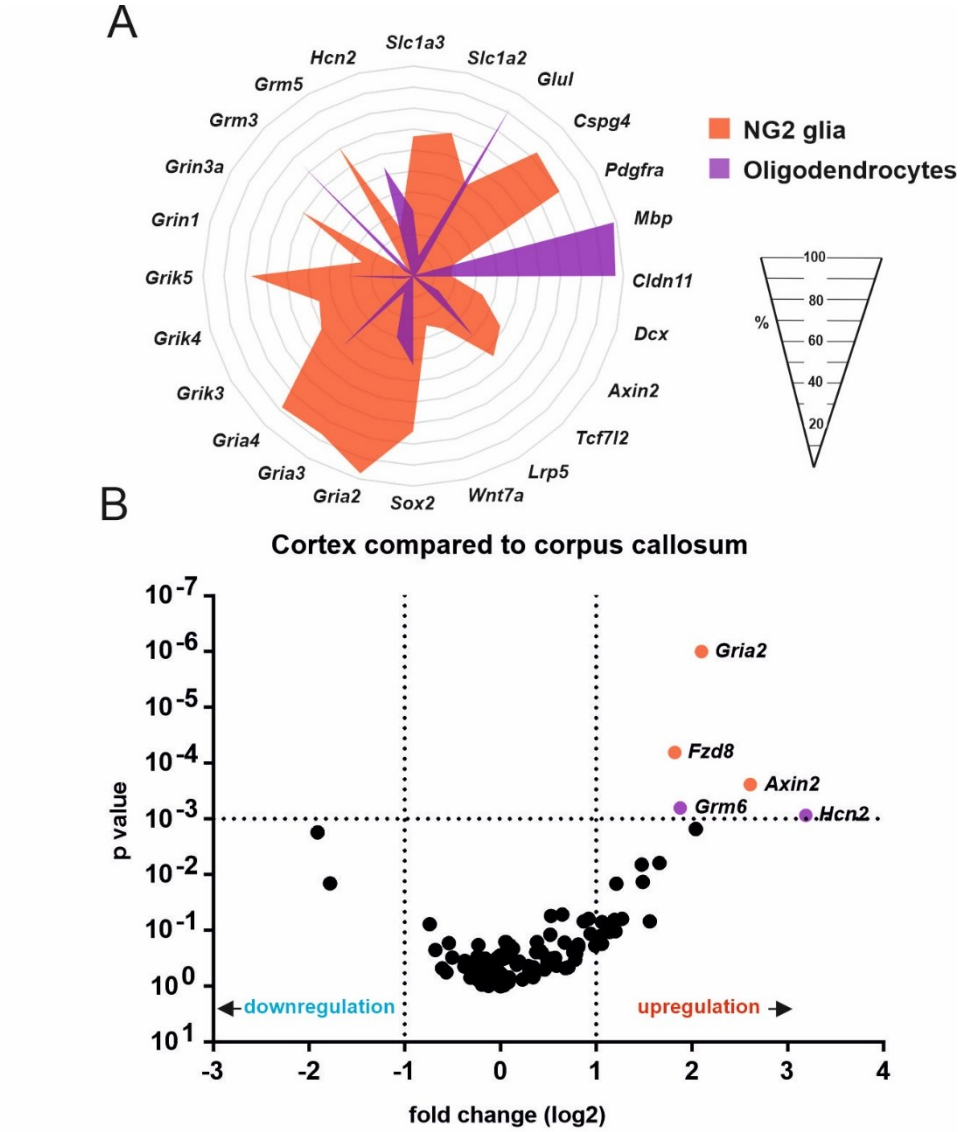

Figure 23: A) NG2 glia and oligodendrocytes isolated from uninjured mice differ in percentage of cells expressing particular genes. B) Volcano plots showing higher levels of expression (red) of several genes in the cortex (CTX) compared to corpus callosum (CC) in NG2 glia (orange) or oligodendrocytes (purple). Statistics were calculated using multiple t-test. In the case of B, only statistically significant differences with $p < 0.05$ are shown. In the case of C, only statistically significant differences with $p < 0.001$ and log fold change > 1 are shown. FCI, focal cerebral ischemia; SW, stab wound; DEMY, demyelination; CTRL, control.

4.2.2 Gene expression profiles of NG2 glia following CNS disorders

To compare NG2 glia heterogeneity following different pathophysiological conditions of the brain, we collected single cells seven days after the induction of three different types of brain disorders: CTX after FCI (n = 127 cells), SW (n = 87 cells), and DEMY (n = 93 cells) and CC after DEMY (n = 88 cells). We merged all the cells from uninjured CTX (n = 75 cells) and CC (n = 80 cells) with their injured counterparts and performed SOM analyses, which revealed eight distinct cell subpopulations: four subpopulations of NG2 glia and four subpopulations of oligodendrocytes (Fig. 24A). Two subpopulations of NG2 glia were termed NG2 glia (S1) and NG2 glia (S2), characterized by a high percentage of cells expressing typical markers of NG2 glia, such as *Cspg4* and *Pdgfrα* (Fig. 25A, B). The expression pattern of these two groups was similar to NG2 glia from the uninjured brain, except for the fact that NG2 glia (S2) had a higher expression of several genes compared to the NG2 glia (S1). The difference is visible at the level of the percentage of cells expressing the given gene (Fig. 25A, B). The most pronounced difference is the percentage of cells expressing *Glul* within each subpopulation, 67.2±6.4 % of NG2 glia (S2), compared to 19.0±5.3 % of NG2 glia (S1) (Fig. 25A, B).

The third population of NG2 glia is a specific group of cells characterized by the highest number of cells expressing astroglial markers *Gfap* (37.5±7.1 %) and *Vim* (92.9±1.2 %) (Fig. 25C) and was further termed astrocyte-like NG2 glia. These genes for intermediate filaments are typically upregulated in reactive astrocytes (Pablo et al., 2013), which could highlight the astrogliogenic potential of these cells. In this subpopulation, the expression of *Cspg4* and *Pdgfrα* is lower (4.8±2.2 log2E and 9.3±2.3 log2E respectively) than in NG2 glia (S2) (6.8±2.1 log2E and 11.2±1.2 log2E respectively; Fig. 25E), which could also indicate differentiation to astrocytes. When NG2 glia differentiate to oligodendrocytes, they gradually lose the expression of *Cspg4* and *Pdgfrα,* and enter an intermediate pro-oligodendrocyte stage before finally expressing the markers of mature oligodendrocytes (Polito and Reynolds, 2005). Astrocyte-like NG2 glia display a decreased percentage of cells expressing *Grm5* (53.6±5.7 %) and its expression level is also reduced (3.1±0.4 log2E), the opposite to NG2 glia (Fig. 25C). Both NG2 glia (S2) and astrocyte-like NG2 glia subpopulations are characterized by a high expression of *Dcx* (55.2±7.0 % and 67.9±7.0 % respectively), mentioned above as a marker of cell motility (Fig. 25B, C). Moreover, astrocyte-like NG2 glia are characterized by their proliferation potential as this subpopulation has the highest percentage of cells expressing *MKi67* (39.3±7.0 %), a marker of proliferation (Fig. 25C), and its highest expression (3.1±0.6 log2E) when compared to all

subpopulations (Fig. 25E). This suggests that astrocyte-like NG2 glia retain the ability to proliferate thus differing to oligodendrogliogenesis, when this ability is lost (Hassannejad et al., 2019).

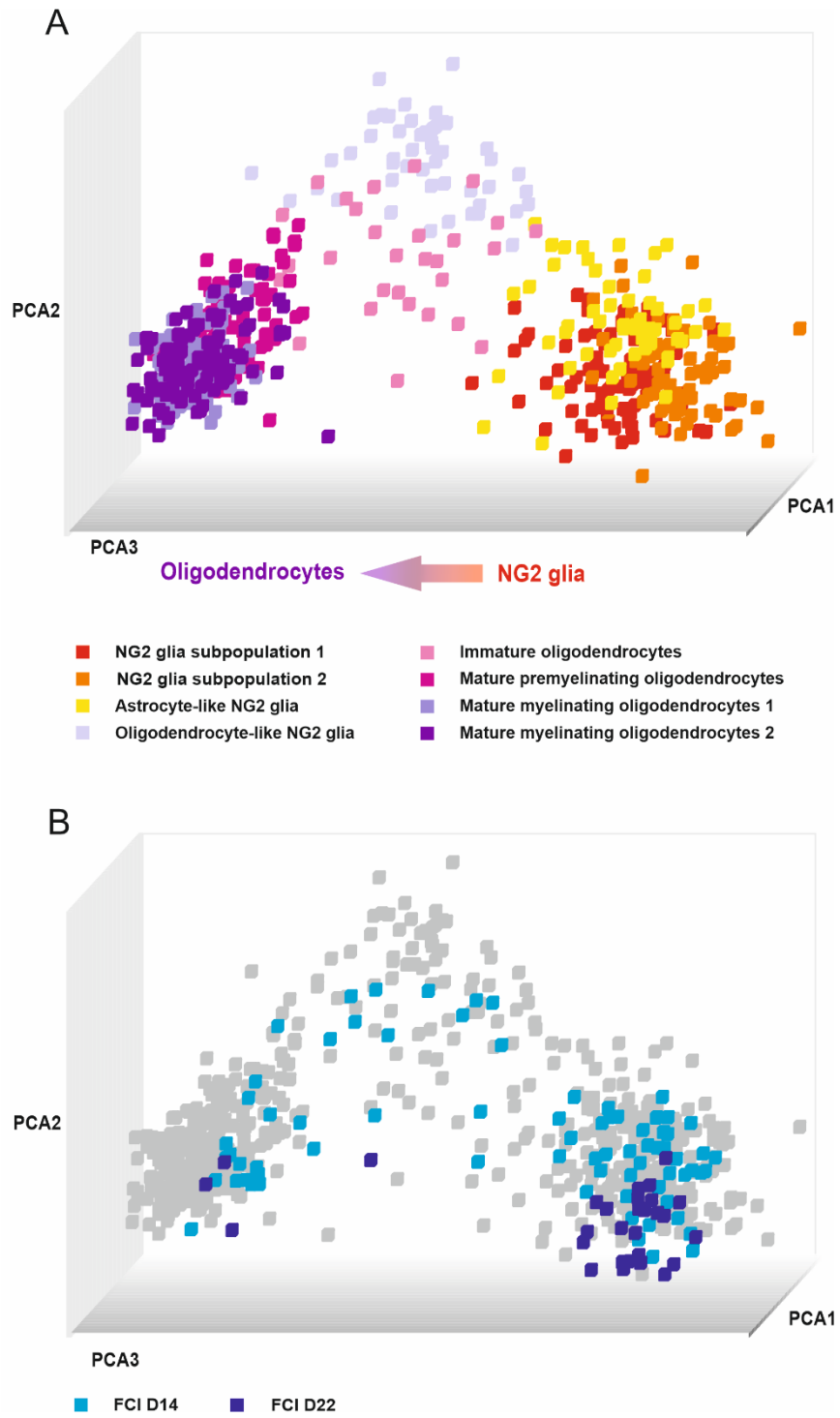

Figure 24: (A) Principal component analysis (PCA) showing the distribution of four subpopulations of NG2 glia and four subpopulations of oligodendrocytes seven days after injury. (B) PCA showing the distribution of cells from two additional time points (14 and 22 days) after focal cerebral ischemia across the subpopulations of NG2 glia and oligodendrocytes.

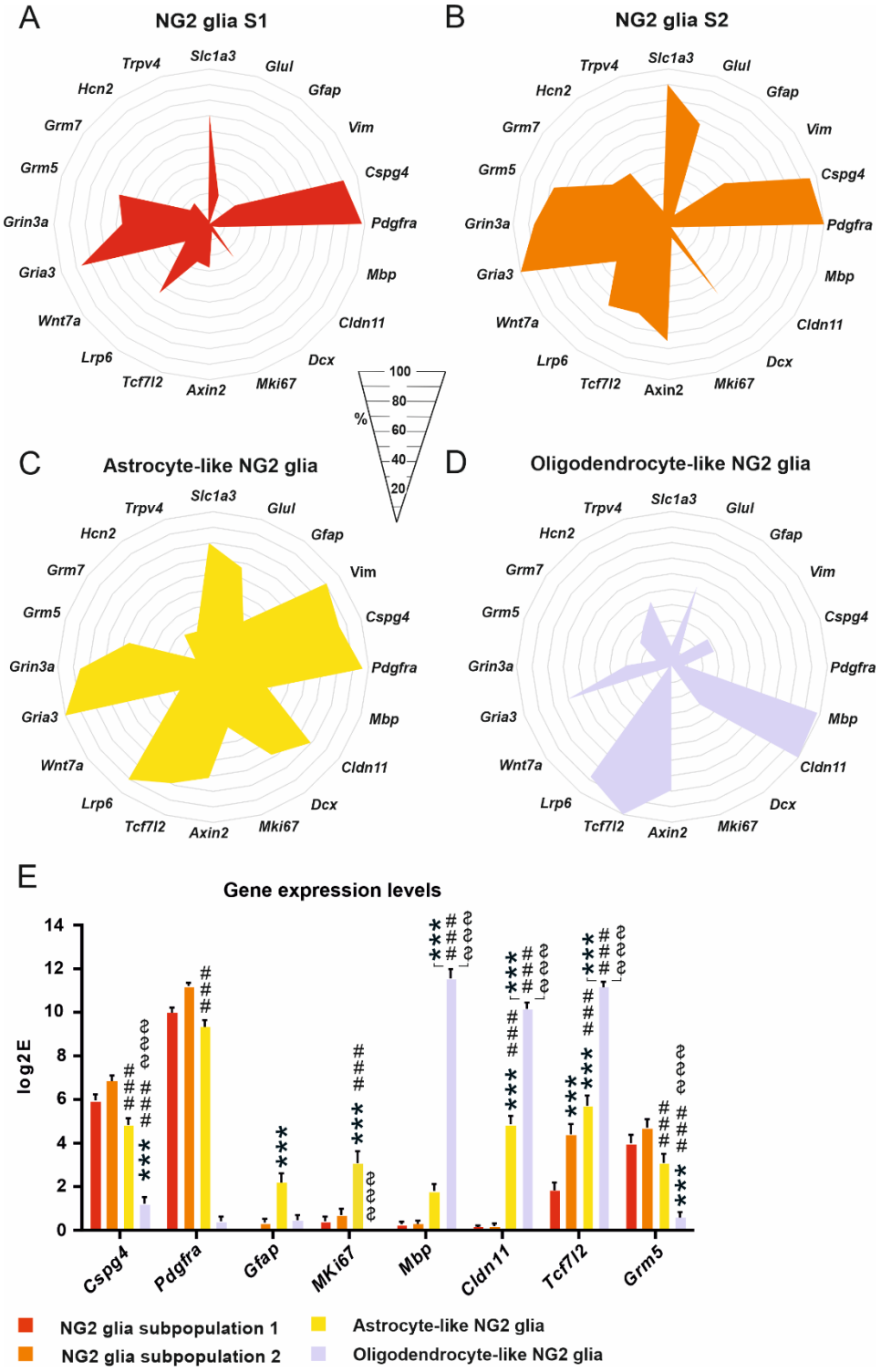

Figure 25: Four NG2 glia subpopulations identified using self-organizing map analysis. NG2 glia subpopulation 1 (A), NG2 glia subpopulation 2 (B), astrocyte-like NG2 glia (C), and oligodendrocyte-like NG2 glia (D) differ in the percentage of cells expressing genes or in gene expression levels (E). (A-D) Only genes, of which expression is changed significantly ($p < 0.05$), are depicted, with the exceptions of the marker genes. (E) Asterisks show significance compared to the NG2 glia subpopulation 2. Hashtags show significances compared to the astrocyte-like NG2 glia subpopulation. Dollar show significances compared to the oligodendrocyte-like NG2 glia subpopulation. ***, ###, $$$ $p < 0.001$. Statistics are calculated using multiple t-test or two-way ANOVA, comparing each subpopulation with each other. S, subpopulation.

The fourth subpopulation is oligodendrocyte-like NG2 glia, characterized by a high percentage of cells expressing oligodendrocyte-committed genes, such as *Mbp* (98.0±3.8 %), *Cldn11* (100.0±0.0 %), and *Tcf7l2* (100.0±0.0 %) and a lower percentage of NG2 glia-committed genes, such as *Cspg4* (28.6±5.4 %) and *Pdgfrα* (8.2±3.7 %) (Fig. 25D). Interestingly, some astrocyte-like NG2 glia expressed *Mbp* (39.3±4.7 %), *Cldn11* (80.4±8.5 %), and *Tcf7l2* (76.8 ± 4.9 %; Fig. 25C, D) but their expression was much lower (*Mbp*, 1.8±0.3 log2E; *Cldn11*, 4.9±0.4 log2E; *Tcf7l2*, 5.71±0.5 log2E) than in oligodendrocyte-like NG2 glia (*Mbp*, 11.6±0.4 log2E; *Cldn11*, 10.2±0.3 log2E; *Tcf7l2* 11.2±0.3 log2E; Fig. 25E). In oligodendrocyte-like NG2 glia, we found a decreased expression of *Grm5* (10.2±4.0 %; Fig. 25E), while *Grm3* expression was not detected. Another feature of this subpopulation is the expression of *Trpv4*, which was also described by Marques et al. in committed OPC (Marques et al., 2016) (Fig. 25D).

The distribution of the four NG2 glia subpopulations varied among the regions of the uninjured brain, as well as in response to pathological stimuli. The proportion of the two subpopulations of NG2 glia between CTX and CC is already significantly different in the uninjured brain. There is a large number of NG2 glia (S2) that has a higher expression of several genes than NG2 glia (S1), differing to that in CC (Fig. 26A). Oligodendrocyte-like NG2 glia are equally distributed in the gray (CTX) and white (CC) matter and no astrocyte-like NG2 glia are present in the uninjured brain (Fig. 26A). Interestingly, astrocyte-like NG2 glia represent the prevailing subpopulation (48.5±8.5 %) after FCI, at the expense of NG2 glia (S1) and (S2). With regards to the DEMY CTX two transitions states, namely oligodendrocyte- and astrocyte-like NG2 glia, these disappear completely, and we found only a few transitions of NG2 glia in DEMY CC (Fig. 26A). In the case of SW, the distribution was similar to its corresponding CTRL (Fig. 26A).

In order to determine whether FCI-specific astrocyte-like NG2 glia is permanent or transient subpopulation within NG2 glia subpopulations, we performed single-cell RT-qPCR analysis 14 and 22 days after FCI (Fig. 24B). This subpopulation was still present 14 days after FCI, but with a decreasing tendency (Fig. 26C). In the late stages (22 days) astrocyte-like NG2 glia were not observed which was at the expense of NG2 glia (S2) similarly to oligodendrocyte-like NG2 glia (Fig. 26C).

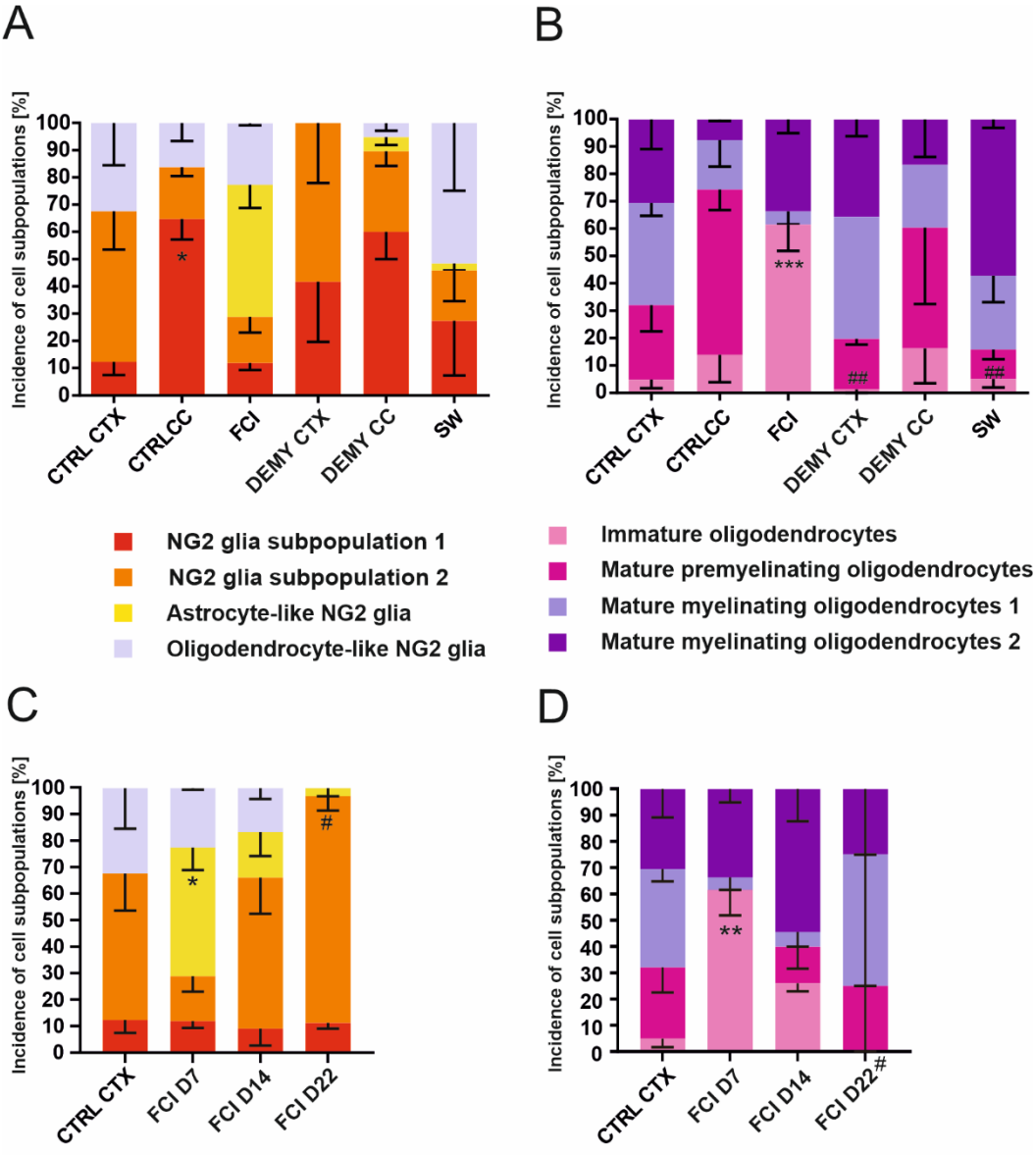

Figure 26: Distribution of four subpopulations of NG2 glia (A) and four subpopulations of oligodendrocytes (B) is unequal in controls (CTRLs) and following injuries. Note that astrocyte-like NG2 glia only become greatly emerged after focal cerebral ischemia (FCI). Changes in the distribution of four subpopulations of NG2 glia (C) and four subpopulations of oligodendrocytes (D) at different time points after focal cerebral ischemia. Statistics were calculated using two-way ANOVA, comparing incidences of a particular subpopulation among groups. The percentage of subpopulations was calculated as an average of the percentage from different mice. In the case of A, asterisks show significances between CTRLs. In the case of B, asterisks show significance compared to CTRL and hashtags show significances compared to FCI. * $p < 0.05$; ## $p < 0.01$; *** $p < 0.001$. CTX, cortex; CC corpus callosum; DEMY, demyelination; SW, stab wound.

4.2.3 Different oligodendrocyte subpopulations after CNS injuries

Besides the NG2 glia subpopulations, we also identified four subpopulations of oligodendrocytes. We classified them according to (Guo et al., 2015, Valny et al., 2018) as immature oligodendrocytes, mature premyelinating oligodendrocytes, and two subtypes of

mature myelinating oligodendrocytes (1 and 2) (Fig. 27). The first two groups of oligodendrocytes have the residual expression of *Cspg4* and other genes typical for NG2 glia, such as *Grm5*, *Axin2,* and *Gria3* (Fig. 27A, B). Interestingly, in immature oligodendrocytes, only 77.4±6.6 % cells expressed *Mbp* and 71.0±8.8 % cells expressed *Cldn11* unlike oligodendrocyte-like NG2 glia *(Mbp* 98.0±3.8 %, *Cldn11* 100.0±0.0 %; Fig. 27A; Fig. 25D). Additionally, there was a relatively lower incidence of cells expressing *Glul* and *Grm3* (including their expression levels) within immature oligodendrocytes (Fig. 27A, E). The tendency is that the expression pattern of these genes within oligodendrocytes subpopulations increases (Fig. 27E) with the progressing maturation of oligodendrocytes. The number of cells expressing the gene of Shh signaling *Ptch1* increases with the maturation of oligodendrocytes (Fig. 27). Shh signaling is implicated in controlling both the generation of oligodendrocytes during embryonic development, and their production in adulthood (Loulier et al., 2006, Wang and Almazan, 2016). The need for the Shh genes in the oligodendroglial lineage is due to *Shh* signaling not only being involved in differentiation but also in oligodendrocyte branching once they are mature (Wang and Almazan, 2016), and it is a necessary factor playing a positive role during demyelination/remyelination (Ferent et al., 2013). Thus, an increased transcription of suppressor receptor *Ptch1* in mature myelinating oligodendrocytes 2 suggests that the Shh pathway is no more needed. The *Hcn2* gene could serve as an indicator at the stage of oligodendrocyte differentiation. This gene is barely expressed in immature and premyelinating oligodendrocytes (0.7±0.4 log2E; 0.5±0.2 log2E), while in the both mature stages it is highly expressed (8.5±0.2 log2E; 9.6±0.2 log2E) (Fig. 27A, B, C, D, E). Moreover, the number of cells expressing the subunits of AMPA receptors, *Gria2* and *Gria3,* gradually decreases with oligodendrocyte maturation. The exception is that within the subpopulation of mature myelinating oligodendrocytes 2, a relatively high number of cells express *Gria2* (35.0±6.4 %) compared to the mature myelinating oligodendrocytes 1 (Fig. 27C, D). This is one of the characteristics of mature myelinating oligodendrocytes 2 which distinguishes them from mature myelinating oligodendrocytes 1, as comparably described by Valny and colleagues (Valny et al., 2018). The overexpression of *Gria2* stimulates the transcriptional activities linked to myelin formation, even in the absence of injury (Khawaja, 2019). Moreover, Ca^{2+}-permeable AMPA receptors were shown to mediate ischemia-induced excitotoxic damage in oligodendrocytes (Leuchtmann et al., 2003, McDonald et al., 1998, Dewar et al., 2003). This suggests that the upregulation of *Gria2* can be beneficial to oligodendrocyte repair in pathology, and it protects them from Ca^{2+} overloading. Another difference between the two

mature subpopulations was observed in the expression and the number of cells expressing kainate receptor subunit *Grik5* (Fig. 27C, D, E), making them vulnerable to glutamate excitotoxicity (Alberdi et al., 2002, Sanchez-Gomez et al., 2011). The role of another highly expressed subunit of glutamate receptors, *Grm7* (Fig. 27E), which is known to be involved in the regulation of proliferation, remains elusive in mature oligodendrocytes 2 as they are apparently terminally differentiated (Xia et al., 2015). Unlike NG2 glia subpopulations, the distribution of oligodendrocyte subpopulations was comparable between the gray and white matter (Fig. 26B). Following FCI, no premyelinating oligodendrocytes were present, but there was a significantly higher incidence of immature oligodendrocytes (Fig. 26B). This was in the contrast to DEMY in CTX and following cortical SW, where the immature subpopulation of oligodendrocytes was barely present (Fig. 26B). This might be due to the various rates of remyelination caused by the different severity of injury. This idea is supported by data from late stages following FCI where premyelinating oligodendrocytes appeared after 14 days, and after 22 days, the proportion of oligodendrocyte subpopulations was similar to that from CTRL CTX (Fig. 26D).

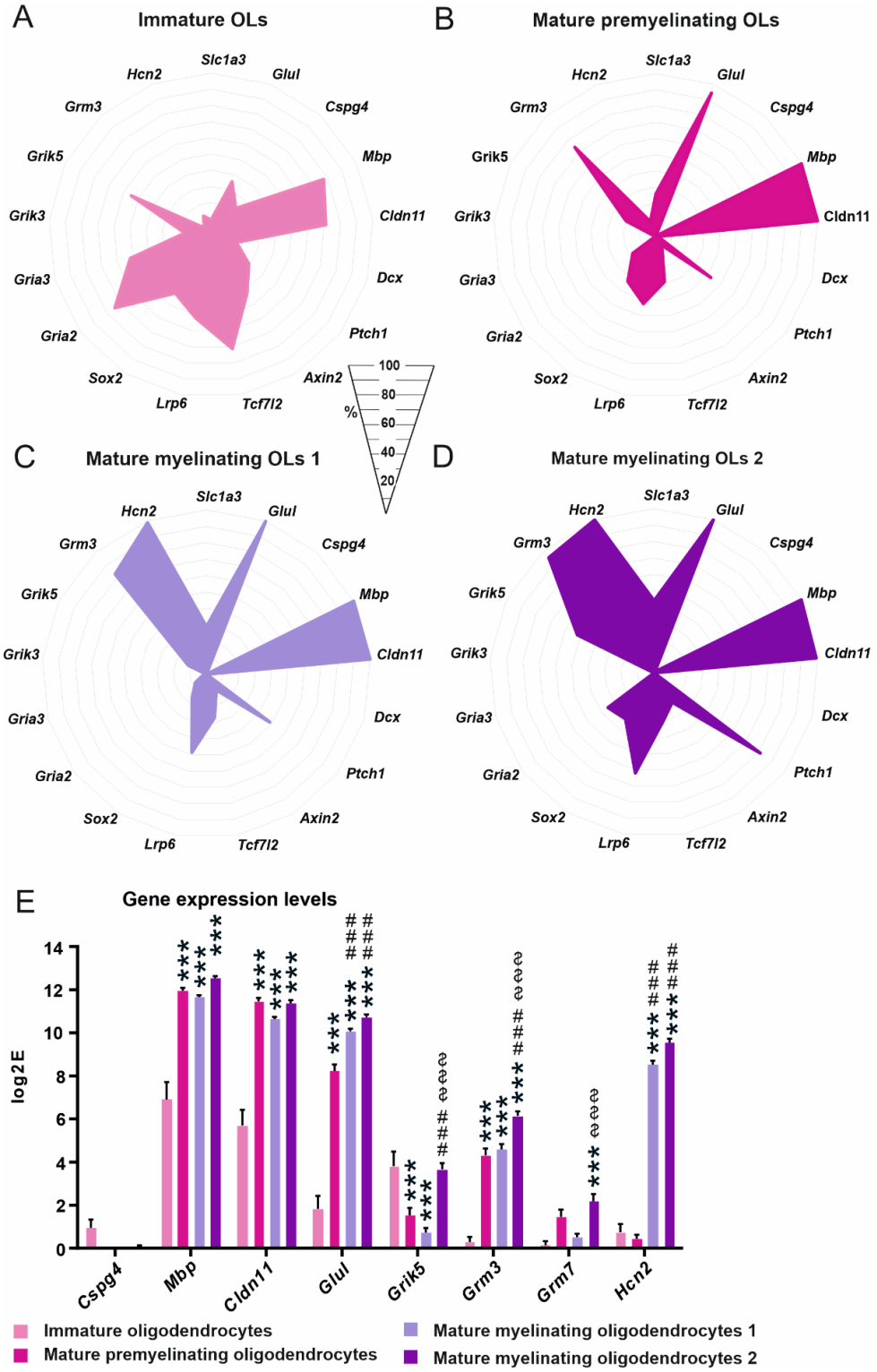

Figure 27: Four oligodendrocyte (OL) subpopulations identified using self-organizing map analysis. Immature OLs (A), mature premyelinating OLs (B), mature myelinating OLs 1 (C) and mature myelinating OLs 2 (D) differ in the percentage of cells expressing genes or differ in gene expression levels (E). (A-D) Only genes, where expression is changed significantly ($p < 0.05$), are depicted, with the exception of the marker genes. (E) Asterisks show significance compared to the immature OLs. Hashtags show significances compared to the mature premyelinating OLs. Dollar show significances compared to the mature myelinating OLs 1. ***, ###, $$$ $p < 0.001$. Statistics were calculated using multiple t-test or two-way ANOVA, comparing each subpopulation with each other.

4.2.4 Immunohistochemical identification of NG2 glia progeny following CNS injuries

To further verify the phenotypic differences of identified tdTomato$^+$ subpopulations we stained uninjured brains, and those following FCI, SW or DEMY, against the combinations of cell-type-specific markers, such as GFAP, AlDH1L1 (astrocytes) and, APC, the cell-body marker of oligodendrocytes and proliferation markers (PCNA, KI67). The overlap of signals from tdTomato with an appropriate marker (Fig. 28, Fig. 29), was detected in the depicted areas of the brain (Fig. 15). To assess proliferation rate of NG2 glia, we employed two frequently used markers, PCNA and KI67. According to PCNA staining, proliferation was increased in response to each type of injury, when compared to the corresponding CTRL. The highest number of proliferating cells was in the CTX and CC, following DEMY (Fig. 28A). Interestingly, KI67 staining showed different results. The proliferation was only increased in the BBB -damaging CNS disorders (FCI and SW) and not in DEMY (Fig. 28B). NG2 glia differentiation into oligodendrocytes is very well known. Notably, the most pronounced oligodendrogliogenesis was detected in the CTX after SW (24.5±2.4 %), while following FCI and DEMY, it was comparable with the CTRL (Fig. 28C). As we expected, oligodendrogliogenesis differs between the brain regions in the CTRLs, as well as after DEMY; it is much higher in white matter than in the gray matter (Fig. 28C).

We used immunohistochemistry to confirm that astrocyte-like NG2 glia only arise after FCI. We clearly showed that tdTomato/GFAP$^+$ cells are only present after FCI in a higher number (31.4±1.9 %), compared to the CTRLs or the other types of injury (Fig. 29A). These cells were mainly located on the border of ischemia between NG2 glia and astrocytes (Fig. 29A) in the close vicinity of the lesion as already observed by Valny et al. (Valny et al., 2018). Another astrocytic marker, ALDH1L1, did not confirm the increased number of astrocyte-like NG2 glia (Fig. 29C), however, other studies showed that GFAP$^+$ cells may not necessarily be positive for ALDH1L1 (Hackett et al., 2018). For that reason, we used another very typical marker of reactive astrocytes-VIM, which was also increased following FCI, but not as much as was GFAP (Fig. 29D). To validate single-cell RT-qPCR results from late stages following FCI, we did also double-labelling for tdTomato/GFAP mice in the 14 and 22-30 days after FCI. We observed a GFAP immunoreactivity decay already at 14 days (Fig. 29B). This suggests that astrocyte-like NG2 glia represent a transient subpopulation, but unique to FCI. In summary, NG2 glia only form astrocyte-like NG2 glia following severe ischemic damage, while cortical SW or DEMY are not able to evoke such NG2 glia multipotency.

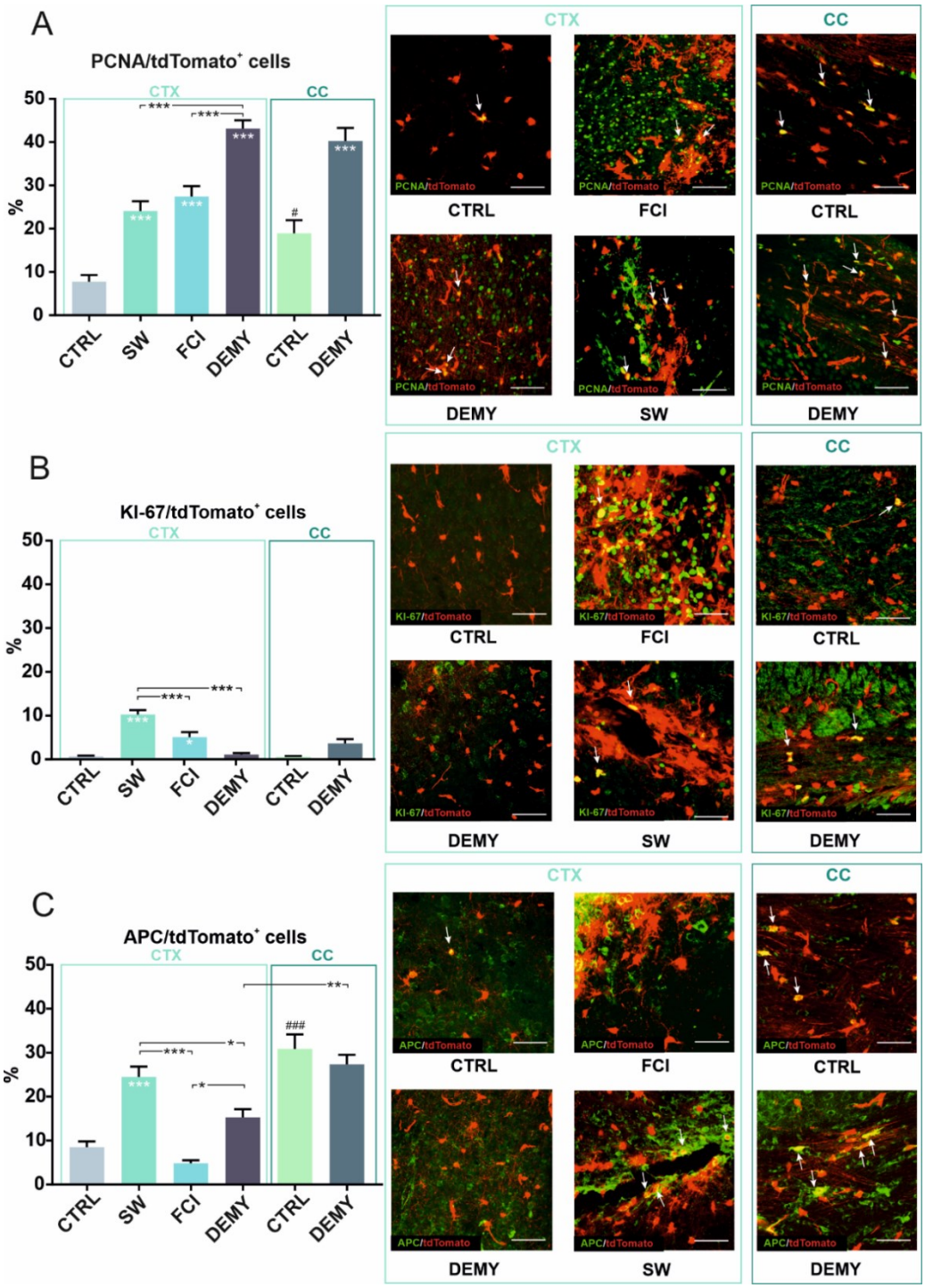

Figure 28: Graphs showing the percentage of tdTomato$^+$ cells expressing a given marker, and their representative images depicting the co-localization of proliferation and oligodendrocyte markers under physiological and pathological conditions. (A) Showing tdTomato$^+$ NG2 glia expressing proliferating cell nuclear antigen (PCNA), (B) showing tdTomato$^+$ NG2 glia expressing proliferation marker KI67, (C) showing tdTomato$^+$ NG2 glia expressing oligodendroglial marker, adenomatous polyposis coli (APC). (A-C) Arrows indicate the co-localization of green and red signals. Statistics were calculated using one-way ANOVA. Asterisks show significance compared to the corresponding control (CTRL) unless otherwise indicated. Hashtags show significances between CTRLs (CTX, CC). *, #, $p < 0.05$; ** $p < 0.01$; ***, ### $p < 0.001$. Scale bars, 50 µm. CTX, cortex; CC corpus callosum; FCI, focal cerebral ischemia; DEMY, demyelination; SW, stab wound.

4.2.5 Astrocyte-like NG2 glia features

To characterize astrocyte-like NG2 glia on a genome-wide level, we performed a single-cell RNA-seq experiment using Cspg4/tdTomato mice. We analyzed three uninjured (CTRL) and three post-ischemic mice (day seven) using high-throughput platform Chromium Single-Cell Gene Expression. NG2 glia and astrocytes were enriched using FACS selection of tdTomato$^+$ and ACSA-2$^+$ cells, a recently identified marker of astrocytes (Kantzer et al., 2017). Single- and double-positive populations were collected and analyzed. In total, we acquired a single-cell transcriptome of 4634 cells (1656 in CTRLs and 2978 in ischemic animals). The preliminary analysis identified clusters of various cell types. Some of them were expected, e.g. various maturation stages of oligodendrocytes or Cspg4$^+$ pericytes, other were rather surprising, e.g. clusters composed of myeloid or vascular cells. For further analysis, we only selected cells expressing typical NG2 glia and astrocyte markers, resulting in 1134 cells. Unfortunately, we only collected seven NG2 glia in the CTRL animals, where the majority of tdTomato$^+$ cells were identified as pericytes, therefore we further limited our analysis only to cells under ischemic conditions (549 cells).

In the ischemic animals, we identified four cell clusters (Fig. 30A). Two clusters expressed typical markers of NG2 glia and astrocytes (Fig. 30B), whereas the remaining two represented separate subpopulations sharing the expression of both cell type markers (Fig. 30B). It was noted that both subpopulations demonstrated a similar level of *Gfap* expression (Fig. 30B) as well as the percentage of *Gfap*$^+$ cells, compared to astrocytes, and a similar expression level and positivity of the *Cspg4* gene, in comparison to NG2 glia (Fig. 30B). To characterize these transient subpopulations, we performed a DE analysis identifying 288 and 353 marker genes that were upregulated in the subpopulations (fold change > 2, adjusted p value < 0.05).

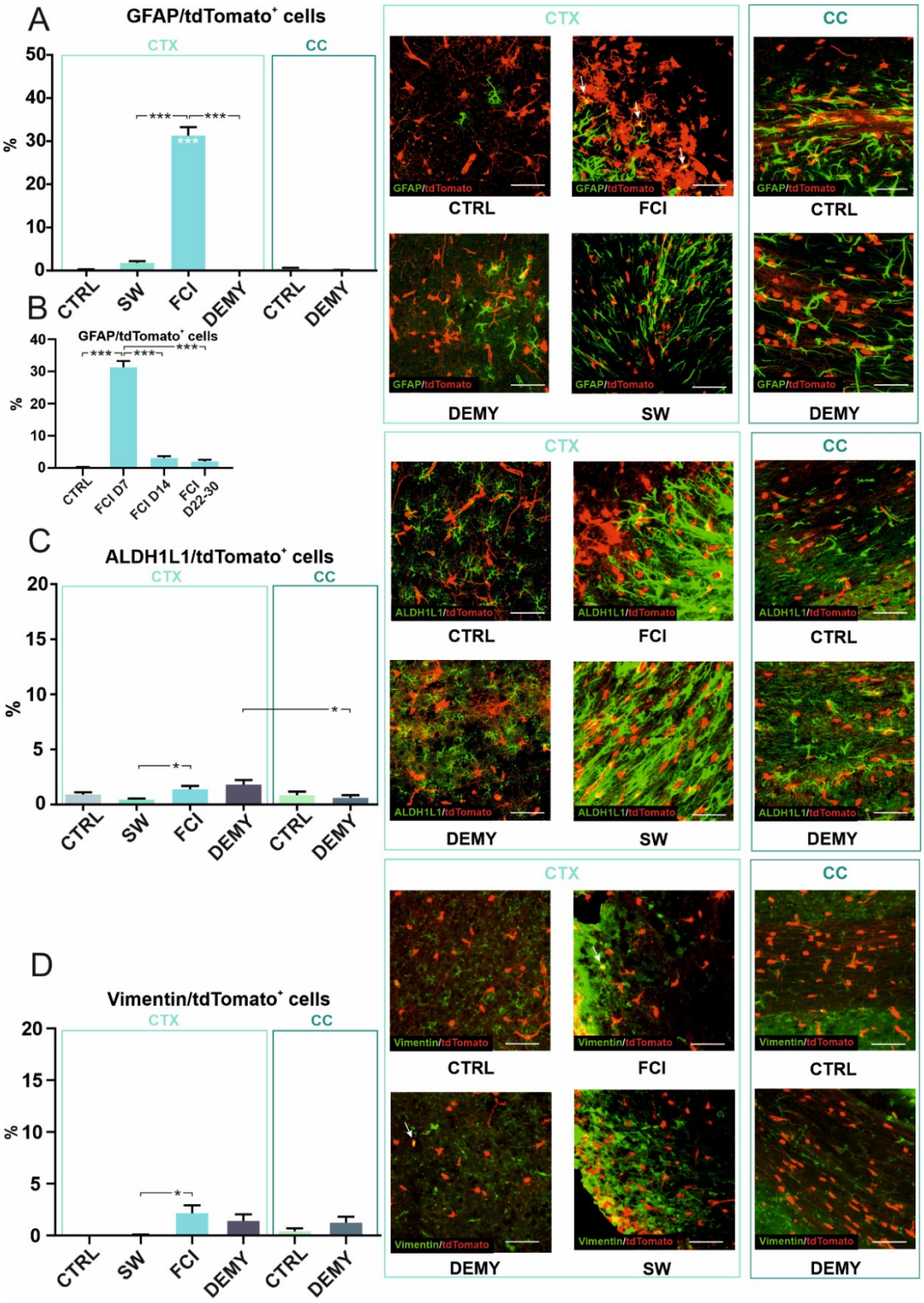

Figure 29: Graphs showing the percentage of tdTomato$^+$ cells expressing a given marker and their representative images depicting the co-localization of astrocyte markers under physiological and pathological conditions. (A-B) Showing tdTomato$^+$ NG2 glia expressing astrocyte markers glial fibrillary acidic protein (GFAP), (C) aldehyde dehydrogenase 1 family member L1 (ALDH1L1) and (D) vimentin (VIM). (A-D) Arrows indicate the co-localization of green and red signals. Statistics are calculated using one-way ANOVA. Asterisks show significances compared to the corresponding CTRL unless otherwise indicated. * $p < 0.05$; *** $p < 0.001$. Scale bars, 50 µm. CTRL, control; CTX, cortex; CC corpus callosum; FCI, focal cerebral ischemia; DEMY, demyelination; SW, stab wound.

The first transient subpopulation we termed as pericytes (detached; 15 cells) because, in addition to *Gfap* and *Cspg4* expression, this subpopulation showed a high expression of genes typically found in pericytes (e.g. *Vtn, Rgs5*; Fig. 30D). These were characterized by the positive regulation of the cell migration, angiogenesis, and wound healing (Fig. 30C). We speculate that these cells represent a unique population of pericytes, which migrate into the ischemic lesion and differ from classic pericytes which are attached to the capillaries and venules (Fig. 30B). Notably classic pericytes were removed from the analysis during the preprocessing steps, so we may assume that this is a unique population of pericytes sharing the expression of some typical astrocytic genes (*Aqp4, Gjb6, Aldh1l1*; Fig. 30B). Interestingly, a recent report studying the role of pericytes in fibrotic scarring, identified a population of pericytes displaying a distinctive morphology that was located close to the glial-fibrotic lesion (Dias et al., 2020). We suggest that the close vicinity of astrocytes and pericytes at the ischemic border may initiate transcriptional changes, making pericytes similar to astrocytes. However, the validity of this hypothesis needs to be confirmed by additional studies.

The second transient subpopulation was identified as astrocyte-like NG2 glia (50 cells), because they shared typical markers of both astrocytes (*Gfap, Glul, Gja1, Aqp4, Gjb6;* Fig. 30B) and NG2 glia (*Cspg4, Pdgfrα*; Fig. 30B). Moreover, within the 10 top DE genes of astrocyte-like NG2 glia population, there are genes typical for NG2 glia (*Ube2c, Rrm2, Pbk, Birc5, Spc24*), and also genes typical for astrocytes (*Top2a, Hells*; Fig. 30D) (Zhang et al., 2014, Cahoy et al., 2008). Furthermore, the list of top10 DE genes in the astrocyte-like NG2 glia included genes associated with the cell cycle and mitosis (e.g. *Top2a, Cdk1*; Fig. 30D). Interestingly, this population differentially expressed *Kcne1*, encoding the accessory subunits of acetylcholine-inhibited channels, *Kcnq1* and *Kcnq4*, which has already been identified as a typical marker of astrocytes (Cahoy et al., 2008). Moreover, this subpopulation may respond to intracellular Ca^{2+} signals because the cells express *S100a10*, a Ca^{2+}-binding protein that generally modulates cellular target proteins. It is known to be expressed in multiple neuronal cell types, but the group of Milosevic showed that *S100a10* is expressed by astrocytes and a small population of NG2 glia (Milosevic et al., 2017). To gain a deeper insight into the role of the two transition populations, we performed gene over-representation analysis. The analysis revealed the upregulation of processes associated with mitotic cell cycle division and chromosome segregation in astrocyte-like NG2 glia (Fig. 30C). These data accord well with our recent work, which showed that up to 75 % of NG2 glia have to undergo cell division before they start to express markers of astrocytes, including

the production of GFAP protein (Valny et al., 2018). Additionally, this subpopulation is characterized by upregulated processes of cellular homeostasis, a regulation of signaling, and a positive regulation of cell-cell communication (Fig. 30C).

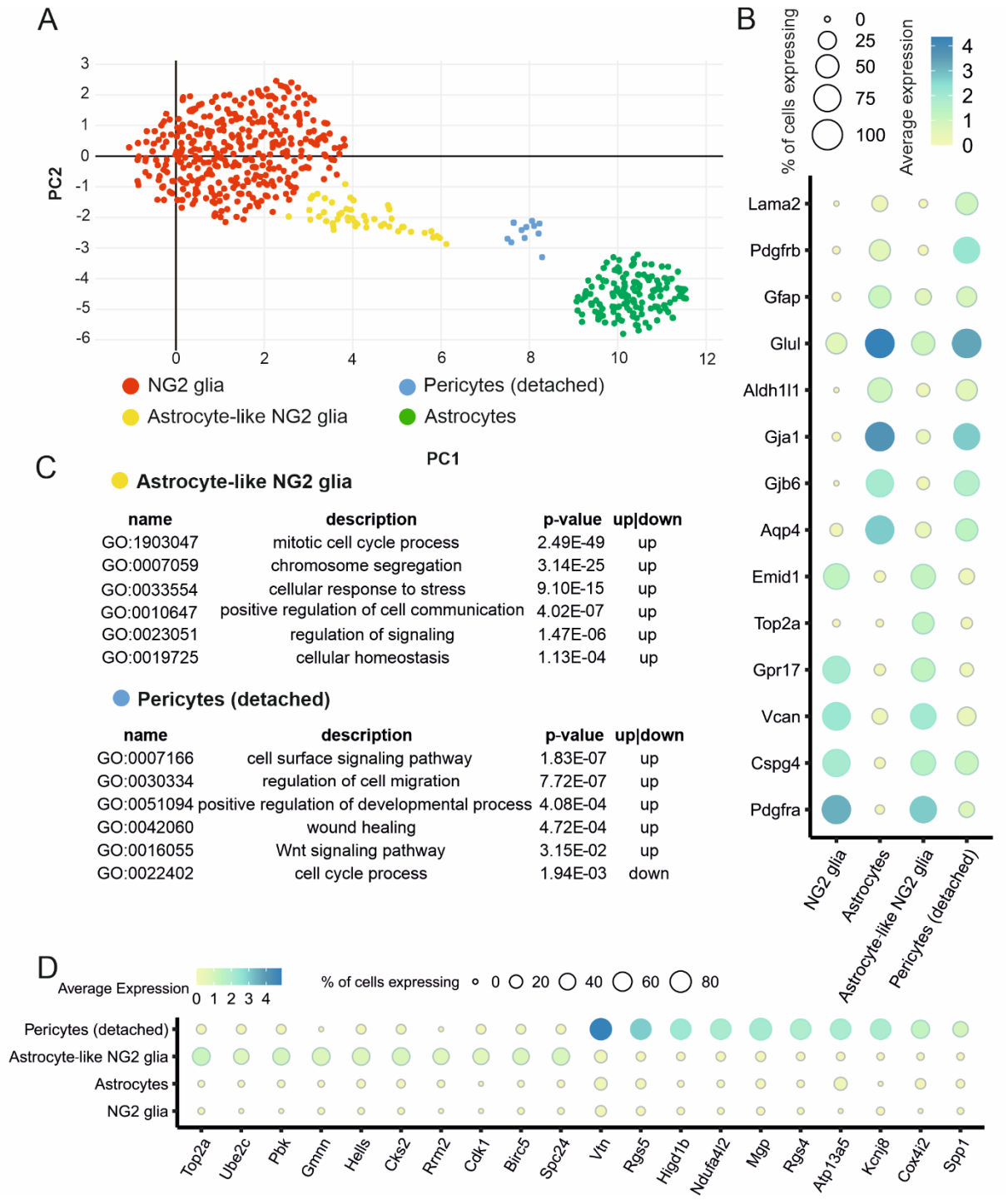

Figure 30: Single-cell RNA-Seq analysis of NG2 glia and astrocytes seven days following focal cerebral ischemia. (A) Uniform Manifold Approximation and Projection (UMAP) visualization of 549 cells expressing markers of NG2 glia and/or astrocytes, (B) Marker genes of astrocytes, NG2 glia, astrocyte-like NG2 glia and pericytes (detached); (C) Functional annotation of two transient subpopulations - astrocyte-like NG2 glia and

pericytes (detached) - shown selection of representative GO terms (Fisher's exact test). (D) Expression of canonical markers of NG2 glia, astrocytes, astrocyte-like NG2 glia and pericytes.

4.2.6 Electrophysiological characteristics of astrocyte-like NG2 glia

Based on the RNA-seq data, we found that astrocyte-like NG2 glia is a specific and distinct subpopulation of NG2 glia, only arising after FCI. Therefore, it was of interest to determine the electrophysiological properties of astrocyte-like NG2 glia seven days after FCI. Here, we cross-bred Cspg4/tdTomato mice with Gfap/EGFP mice, which enabled the measurement of astrocytes ($EGFP^+$ cells), NG2 glia ($tdTomato^+$ cells), and astrocyte-like NG2 glia ($EGFP^+$/$tdTomato^+$ cells) (Fig. 14B). The membrane currents were recorded from all the above-mentioned cells at the ischemic lesion border (CTX) of adult mice, using the patch-clamp technique in the whole-cell configuration. The predicted electrophysiological recordings revealed a complex current pattern typical of NG2 glia, i.e., they displayed K_{DR}, K_A, and K_{IR} currents (Honsa et al., 2012, Schools et al., 2003). Their average resting membrane potential (V_m) measured by our group was −71.9±3.5 mV (n=9), IR was 160.2±41.6 MΩ, and C_m was 8.1±1.0 pF. The current densities were 14.7±3.0 pA/pF for K_{IR} currents, 28.7±8.3 pA/pF for K_{DR} currents, and 50.6±14.3 pA/pF for K_A currents (Fig. 31A). In general, ischemic astrocytes elicit predominantly time- and voltage-independent currents. This type of membrane current, carried primarily by K^+ ions, has been shown to be typical of mature astrocytes (Pivonkova et al., 2010, Wallraff et al., 2004, Zhou et al., 2006). Their average V_m was −75.3±3.3 mV (n=8), IR was 115.5±34.9 MΩ and C_m was 8.4±1.2 pF. The current densities were 5.6±1.9 pA/pF for K_{IR} currents, and 2.4±1.4 pA/pF for K_{DR} currents (Fig. 31C). Astrocyte-like NG2 glia membrane currents resulted in a shift between the current pattern of NG2 glia and astrocytes (Fig. 31B). Their passive membrane properties did not significantly differ from NG2 glia/astrocytes after FCI. However, they had considerably reduced K_{IR} (3.5±0.8 pA/pF), K_{DR} (4.2±1.1 pA/pF) and K_A (0.2±0.2 pA/pF) current densities, when compared to NG2 glia, while they did not differ from those obtained in cortical astrocytes (Fig. 31B).

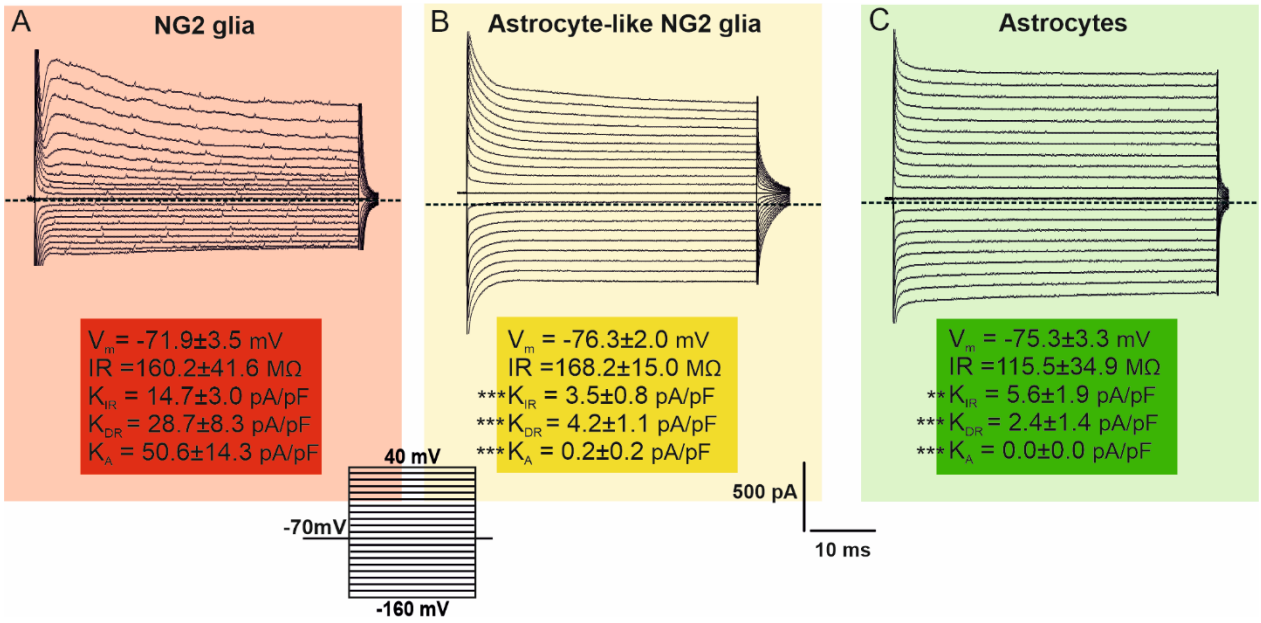

Figure 31: Current patterns of NG2 glia, astrocyte-like NG2 glia, and astrocytes seven days after focal cerebral ischemia (FCI). Typical current patterns of (A) NG2 glia, (B) astrocyte-like NG2 glia, (C) and astrocytes were obtained by hyper- and depolarizing the cell membrane from the holding potential of -70 mV to the values ranging from -160 mV to 40 mV, in 10 mV increments (see the inset, bottom). Zero current is marked by the dashed line. Statistics were calculated using one-way ANOVA. Asterisks show significances compared to NG2 glia, ** $p < 0.01$; *** $p < 0.001$.

4.3 Interaction between stroke and aging at the genome-wide level using model of FCI

To explore the difference in the response to ischemia between young and aged brain leading to impaired regeneration, we performed 3' mRNA sequencing of CTX isolated from 3-month-old (young) and 18-month-old (aged) female mice at three days after FCI and from their age-matched CTRLs (in total 4 groups, 6 animals per group).

4.3.1 Aging is accompanied with increased neuroinflammation involving primarily glial cells

We first explored factors that may contribute to the increased vulnerability of the aged brain to ischemia. We compared DE genes between young and aged CTRLs and analyzed them using Gene set enrichment analysis (Subramanian et al., 2005). We identified 52 upregulated and only 13 downregulated genes ($log_2FC > 1$, $p_{adj} < 0.05$). GSEA revealed upregulation of defense response-related processes, positive regulation of immune response, and increased secretion of cytokines and protein catabolism (Fig. 32A). Concomitantly, downregulated processes mapped to positive regulation of protein polymerization, dendrite

development and axon projection, altogether pointing towards increased inflammation and axonal degeneration in the aged brain. To see better cell-specific context of observed transcriptional changes, we searched in the literature for transcriptomic datasets related to brain aging, neuroinflammation and stroke, and quantified overlap with our lists of differentially expressed genes (Fig. 32B). There was a significant overlap between the genes upregulated within the aged CTRLs and signatures of aged astrocytes (such as *Gfap, Anln, Pcdhb6, C4b, Serpina3n, Lyz2, Neat1, Plin4*)(Boisvert et al., 2018, Clarke et al., 2018), aged microglia (such as *Clec7a, Cst7, Cybb, Lgals3, Mmp12, Spp1, C4b, Ccl8*) (Grabert et al., 2016, Holtman et al., 2015), aging OPCs (such as *Rab37, Tnfaip2*)(Spitzer et al., 2019), in lipopolysaccharide (LPS)-treated microglia (such as *Bcl3, C3ar1, Ccl3, Ccl4, Cst7, Cybb, Tnfaip2*) (Erny et al., 2015, Srinivasan et al., 2016)(Erny et al., 2015; Srinivasan et al., 2016) and/or LPS-treated astrocytes (such as *Casp1, Flnc, Mpeg1, Runx1, Serpina3n*) (Srinivasan et al., 2016), as well as with genes that are part of the common inflammatory signature (such as *Ptprc, Rab32, Slc11a1, St14, Tep1, Trem2, Tyrobp*) (Wang et al., 2012). We also found significant upregulation of genes enriched in bone marrow-derived macrophages (BMDMs) versus brain-resident microglia (such as *Cdkn2a, Itgax, Tep1*), while microglia-enriched genes (such as *Cask, Gda, Nav3, Nrep, Sox4*) were downregulated, indicating the convergence of microglial and macrophage signatures with aging, as previously suggested (Grabert et al., 2016, Friedman et al., 2018). Furthermore, aging-upregulated genes strongly overlapped with the neurodegeneration-related transcriptional profile of microglia (Friedman et al., 2018) and also with *Ccl4*-expressing subpopulation of microglia that expand during aging, injury (Hammond et al., 2019) and neurodegeneration (Mathys et al., 2017). Overall, these results suggest that aged brain presents alteration in the neuroinflammatory environment, involving particularly glial cells. A subset of pro-inflammatory primed microglia and/or astrocytes may contribute to aggravation of the ischemic injury in aged animals.

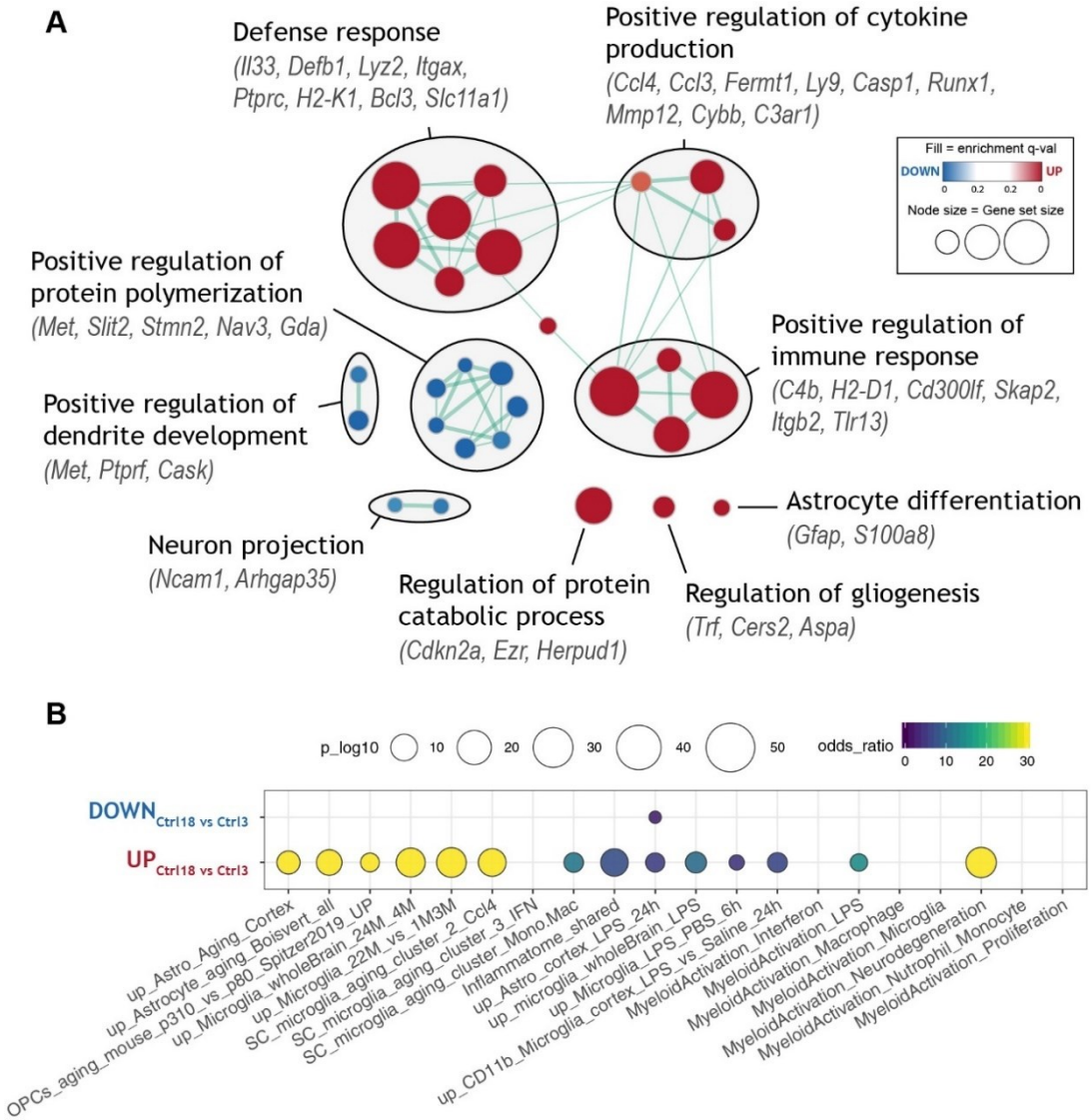

Figure 32: Gene sets with altered expression during normal aging A) Enrichment map of significantly up- or down-regulated gene ontology (GO) terms between aged (18 months) and young adult (3-month-old) control mice. Nodes represent gene sets. Highly similar gene sets are connected by edges, grouped in sub-clusters and annotated manually. B) Meta-analysis showing enrichment of selected transcriptional signatures from literature. Several inflammatory and glial cell activation-related states are significantly upregulated.

4.3.2 Aging alters the magnitude of the transcriptional response to ischemia in brain

As the next step, we explored transcriptional changes three days following ischemia in young and aged mice relative to their age-matched CTRLs. Large number of genes were DE in both young (2556) and aged (3435) mice, with a high prevalence of upregulation, both in terms of number of regulated genes and the fold-change (Fig. 33A). There was a substantial overlap between DE genes in young and aged mice, when aged mice differentially regulated more genes, often with a greater magnitude (Fig. 34A). Functional analysis with GSEA showed

hundreds of significantly enriched gene ontology (GO) terms. The GO terms were related to inflammatory response (such as IFN-I signaling, cytokine production, neutrophil degranulation), cell-cell interactions (such as integrin cell-surface interaction, extracellular matrix organization) and cell-cycle (such as regulation of DNA replication) and were upregulated to a greater extent in aged animals after injury (Fig. 33B). Similarly, gene sets associated with synaptic signaling and plasticity, neurotransmitter transport and potassium ion channels were downregulated exclusively, or to a greater extent in aged animals after ischemia (Fig. 33B). These results suggest that in addition to common genes, aged brain activates/represses distinct cellular processes in response to ischemic impact. Surprisingly, almost no functional gene sets were induced or repressed exclusively in young animals (Fig. 33B).

4.3.3 Stroke does not activate exclusive neuroprotective pathways in young compared to aged mice

Since we did not identify any unique gene set specifically responding in young mice, we took a step back and focused on individual genes that showed a greater upregulation in young mice compared to the aged group ("more up MCAO3", MCAO=FCI). We postulated that such genes may display a neuroprotective effect (considering the better outcome of stroke in young animals). We found that some genes do show upregulation upon FCI in young mice ($log_2FC_{young} >> log_2FC_{aged}$), almost all of them are also upregulated in aged CTRLs compared to young CTRLs (Fig. 34B, left) and their abundance levels in young stroke group do not rise above the levels in aged stroke group (Fig. 34B, right). Considering the inflammatory nature of these genes, the strong overlap with markers of aged and activated microglia (Hammond et al., 2019, Mathys et al., 2017, Mrdjen et al., 2018), as well as the presence of reactive astrocyte marker (*Gfap*), it is apparent that these genes reflect age-induced glial activation, which is partially saturated after stroke in aged mice. These results suggest that the group of genes showing stronger activation after ischemia in young animals does not involve exclusive neuroprotective pathways, but rather reflects the resting baseline level of microglia and astrocytes in young CTRL animals and a more polarized baseline state in aged CTRL animals.

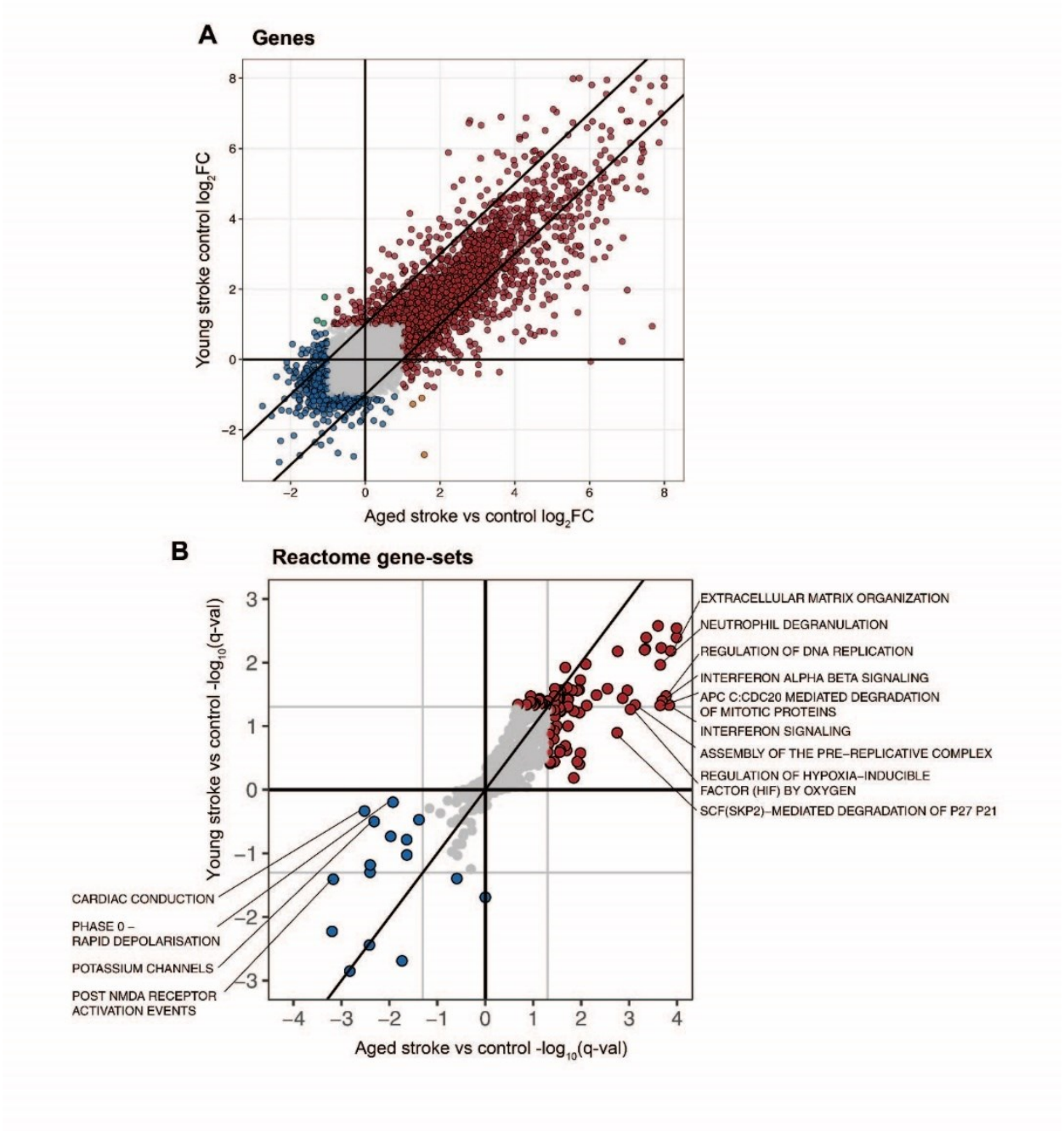

Figure 33: Comparison of differentially expressed genes and gene sets after ischemia between young and aged mice. A) Scatter plot comparing stroke-induced $\log_2$ fold-change in young and aged mice. Genes with $|\log_2 FC| > 1$ are highlighted in color. B) Scatter plot comparing ischemia-induced alteration of Reactome pathways in young and aged mice. Pathways wih q-val < 0.05 are highlighted in color. Sign depicts UP (+) or DOWN (-) regulation.

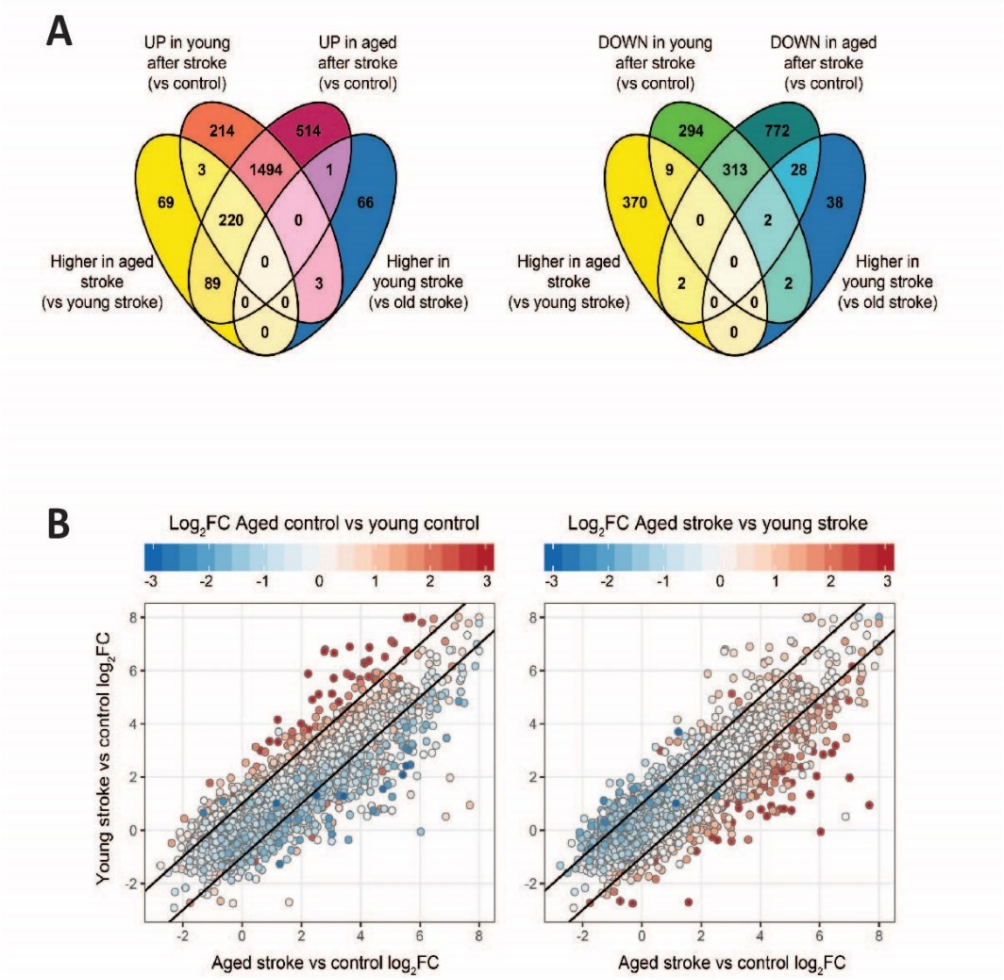

Figure 34: Comparison of differentially expressed (DE) gene sets after ischemia between young and aged mice A) Venn diagrams showing overlaps of DE genes between selected pairwise comparisons. B) Scatter plots of ischemia-induced $\log_2$ fold-change in young and aged mice. Color maps to $\log_2$ fold-change between aged and young controls (left) or between aged and young ischemia groups (right). Genes with larger stroke-induced upregulation in young mice tend to increase in expression during normal aging. Sign depicts UP (+) or DOWN (-) regulation.

4.3.4 Combination of aging and stroke leads to massive activation of type-I interferon signaling and aggravated inflammatory response

We then explored the genes showing upregulation after ischemic impact in aged mice, which are likely to have detrimental effects ("more up MCAO18"). There were more than 400 such genes, of which a great proportion were related to immune system (Fig. 35). GO and pathway enrichment analysis revealed T-cell activation, cell adhesion, chemotaxis and leukocyte migration, as the ones of the most strongly enriched functional clusters, suggesting an increased infiltration and activation of peripheral immune cells (Fig. 35). We found strong enrichment of genes associated with antigen processing and presentation, MHC class I, and cytokine secretion. Several signaling pathways, namely ERK/MAPK signaling and

cAMP/cGMP mediated signaling were also significantly enriched, as were the GO terms associated with lipid metabolism, transport of fatty acids and oxidative phosphorylation. Pathway enrichment showed clusters of extracellular matrix organization and cluster of pathways mediating regulation of cell cycle, suggesting that cellular proliferation may be increased in aged post-ischemic mice (Fig. 35). Genes that are more induced by ischemia in aged mice also significantly overlapped with several inflammation and aging associated signatures from the literature. However, an interesting feature was the strong overlap with the LPS-induced / A1 pro-inflammatory astrocytic profile. Previously, it has been reported that FCI induces a beneficial A2 astrocytic profile (Zamanian et al., 2012). Our result suggests this may not be the case in the aged brain, which would be consistent with reports that aging promotes inflammatory A1 profile of astrocytes (Clarke et al., 2012, Boisvert et al., 2018) and accelerates injury-induced astrocyte reactivity (Badan et al., 2003, Gordon et al., 1997, Popa-Wagner et al., 2007). Another striking characteristic was overrepresentation of ISG, indicating that specifically IFN-I signaling pathway is much strongly activated by ischemia in aged animals (Fig. 33A).

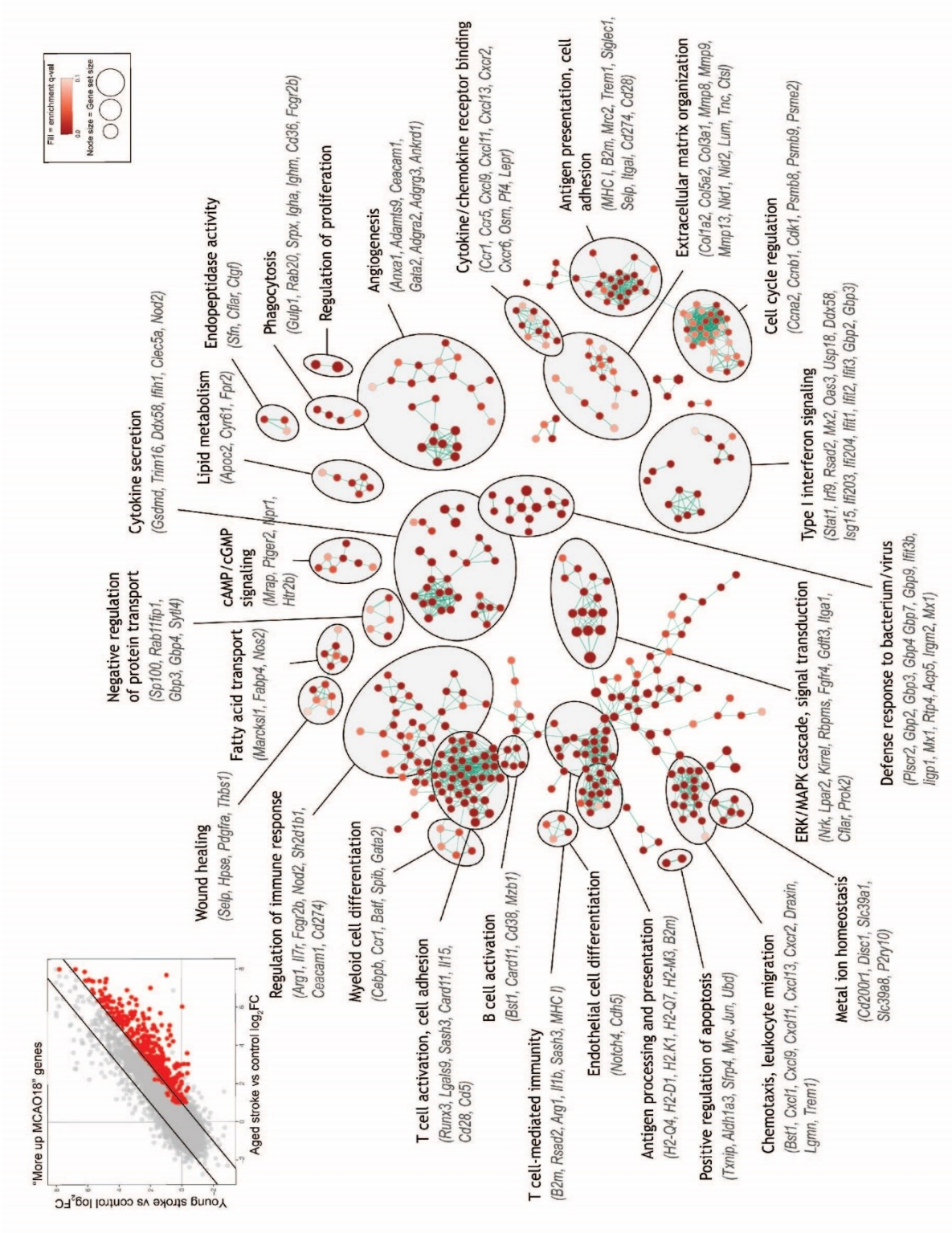

Figure 35: Functional annotation of genes with different quantitative response to ischemia between young and aged mice. Enrichment map showing significantly enriched gene ontology (GO) terms (circles) and pathways (hexagons) for genes with greater upregulation after ischemia in aged mice ("more up MCAO18"). Similar gene sets are grouped into sub-clusters and annotated manually.

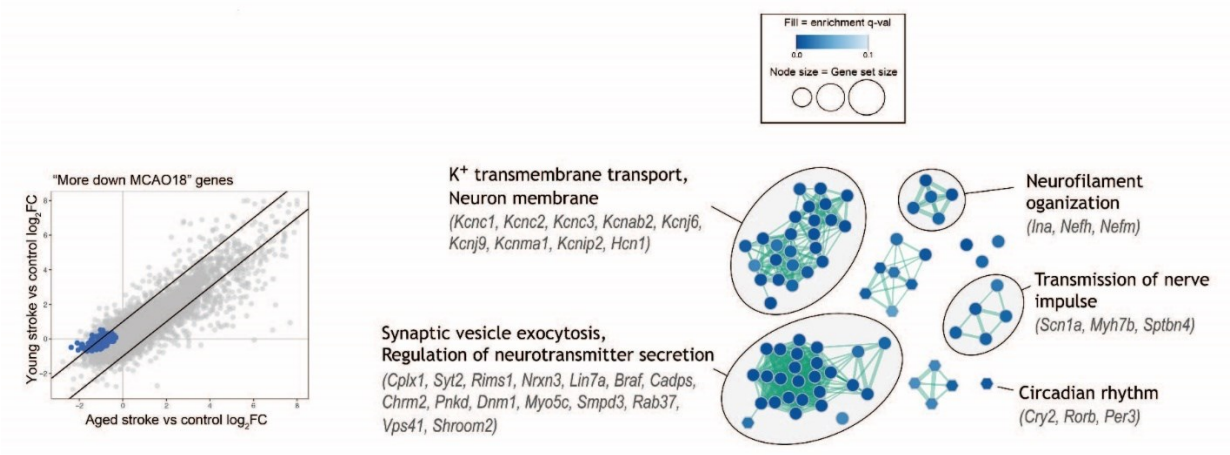

Figure 36: Functional annotation of genes with different quantitative response to ischemia between young and aged mice. Enrichment map showing significantly enriched gene ontology (GO) terms (circles) and pathways (hexagons) for genes with greater downregulation after ischemia in aged mice ("more down MCAO18"). Similar gene sets are grouped into sub-clusters and annotated manually.

In concordance to larger upregulation, aged mice also downregulated larger number of genes after ischemia, often with a greater magnitude ("more down MCAO18") (Fig. 36). Functional annotation of the "more down MCAO18" gene set showed significant enrichment of K^+ transmembrane transport (*Atp1b1, Hcn1*), voltage-gated K^+ channels (*Kcnc1, Kcnc2, Kcnc3, Kcnj6, Kcnj9, Kcnma1, Kcnt1*) and their regulatory subunits (*Kcnab2, Kcnab3, Kcnjp2*), neurofilament proteins (*Nefh, Nefm, Ina*) and genes involved in synaptic vesicle exocytosis regulation and neurotransmitter release (such as *Cadps, Pnkd, Lin7a, Braf, Dnm1, Rims1, Cplx1,Syt2, Nrxn3*) (Fig. 36). These genes mainly localize along the presynaptic and neuron projection membranes, indicating greater axonal damage and impaired synaptic communication in aged post-ischemic mice. "More down MCAO18" genes were also enriched with genes involved in the regulation of circadian rhythm (such as *Cry2, Rorb, Per3*). An impact of ischemic stroke on circadian rhythm has been observed before (Meng et al., 2008) and our results suggest that aged animals may be more susceptible to its destabilization, which is linked to sleep, mood and post-stroke depression, and may therefore impact recovery (Duss et al., 2017, Sterr et al., 2018). Overall, analysis of age-ischemia interacting genes revealed an increased neuroinflammatory environment in aged animals, which is connected to higher infiltration and activation of peripheral immune cells, pro-inflammatory cytokine secretion and activation of signaling pathways (ERK/MAPK, IFN-I) that may contribute to secondary injury. On the other hand, K^+ transmembrane channels, neurofilament and synaptic communication proteins were specifically repressed in aged animals.

4.3.5 Transcriptome deconvolution reveals cell type composition changes during aging and after stroke

In order to provide cell-specific context to the observed transcriptional profiles, we estimated relative changes of cell type proportions by computational deconvolution. First, we built a reference of cell-specific genes for major CNS cell types (for details see Methods). We then used the *markerGeneProfile* R package (Mancarci et al., 2017), which summarizes expression of multiple cell-specific genes into a single marker gene profile (MGP). To validate the estimates, we used transcriptome deconvolution algorithm CIBERSORT (Newman et al., 2015) (see Methods). Except for astrocytes, concordance analysis confirmed the robustness of the results. Closer inspection showed that astrocyte-specific genes do not significantly overlap with any DE geneset (Fig. 38A), and cluster into different co-expression modules (see below), which may be due to heterogeneity of astrocytic response or intrinsic transcriptional regulation of large part of astro-specific genes. To ease the interpretation, we report the relative changes in cell type proportions as MGPs selected by *markerGeneProfile* R package (Fig. 37).

We found a significant increase in the MGPs of all non-neuronal cell types following stroke in both age groups (p_{adj} < 2.2e-16; Fig. 37). The largest increase was in microglial and endothelial marker genes (log_2FC 1.26-1.77) and the lowest in oligodendrocytic markers (log_2FC 0.47-0.60), which also significantly increased with normal aging (p = 1.20e-19; Fig. 37). Glial marker genes had generally higher expression in aged ischemic group compared to young ischemic group, although the magnitudes of their activation by stroke were relatively comparable between both ages. The most prominent difference was in endothelial cell markers (log_2FC_{young} = 1.26, log_2FC_{aged} = 1.74), which were also significantly overrepresented among “more up MCAO18” genes (Fig. 38A). Furthermore, cell type proportion estimates revealed significant depletion of pyramidal/excitatory neurons during aging and following ischemia in both age groups (p_{adj} < 1.00e-06, log_2FC_{young} = -0.56, log_2FC_{aged} = -0.63, Fig. 37).

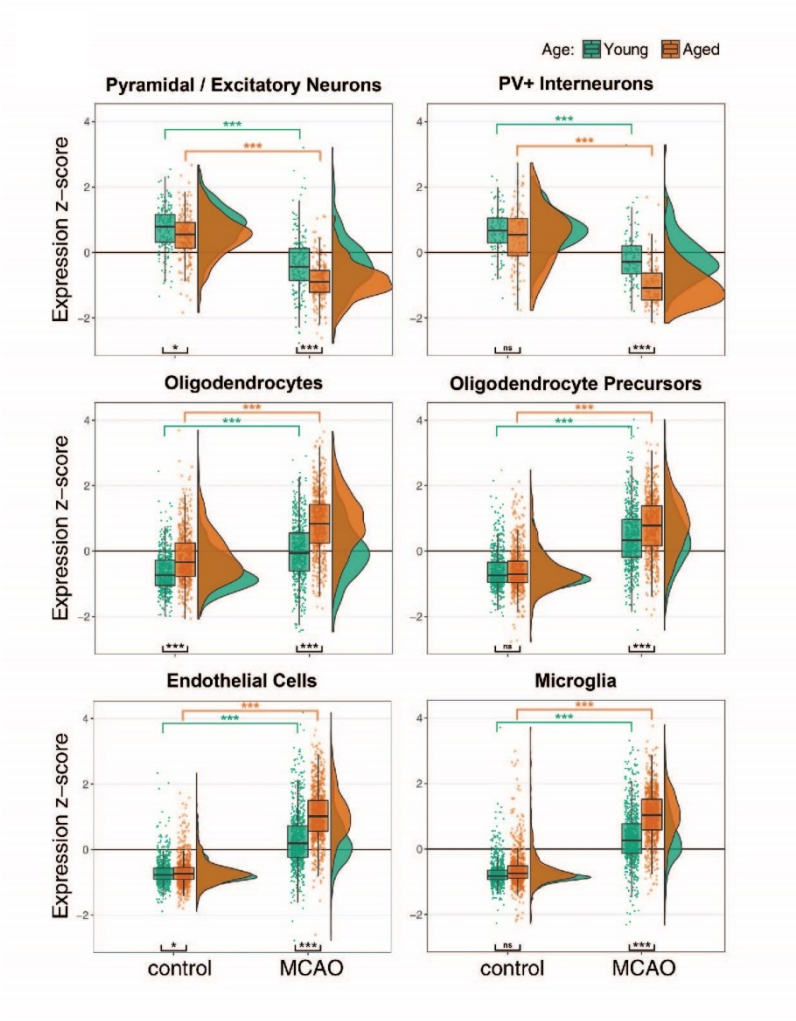

Figure 37: Cell type proportion estimation by transcriptome deconvolution. Raincloud plots showing z-scored expression of selected marker genes for major brain cell populations. Asterisks show Holm-corrected post-hoc t-test p-values.

4.3.6 Aged ischemic brain is characterized by selective downregulation of Parvalbumin$^+$ interneuron-associated expression and increased infiltration of peripheral leukocytes

Unlike pyramidal/excitatory neurons, parvalbumin-positive (PV^+) GABAergic interneuron markers were downregulated after FCI to a greater degree in aged animals (log_2FC_{young} = -0.42, log_2FC_{aged} = -0.89, $p_{interaction}$ = 6.22e-08; Fig. 37), which was supported by the significant overlap with "more down MCAO18" gene set (Fig. 38A), suggesting that this neuronal class may be particularly vulnerable to ischemia in aged mice. PV^+ interneurons play key roles in cortical plasticity and thus may have profound effect on post-ischemic recovery (Tsuiji et al., 2017, Hu et al., 2014). Testing for enrichment of independent set of marker genes of six phenotypically well-defined interneuron populations (Paul et al., 2017) also revealed significant overlap of "more down MCAO18" genes with markers of PV^+ fast-

spiking basket cells, but not other interneuron populations. Recently, it has been reported that decreased PV^+ signal may occur not only due to loss of PV^+ interneurons, but also transcriptional downregulation (Filice et al., 2016). For this reason, we counted the numbers of $NeuN^+$ and PV^+ cells by immunohistochemistry (Fig. 39A, B). We found that reduction of both $Neun^+$ and PV^+ cells after FCI was similar in both age groups, suggesting that the greater decrease of PV^+ associated expression in aged mice is a result of transcriptional downregulation, rather than greater PV^+ cell loss.

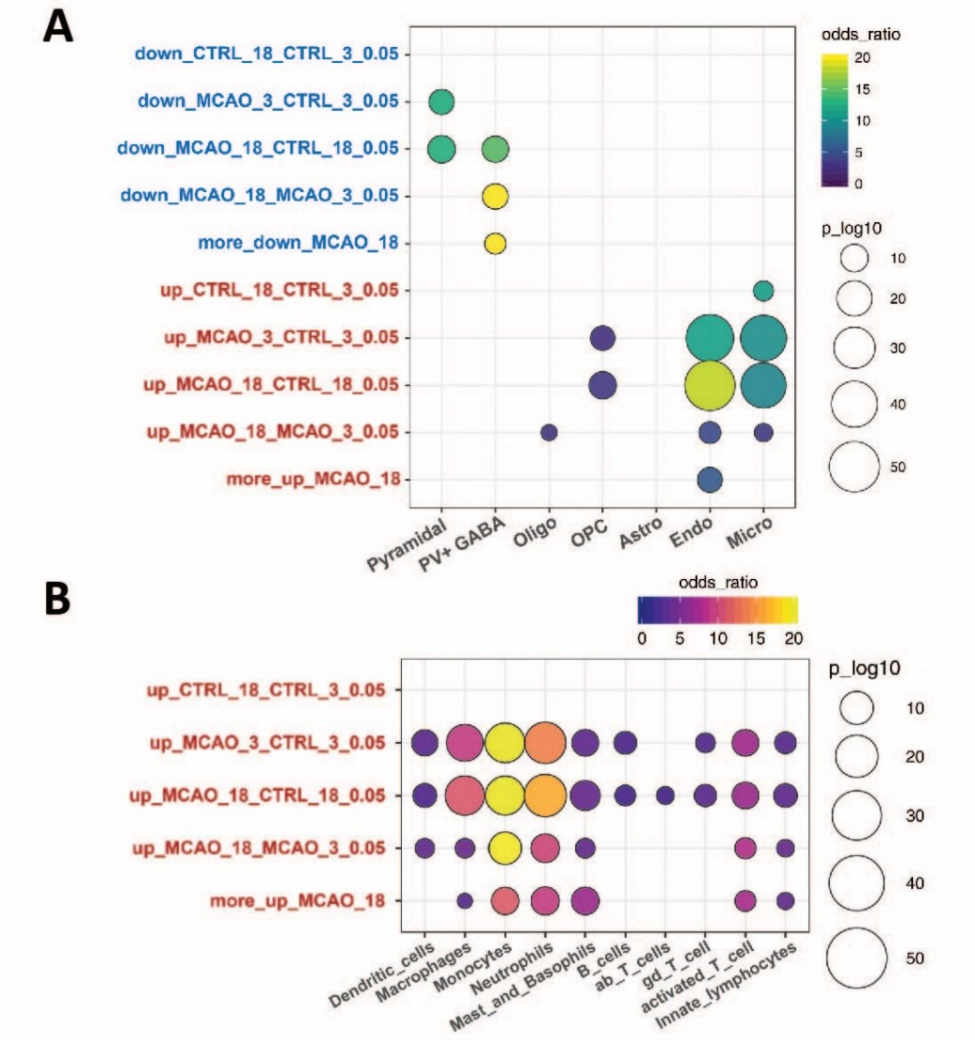

Figure 38: Cell type proportion estimation by transcriptome deconvolution. A) Overlap between cell marker gene sets and the sets of differentially expressed genes. B) Overlap between sets of aging/ischemia upregulated genes and the marker genes of the major leukocyte populations.

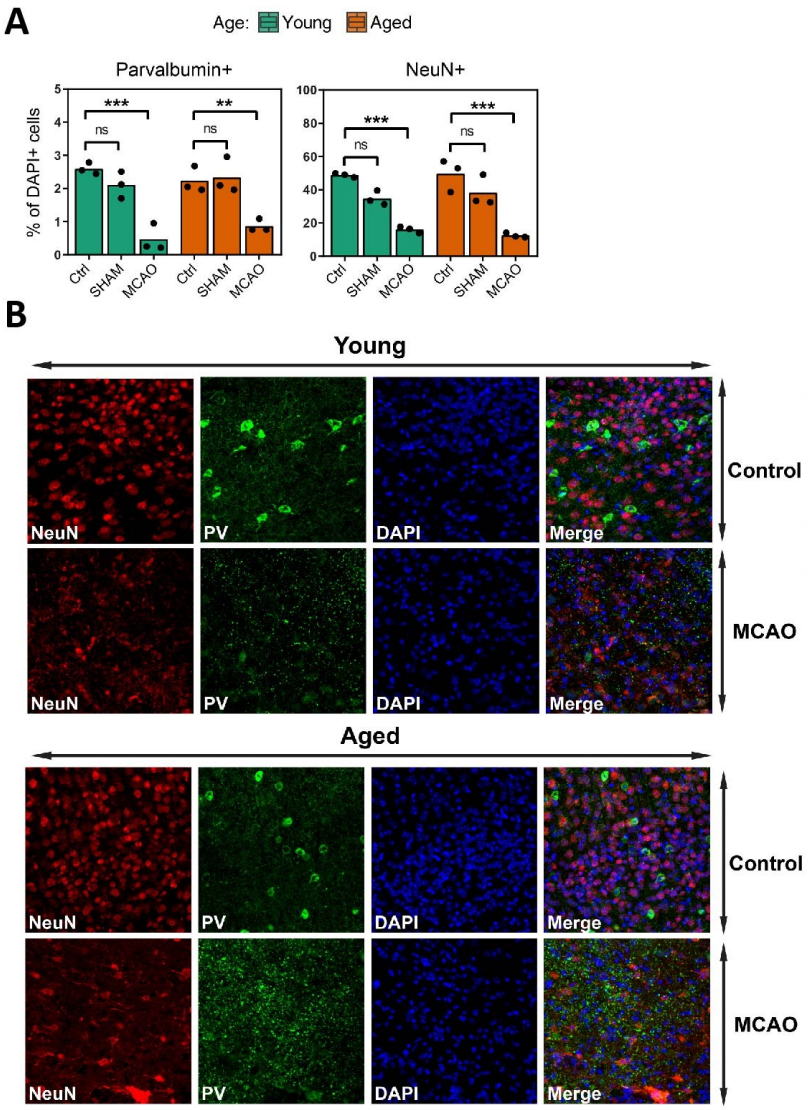

Figure 39: A) Immunohistochemical quantification of Parvalbumin (PV) and NeuN-positive cells. Asterisks show significance of Sidak-corrected post-hoc pairwise comparisons. Results of two-way ANOVA are shown on the right. B) Representative images of immunostaining for Parvalbumin (PV) and NeuN proteins in cortex of control and MCAO-treated young and aged mice. Significance codes (***) <0.001; (**) <0.01; (*) <0.05; (ns) >0.05.

Since peripheral immune cells can infiltrate the brain following the disruption of BBB after ischemia, we assessed their contribution by analyzing the overlap of DE gene sets with cell-specific genes of several leukocyte populations (Fig. 38B). Ischemia-induced genes in both age groups were highly enriched with macrophage-, monocyte- and neutrophil-specific genes ($p \leq 4.19e\text{-}14$) and less strongly with mast cell/basophil-, dendritic cell- and activated T-cell-specific genes ($p \leq 1.18e\text{-}5$). Taken together, the analysis of relative cell type proportions highlighted similarities including proliferation of non-neuronal cells (particularly of microglia and endothelial cells) and dissimilarities manifesting in greater

downregulation of PV^+ interneuron-associated expression, in response to stroke between the two age groups.

4.3.7 Age-dependent activation of type-I IFN regulatory modules after ischemia

A hallmark of the differential response of aged animals to ischemia was activation of IFN-I signaling pathway (Fig. 40A). IFN-Is are key antiviral cytokines that elicit prototypical ISGs encoding antiviral and inflammatory mediators (Owens et al., 2014) and also activate other signaling pathways including MAPK cascades, other cytokines, chemokines and cell-cell interaction modifiers (MHC-I, *Lgals9)* (Mostafavi et al., 2016). It has been showed that blocking the IFN-I signaling improves ischemia outcome in young mice (Zhang et al., 2017). IFN-I signaling may therefore act as the central player in the increased neuroinflammatory signature that we detected in the aged animal post-ischemia, worsening the neuronal injury.

To explore this signaling component in better detail, we verified the upregulation of ISGs in aged animals by mass spectrometry, showing that the observed changes are carried over to the protein level (Fig. 40B). We then mapped our expression data onto the recently published cross-species IFN-I regulatory network (Mostafavi et al., 2016) (Fig. 40C, D). IFN-I network is divided into five regulatory clusters (C1-C5) with functional differences and variable disease associations. Mapping our data against the network revealed that cluster C3 (composed mainly of antiviral effector genes) and C5 (enriched in inflammation mediators and regulators) were upregulated after FCI in both aged and young animals while the remaining three clusters were non-responsive (Fig. 40D). Of the two responsive clusters only cluster C3 was differentially induced between young and aged animals ($p = 3.63e\text{-}36$). C3 represents a supposed cluster containing predominantly genes under control of ISGF3 transcription factor complex composed of STAT1, STAT2 and IRF9 (Mostafavi et al., 2016). In accordance, several regulators of the C3 cluster including components of ISGF3 complex were part of "more up MCAO18" DE set (Fig. 40C), and the phosphorylation status of STAT1 and protein levels of STAT1 and IRF9 were increased (Fig. 40E).

4.3.8 Post-ischemic temporal dynamics of IFN-I signaling in young and aged mice

IFN-I signaling is typically characterized by rapid ISG induction, which is afterwards quickly attenuated by negative feedback mechanisms (Mostafavi et al., 2016). As the outcomes of the IFN-I signaling within the CNS may depend on a delicate balance (Blank and Prinz, 2017, Owens et al., 2014), we asked if the increased IFN-I signaling in the aged post-ischemic mice is due to constitutively greater expression or rather altered expression

dynamics relative to young mice. To answer this question, we analyzed the expression of IFN-Is, IFN receptors, ISGs and other selected genes by microfluidic RT-qPCR at several time points following FCI (Fig. 40F).

As expected, all 23 ISGs changed in a largely coordinated fashion throughout the time course, albeit with varying fold-changes (Fig. 40F). Expression of ISGs in young animals initially slightly decreased at three hours post FCI and then started to increase, with peak at seven days after FCI (average $log_2FC = 3.30$; n = 23 ISGs). In aged mice, the increase of ISG levels was on average four times greater at day one and day three compared to the increase in young animals. Unlike in young mice, the expression of ISGs did not further fluctuate, but remained at elevated levels until the latest investigated time point (14 days, average $log_2FC = 2.66$). Together, these results show that activation of IFN-I signaling occurs early, but not sooner than three hours after FCI, and both timing and overall magnitude of ISG expression are important factors in the different response of aged brain to ischemic injury.

4.3.9 Cell-specific analysis of IFN-I signaling in young and aged mice after ischemia

Stat1 activation in neurons (Takagi et al., 2002) and more recently increased IFN-I signaling in microglia (McDonough et al., 2017a) following transient MCAO have been demonstrated in young animals. However, little is known about the IFN-I signaling in other cell types following ischemia, and no cell type specific data are available in the aged brain. We have therefore focused on the key players in the brain inflammatory responses – glia and endothelial cells (Lecuyer et al., 2016) – and aimed to identify how they contribute to IFN-I signaling following stroke. We have FACS-sorted populations of astrocytes ($GFAP^+$), microglia ($CD11b^+$), oligodendrocytes ($O4^+$) and endothelial cells ($CD31^+$) from young and aged mice three days after FCI as well as from the age-matched controls and measured expression of ISGs and other selected genes by microfluidic RT-qPCR (Fig. 40G).

Microglia and oligodendrocytes heavily upregulated ISG expression following FCI in both young and aged animals (Fig. 40G). Endothelial cells displayed opposite behavior and significantly downregulated vast majority of measured ISGs in young, and to a much lesser extent in the aged mice. In astrocytes, 9 out of 23 ISGs were undetected. The expression of the remaining 14 ISGs did not change in a synchronized fashion, altogether showing a limited response of astrocytes to IFN after stroke in both age groups. In addition, astrocytes

and microglia, but not endothelial cells and oligodendrocytes, showed significant ISG upregulation with normal aging (Fig. 40G).

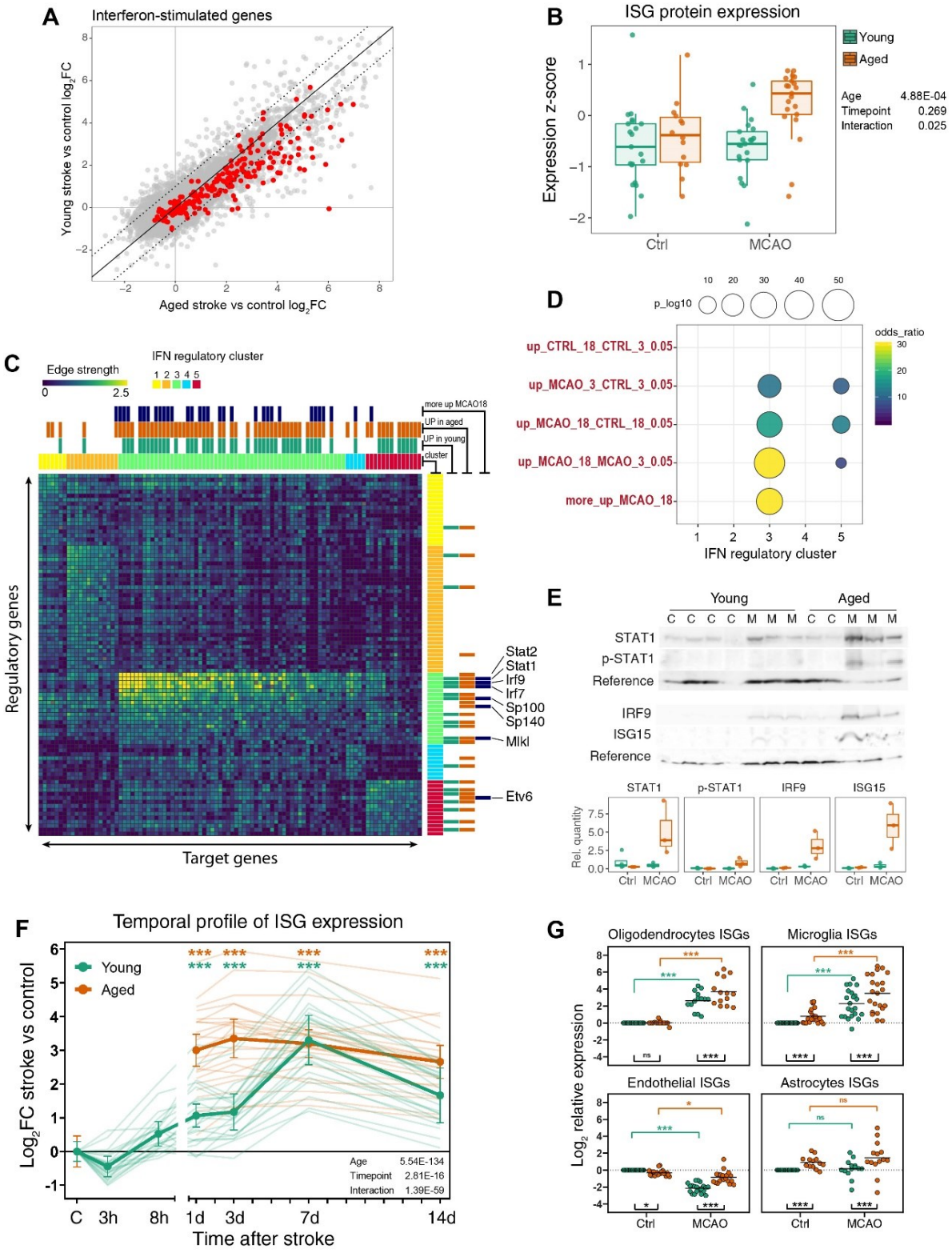

Figure 40: Transcriptional response of IFN-I signaling after ischemia in young and aged mice. A) Scatter plot of ischemia-induced $\log_2$ fold-change in young and aged mice. Highlighted is a set of 207 interferon-stimulated genes. B) Z-scored protein expression of ISGs from "more up MCAO18" gene set measured by quantitative mass spectrometry. N = 7 proteins. P-values for each factor and their interaction are shown at the right (linear

mixed model). C) Heatmap of IFN-I network regulatory links between regulators (kinases, phosphatases, transcription factors) and target genes reconstructed from (Mostafavi et al., 2016). Binarized mapping of genes to ischemia-upregulated gene sets in young/aged mice is shown on top and right. D) Enrichment of IFN-I regulatory network clusters from (Mostafavi et al., 2016) in aging/ischemia upregulated gene sets. E) Western blot analysis of STAT1, p-STAT1, IRF9 and ISG15 proteins. C = control, M = MCAO. F) Time-course analysis of ISG expression after stroke in young and aged mice. Bold line shows average expression of 23 ISGs measured by RT-qPCR. Error bars show standard deviation of biological replicates (n = 2-5). Thin lines show average expression of each gene. Asterisk show significant difference relative to control for each age separately (mixed model with post-hoc t-tests). Mind the break in x-axis. Due to limited number of 18-month-old animals, 3h and 8h time points were omitted for the aged group. G) ISG expression in purified cell populations 3 three days after FCI from young and aged mice. Asterisks show Holm-corrected post-hoc t-test p-values. Significance codes: (***) <0.001; (**) <0.01; (*) <0.05; (ns) >0.05.

5 DISCUSSION

5.1 Proliferation and differentiation potential of NG2 glia following FCI

The was majority of studies about proliferation, differentiation and maturation of oligodendrocytes and their precursors under physiological and pathological conditions focus on oligodendroglial lineage in context of myelination/remyelination (Spitzer et al., 2016, Hughes and Appel, 2016, Chamberlain et al., 2016, Wheeler and Fuss, 2016). Nonetheless, there are some evidences about NG2 glia ability to give rise to the other cell type beside the oligodendrocytes during development or after injury, such as FCI, SW injury or demyelinating injury (Zhu et al., 2008, Tripathi et al., 2010, Zawadzka et al., 2010, Honsa et al., 2012, Dimou et al., 2008). Therefore, we analyzed the gene expression profile of NG2 glia from the ischemic mouse brain. This analysis revealed the heterogeneity of NG2 glia, which becomes much greater after FCI. We identified four phenotypically distinct subpopulations of NG2 glia emerging after FCI and concluded that NG2 acquired FCI-induced multipotent character.

5.1.1 tdTomato$^+$ cells expression pattern in uninjured cortex

We detected several differences in the expression pattern of genes, which are generally considered as astrocyte-specific, between NG2 glia and oligodendrocytes. Dramatically higher expression of *Slc1a2* and *Slc1a3* in NG2 glia compared to oligodendrocytes fits well with the results of (DeSilva et al., 2009, Martinez-Lozada et al., 2014) who showed that glutamate transporters are expressed in the white matter NG2 glia and play a role in the regulation of oligodendrocyte maturation and differentiation. The widespread role of glutamate and its receptors in oligodendroglial lineage was reviewed by (Spitzer et al., 2016). In our analysis we detected the expression of glutamate receptors predominantly in NG2 glia. Interestingly we observed the DE glutamate receptors: mGlur 3 and 5. The expression of both glutamate receptors on mRNA as well as functional level was shown earlier and their role in proliferation and differentiation of oligodendroglial cells was suggested (Marques et al., 2016, Luyt et al., 2003, Haberlandt et al., 2011). As mGlur5 was shown to enhance proliferation and mGlur3 inhibits it, the oligodendroglial *Grm5*/*Grm3* developmental switch fits well with the precursor nature of NG2 glia compared to oligodendrocytes and represents novel possibility to distinguish between these two types.

5.1.2 Multipotency of NG2 glia contributes to glial scar formation

Following CNS injuries NG2 glia start to proliferate massively and migrate to the site of injury (Anderova et al., 2011, Sirko et al., 2013). Besides that, NG2 glia are able to differentiate into reactive astrocytes; however, the rate of differentiation is injury-dependent as reviewed by (Dimou and Gallo, 2015). Here we identified three subpopulations of NG2 glia emerging following FCI, which are phenotypically distinct from uninjured NG2 glia. Whereas the most P-NG2 cells and A-NG2 cells were detected three days after FCI, OL-NG2 cells peaked at day seven after FCI. These results suggest that FCI induces preferentially rapid proliferation of NG2 glia and their participation in glial scar formation rather than generation of new oligodendrocytes.

Interestingly, using the post-ischemic TX scheme, we observed very little OL-NG2 cells and no A-NG2 cells. The vast majority of the identified cells were P-NG2 glia, which fits well with the massive increase in the number and proliferation rate of NG2 glia three days after ischemia (Anderova et al., 2011, Simon et al., 2011, Honsa et al., 2012). A complete absence of A-NG2 cells encouraged us to think that they might be the phenotypically most distinct subpopulation among all NG2 glia. Besides that, this result negates the possibility that reactive astrocytes could start express *Cspg4* after FCI, otherwise we would detect them. The differentiation of NG2 glia into reactive astrocytes is modulated by Shh signaling activation/inhibition as was showed previously (Honsa et al., 2016). Since the Smo agonist was shown to increase the number of NG2 glia-derived astrocytes and about 40 % of P-NG2 cells express this agonist, we hypothesized that activation of smoothened in P-NG2 cells favors their asymmetric division to form new NG2 glia and NG2 glia-derived astrocytes.

5.2 Appearance of NG2 glia-derived astrocytes between different types of CNS disorders

The capacity of NG2 glia to proliferate and differentiate into other cell types has been extensively investigated in several genetically modified mice (Zhu et al., 2008, Zhu et al., 2011, Kang et al., 2010, Huang et al., 2018, Huang et al., 2019, Huang et al., 2014, Guo et al., 2009, Aguirre and Gallo, 2004). It is generally accepted that NG2 glia are restricted to the oligodendroglial lineage (Kang et al., 2010, Zawadzka et al., 2010), but numerous reports describe their differentiation into astrocytes (Huang et al., 2019, Huang et al., 2014, Honsa et al., 2012, Honsa et al., 2016, Dimou et al., 2008). However, the majority of such studies only focuses on one type of injury, such as ischemia (Honsa et al., 2012), cortical SW (Komitova et al., 2011), or a demyelinating injury (Zawadzka et al., 2010). Therefore, it is

difficult to compare these studies which employed various types of cre transgenic mice, different modes of TX administration, and different identification of cell types. In this study, we analyzed NG2 glia and the cells derived from them, under physiological and pathological conditions in Cspg4/tdTomato mice. This approach allowed us to compare NG2 glia heterogeneity after different types of CNS disorders (FCI, SW, DEMY), without any inter-lab variability. Four subpopulations of NG2 glia and four subpopulations of oligodendrocytes that differed according to the region of the brain or type of injury, were identified. In this study, we have proven that the unique subpopulation of astrocyte-like NG2 glia only emerges following FCI, while these cells appear in negligible numbers following SW and DEMY. Using the RNA-Seq and patch-clamp technique, we characterized astrocyte-like NG2 glia as cells which are very active in the cell cycle, and display a current pattern similar to that observed in cortical astrocytes. Our findings suggest that astrocyte-like NG2 glia may represent important players in glial scar formation and the CNS repair process. For the reason that astrocytes do not migrate toward lesion and only a limited number of astrocytes divide (Sofroniew and Vinters, 2010), astrocyte-like NG2 glia could temporarily perform the functions of astrocytes in the vicinity of the lesion.

5.2.1 NG2 glia and oligodendrocytes in the uninjured brain

The difference between NG2 glia and oligodendrocytes starts on the gene expression level. Many studies described a transcriptional continuum between oligodendrocyte populations and their marker genes (Marques et al., 2019, Marques et al., 2016). Our present study is in accordance with the very well-known expression of classic marker genes (*Cspg4, Pdgfra, Mbp, Cldn11*), but suggests the reevaluation of genes that are considered to be marker genes of astrocyte (*Glul, Slc1a3, and Slc1a2*). We also proposed *Hcn2* as the other typically expressed gene in mature myelinating oligodendrocytes, however, to the best of our knowledge there are no reports on *Hcn2* functioning in oligodendrocytes. We confirmed that oligodendroglial lineage cells, at all stages, express glutamate receptors, enabling them to sense and respond to neuronal activity (Spitzer et al., 2016). However, NG2 glia had the highest expression of subunits of ionotropic glutamate receptors compared to oligodendrocytes, in accordance with other studies (De Biase et al., 2010).

5.2.2 Region-specific differences of NG2 glia

Whether NG2 glia represent regionally distinct cell populations is still controversial but regardless, NG2 glia differ in their capability to differentiate into myelinating

oligodendrocytes. For example, NG2 glia from the CC differentiate into myelinating oligodendrocytes more efficiently than NG2 glia from the CTX (Viganò et al., 2013). In line with this, the electrophysiological studies reported that NG2 glia start out as a homogeneous population but become functionally heterogeneous, depending on both the brain regions as well as aging (Spitzer et al., 2019, Chittajallu et al., 2004). It seems that NG2 glial regional heterogeneity is determined by environmental factors rather than being solely regulated by the intrinsic mechanisms or developmental stages (Spitzer et al., 2019). In agreement with the recent work of Marques and coauthors (Marques et al., 2016), we found hardly any differences in the transcriptional profile on NG2 glia between CTX and CC (Fig. 23B). However, after merging all the cells from the uninjured and injured brain, we identified four subpopulations; one of them (NG2 glia (S1)) was not equally distributed between these two regions. Based on our findings (Fig. 25A, B, E) and previous findings from Castelo-Branco`s group (Marques et al., 2018), we consider NG2 glia (S1) less mature when compared to NG2 glia (S2), because they display reduced expression levels in the 20 genes. Interestingly, the incidence of NG2 glia (S1) was significantly higher in the CC, which was not the case in the CTX (Fig. 26A). Since it is well known from previous studies that NG2 glia from white matter have a shorter cell cycle and faster differentiation into oligodendrocytes compared to NG2 glia from gray matter (Young et al., 2013), we hypothesize that the different level of expression of these genes, between NG2 glia subpopulations in the CTX and CC, could serve for predicting their future fate. Thus, a decreased expression of given genes in NG2 glia (S1) may indicate a shorter cell cycle and suitability for differentiation into oligodendrocytes, despite they still do not present oligodendrocyte markers.

5.2.3 Formation of a transient subpopulation of astrocyte-like NG2 glia occurs following focal cerebral ischemia

Three out of four subpopulations of NG2 glia were always present in the uninjured, as well as in the injured, brain. Since a specific subpopulation of astrocyte-like NG2 glia, which emerges following FCI, was already reported in our previous publications (Honsa et al., 2016, Valny et al., 2018) here we clearly state that astrocyte-like NG2 glia represent a unique, FCI-specific subpopulation. It is neither present in the other two types of injuries (DEMY, SW), nor in neurodegenerative diseases such as AD (Valny et al., 2018). The subpopulation of astrocyte-like NG2 glia is not permanent and it disappears during the progression of glial scar, most likely at the expense of NG2 glia subpopulation 2. Nevertheless, it suggests that for a certain period following ischemia, NG2 glia are

multipotential and represent, together with astrocytes, crucial players in post-ischemic regeneration. Some studies demonstrated that NG2 glia can differentiate into reactive astrocytes in addition to their proliferation potential (Dimou et al., 2008, Honsa et al., 2016, Huang et al., 2018, Huang et al., 2014, Komitova et al., 2011), but none of them compared their astrocytic differentiation potential among different types of injuries which would elucidate whether this phenomenon is injury-specific. It has still not been clarified what factors contribute to the differential switch of NG2 glia towards the astrocytic phenotype. Our previous studies suggested Sonic hedgehog as a potential modulator (Honsa et al., 2016), however, additional studies are needed to understand the reprogramming of NG2 glia from oligodendrogenesis to astrogliogenesis. Since massive astrogliosis and inflammation occur following ischemia and have a great impact on the repair processes (Magaki et al., 2018), we hypothesize that the immune response, together with astrogliosis, may only initiate NG2 glia transient increase of astrocytic markers in severe types of CNS injuries. Recent findings show that bone morphogenic protein, which is secreted by astrocytes, inhibits the generation of myelinating oligodendrocytes, and promotes differentiation into the astrocyte phenotype (Magaki et al., 2018). Moreover, neuroinflammatory factor interferon-γ prevents NG2 glia from generating oligodendrocytes, and leads to an increased tendency to generate astrocytes (Tanner et al., 2011). Astrocyte-like NG2 glia, characterized by a high expression of genes typical for reactive astrocytes (*Vim, Gfap*), proliferation (*MKi67*), and motility (*Dcx*) seven days following ischemia, indicate that NG2 glia significantly contribute to the glial scar formation prior to the generation of oligodendrocytes 14 and 22 days following FCI. It is not clear why cortical SW, which also leads to marked astrogliosis and microglia activation, does not result in a similarly increased number of astrocyte-like NG2 glia. A possible explanation for their unique generation following ischemia may dwell from the diverse concentrations of extracellular glutamate/K^+, that occur during FCI and SW (Anderová et al., 2004, Hansen, 1978) and may result in a diverse severity of these CNS injuries.

5.2.4 Oligodendrocytes derived from NG2 glia

Oligodendrogliogenesis is the most noted feature of NG2 glia and therefore, oligodendrocytes and their different stages of maturation are an integral part of NG2 glia differentiation. We detected four subpopulations of oligodendrocytes in the uninjured and injured mouse brain. These types of cells cease to express genes typical of NG2 glia and start to express typical markers of oligodendrocytes. Additionally, oligodendrocytes start to

express a variety of genes such as *Glul, Grm3,* and *Hcn2.* These genes have a great predisposition to become indicators of oligodendrocyte maturation, apart from the classic markers. The distribution of these four oligodendrocyte subpopulations was comparable in the uninjured brain, which was not the case in the injured brain. The subpopulation of immature oligodendrocytes was significantly higher after FCI, when compared to its corresponding CTRL (CTX), but also to DEMY CTX or SW. This suggests that the onset of the remyelination processes starts earlier after DEMY CTX and SW, unlike after FCI. It has been shown that proliferation/differentiation of NG2 glia in the CPZ model of DEMY begins during the administration of CPZ, and remyelination is completed approximately 4 days after its administration (Gudi et al., 2014). In contrast, proliferation and differentiation of NG2 glia only start 2-4 days after FCI (Zhang et al., 2010). For this reason, we suggest that there is a possible shift between the differentiation and final maturation of oligodendrocytes among injuries.

5.2.5 Astrocyte-like NG2 glia can be identified by immunohistochemistry

The different time window of proliferation and differentiation of NG2 glia is well documented by our immunohistochemical analyses. Employing a frequently used marker of proliferation KI67, we demonstrated that seven days after injury, the proliferation is only increased after the BBB-damaging CNS disorders (FCI, SW), while no proliferation was detected after CPZ-induced DEMY. These results suggest an earlier proliferation of NG2 glia, which cannot be detected at seven days after the withdrawal of the CPZ diet but is detectable following FCI and SW. Proliferation cell nuclear antigen staining showed results that do not correlate with KI67 staining. Based on the PCNA staining following all injuries, NG2 glia proliferate and, following DEMY, even more than after FCI and SW. The expression of KI67 and PCNA occurs during very similar phases of the cell cycle (G1/S), which makes them both good markers of cell proliferation. Nevertheless, the fundamental difference is that PCNA has an essential role in nucleic acid metabolism, as a component of the DNA replication and repair machinery (Juríková et al., 2016, Shivji et al., 1992, Essers et al., 2005). This marker therefore represents a less specific proliferation marker, due to its redundant role in the DNA repair. Thus, the immunohistochemical detection of PCNA may not only locate actively dividing cells, but also those undergoing DNA repair (Haneda et al., 1991), which explains the detection of this marker after all types of injury.

To inspect oligodendrogliogenesis, we used the cell-body marker of oligodendrocytes APC. The formation of new oligodendrocytes following FCI and DEMY, did not change

compared to their corresponding CTRLs. Nevertheless, in the uninjured brain there is a higher percentage of newly formed oligodendrocytes in the CC, when compared to the CTX, and a similar trend was identified in these regions following DEMY. These findings correlate very well with the results of Baxi et al., who showed that the dynamics of NG2 glia differentiation varies significantly between white and gray matter. While NG2 glia rapidly repopulate white matter and mature into APC+ oligodendrocytes, differentiation in the gray matter occurs much slower (Baxi et al., 2017). The higher percentage of new oligodendrocytes derived from NG2 glia, surprisingly proved to be in SW. We have already shown that FCI and SW are incomparable injuries, with respect to the appearance of astrocyte-like NG2 glia. A possible explanation for this is that following FCI, these cells develop at the expense of NG2 glia (S2), while in SW, where astrocyte-like NG2 glia are not present, NG2 glia (S2) further differentiate towards a more advanced stage of oligodendrogenesis, specifically oligodendrocyte-like NG2 glia. In addition, the fact that NG2 glia generate transient astrocyte-like NG2 glia following FCI was confirmed on the protein level by immunohistochemical analysis using GFAP, ALDH1L1, and VIM markers. $GFAP^+$ cells arising from NG2 glia were solely present after FCI, and these cells were not positive for another widely used marker, ALDH1L1, and only minimally for VIM. Even though this marker appears to be abundant in the large spectrum of astrocytes, it seems that not all $GFAP^+$ astrocytes necessarily express ALDH1L1 (Hackett et al., 2018).

5.2.6 Astrocyte-like NG2 glia are one of the players in the ischemic glial scar

The unique subpopulation of astrocyte-like NG2 glia detected only after FCI has never been deeply explored, and the role of these cells still needs to be fully explained. Few studies have also reported on NG2 glia as positive for astrocyte markers. The expression of GFAP in astrocyte-like NG2 glia could be a sign of their ability to create fully functional astrocytes. Therefore, using RNA-Seq and the patch-clamp technique, we aimed to reveal some of their properties and functions in the ischemic lesion.

The subpopulation of astrocyte-like NG2 glia expressed typical markers for NG2 glia (*Pdgfrα, Cspg4, Gpr17, Emid1*) and astrocytes (*Aqp4, Glul, Gja1, Gjb6*). In addition, we also found genes that were typical of astrocytes within top10 DE genes, such as *Top2a* or *Hells* (Zhang et al., 2014, Cahoy et al., 2008). This list also clearly included genes typical for NG2 glia, such as *Ube2c, Rrm2, Pbk, Birc5, Spc24* (Zhang et al., 2014, Cahoy et al., 2008). The differentially expressed genes of astrocyte-like NG2 glia, suggest that this group of cells is highly involved in mitotic cell cycle division, chromosome segregation, and

cellular stress response, which makes this subpopulation very active at the border of the ischemic lesion. A similar subpopulation, called OPC cycling, found by the Castelo-Branco`s group (Marques et al., 2018) had 18.4 % of the genes in common with our astrocyte-like subpopulation. One of the common genes is *Gpr17*, often associated with NG2 glia after injury. The subpopulation of NG2 glia expressing *Gpr17* participates in the cell proliferation in the post-acute stages after injury (Boda et al., 2011) and migrates towards the lesion; however, most of these cells remain undifferentiated (Bonfanti et al., 2017). Since the *Gpr17* expression is downregulated when NG2 glia complete their final maturation, it could highlight its involvement in NG2 glia multipotency. Less pronounced but still significantly upregulated in astrocyte-like NG2 glia, are the processes of positive regulation of cell communication, cell differentiation, and cell migration, suggesting that these cells play a key role in glial scar formation, together with astrocytes and classic NG2 glia. Astrocytes in the glial scar show a strong GFAP expression, obvious hypertrophy, and a certain degree of proliferation (He et al., 2020). Similarly to astrocyte-like NG2 glia, a series of stress reactions, including inflammatory reaction and cell division, are triggered after CNS injury, impairing astrocytic metabolism, which accelerates the aggregation, migration, and proliferation of reactive astrocytes (Mori et al., 2008, Zhu and Dahlström, 2007). Based on the *MKi67* level, as well as its incidence in astrocyte-like NG2 glia, we can conclude that they divide considerably (Valny et al., 2018) and, therefore, should be considered important contributors to the glial scar formation. Moreover, since these cells express *Gfap*, a key player in the formation of the glial scar (Nawashiro et al., 2000), astrocyte-like NG2 glia should be taken into consideration in the nervous tissue repair/regeneration via manipulating the glial scar.

Finally, we estimated the basic electrophysiological properties of astrocyte-like NG2 glia and revealed that these cells display passive membrane properties and current patterns, that are comparable with those observed in cortical astrocytes. They have significantly reduced K_{DR}, K_{IR}, and K_A current densities when compared to NG2 glia, while they do not differ from those obtained in cortical astrocytes. Interestingly, passive membrane properties of all three cell types were not significantly different. However, we cannot exclude the possibility that astrocyte-like NG2 glia may have sets of ion channels participating in their passive conductance different from astrocytes, in which two-pore domain K^+ channels play an important role (Zhou et al., 2009). More detailed studies are needed to precisely characterize the electrophysiological properties of astrocyte-like NG2 glia, as they may represent important cellular elements of post-ischemic tissue.

5.3 Interaction between stroke and aging at the genome-wide level using model of FCI

We systematically analyzed the impact of aging, stroke, and their interaction on genome-wide expression profiles. Several studies documented that inflammation is increased in the aged brain (Benayoun et al., 2019, Cribbs et al., 2012, Ori et al., 2015), and it has been reported that the changes occur predominantly in glial cells (Davie et al., 2018, Soreq et al., 2017). Our results are in concordance with these reports as we detected upregulation of large number of pro-inflammatory genes with normal aging. For example, it is known that activated microglia can promote astrocyte reactivity through secretion of modulatory factors (Liddelow et al., 2017), and thus further amplify the neurotoxic environment. It means that these changes probably may sensitize aged brain toward more severe stroke and secondary injury.

5.3.1 Aged ischemic brain is characterized by selective downregulation of Parvalbumin$^+$ interneuron-associated expression

Next, we investigated how adult and aged brain responds to ischemia. The evaluation of cellular differences revealed that genes enriched in PV$^+$ GABAergic interneurons are more greatly downregulated in aged mice after ischemia. Dysfunction or loss of PV$^+$ interneurons is implicated in the pathology of numerous neuropsychiatric disorders, including schizophrenia (Del Pino et al., 2013, Lewis et al., 2005), AD (Verret et al., 2012), and depression (Sauer et al., 2015, Zhou et al., 2015b). Our immunohistochemical analysis showed no change in PV$^+$ cell numbers between age groups, suggesting that decreased PV+ signal may occur through transcriptional downregulation. A similar result was reported in mouse model of autism, where decrease of PV$^+$ signal, previously interpreted as loss of PV$^+$ interneurons, occurs through transcriptional downregulation (Filice et al., 2016). In addition, molecular profiling of the brain at the single-cell level identified correlation between genes underlying axonal and presynaptic functions, preferentially active in PV$^+$ interneurons (Saunders et al., 2018). As the genes are implicated in axonal and synaptic maintenance and transmission, their greater downregulation in aged mice after ischemia may impact the excitation/inhibition balance and neuronal plasticity and thus functional recovery (Carmichael, 2012).

5.3.2 Stroke does not activate exclusive neuroprotective pathways in young compared to aged mice

Surprisingly, we did not detect any exclusive or greater activation of neuroprotective genes in young mice compared to aged mice. Instead, ischemia in young mice induced similar pro-inflammatory signals in activated glia that are already upregulated with normal aging. On the other hand, in aged post-ischemia mice we found markedly stronger upregulation of >400 genes, many of them involved in the processes of the inflammatory cascade. This was accompanied by a greater influx of peripheral leukocytes, particularly neutrophils, which are the strongest producers of ROS and matrix metallopeptidases (MMPs) and promote neuronal injury and BBB disruption (Allen and Bayraktutan, 2009, Strecker et al., 2017, Turner and Sharp, 2016). In agreement, an increased number of neutrophils with changed phenotypic responses was previously seen in aged male mice and human stroke patients compared to their younger counterparts (Ritzel et al., 2018), and an increased neutrophil to lymphocyte ratio has been associated with stroke severity and outcome (Asano et al., 2016). Despite the fact we did not detect any neuroprotective signal in bulk tissue, this does not rule out the possibility of its presence in individual cell types. Our results propose that an increased neuroinflammation and infiltration of circulating immune cells are one of the primary drivers for the exacerbated pathology in aged mice. Genes that were more induced by ischemia in aged mice also significantly overlapped with several inflammation- and aging-associated signatures from the literature. One of them was the strong overlap with the LPS-induced/A1 pro-inflammatory astrocytic profile. Previously, it has been reported that MCAO induces a beneficial A2 astrocytic profile (Zamanian et al., 2012). Our result showed this may not be the case in the aged brain, where the aging promotes inflammatory A1 profile of astrocytes (Boisvert et al., 2018, Clarke et al., 2018) and accelerates injury-induced astrocyte reactivity (Badan et al., 2003, Popa-Wagner et al., 2007, Gordon et al., 1997).

5.3.3 Age-dependent activation of type-I IFN regulatory modules after ischemia

An outstanding feature of differential response of aged animals to ischemic stroke was upregulation of IFN-I pathway, which persisted for at least 14 days. IFN-Is are antiviral cytokines with pleiotropic roles (Prinz and Knobeloch, 2012) implicated in a number of CNS pathologies including MS (Goldmann et al., 2015, McDonough et al., 2017b), ALS (Wang et al., 2011), AD (Friedman et al., 2018, Frigerio et al., 2019, Taylor et al., 2014), spinal cord injury (Roselli et al., 2018), traumatic brain injury (Abdullah et al., 2018, Karve et al., 2016), and ischemia (Chen et al., 2014, McDonough et al., 2017a, Zhang et al., 2017).

Therefore, we have analyzed INF-I signaling in more detail and found that two IFN-I regulatory modules are activated by ischemia irrespective of age, but only the canonical STAT-dependent module is differentially activated in aged animals, likely contributing to an increased neurotoxicity (Zhang et al., 2017). Indeed, *Stat1* and *Irf9* have deleterious roles in ischemia and can act directly on neurons (Chen et al., 2014, Takagi et al., 2002). ISG activation typically requires both IFNAR1 and IFNAR2 receptor subunits (Ivashkiv and Donlin, 2014). Recently, the IFNAR2- and STAT-independent pathway, triggered by IFNβ, was shown to be involved in systemic LPS-induced toxicity (de Weerd et al., 2013). While the genetic or pharmacological blocking of IFNAR1 leads to neuroprotection after transient MCAO (Zhang et al., 2017), the same study reported no effect in IFNAR2−/− mice. This involves the compensatory IFNAR2- and STAT-independent pathways after ischemia, although it has not been explored in aged animals. Our finding of a predominant increase in the IFNAR2- and STAT-dependent module in aged animals suggests that the detrimental effects of IFN-I signaling after stroke may be caused by ISGs that are common to the IFNAR2/STAT-dependent and independent pathways.

5.3.4 Cell-specific analysis of IFN-I signaling in young and aged mice after ischemia

As the cell-specific context to the IFN-I signaling after ischemia has not been well described in the literature, we profiled the responses of the glia and endothelial cells—known as key players in CNS neuroinflammation (Lecuyer et al., 2016). Our results support the perspective that not only microglia, but also oligodendrocytes are active players in the acute inflammatory response after ischemia. On the contrary, endothelial cells expressed the highest levels of ISGs under control conditions, they downregulated IFN-I pathway after ischemia. This discrepancy may be associated with different roles of IFN-I signaling in the endothelial cells, in line with the role IFNb plays in the maintenance of the BBB integrity (Owens et al., 2014).

Analyzed cell populations are not solely contributors of increased ISG expression in the aged post-ischemic brain. Bulk tissue results indicate the involvement of other contributors, such as the early-infiltrating peripheral leukocytes. Previously, the hematopoietic component has been identified as a major source of IFN-I signaling following traumatic brain injury (Karve et al., 2016). In concordance, we detected greater upregulation of granulocyte signature genes in aged animals. Moreover, it has been suggested that IFN levels correlate with severity of injury and differently influence functional outcome. IFN signaling

could be beneficial in context of mild ischemic preconditioning (Marsh et al., 2009, Hamner et al., 2015), but it could be also detrimental following more severe stroke (Zhang et al., 2017). Our findings seem to be consistent with this concept, as aged animals generally suffer more severe ischemia. One potential mechanism could be the greater disruption of BBB, which in turn leads to the greater influx of peripheral leukocytes.

One of the potential limitations of our study is that we utilized only female mice. It has been reported that females may have stronger immune response to various stimuli (Dotson and Offner, 2017), and future work is needed to compare the response to aging with males. Moreover, our study does not discriminate if the observed changes are due to decreased estrogen levels in aged mice, which has a protective role in ischemia (Sohrabji et al., 2019), or are intrinsic to aging. Second limitation is that our RNA-seq data are based on bulk tissue, the expression signal is partly confounded by the cell type composition and the power to detect genes changed in a cell-specific manner is lowered. Another limitation is that our RNA-seq experiment assayed a single time point (three days) after ischemia relative to the control. Although the selected time point can be considered well representative of the subacute phase, informative on early damage as well as initiation of repair processes (Savitz, 2013, Jin et al., 2010), the timing of some events, such as T cell infiltration, may be delayed in aged mice (Ahnstedt et al., 2020, Selvaraj and Stowe, 2017), which leaves a space for future studies analyzing later subacute and chronic phases.

In conclusion, detailed insights into transcriptional response to ischemia described in this study may contribute to our understanding of the interplay between ischemic pathology and aging, and open avenues for the future search for effective therapeutic approaches.

6 CONCLUSIONS

In the present work, we studied the proliferation and differentiation potential of NG2 glia following different types of CNS pathologies and how the pathophysiology of the brain is altered during aging. To be able to examine those different features of NG2 glia we had to crossbreed many different transgenic mice and employed several laboratory methods that helped us to identify changes from mRNA, protein, and functional points of view.

First, analysis of the differentiation potential of NG2 glia confirmed that under physiological conditions, they serve mainly as precursor cells for oligodendrocytes. However, following permanent FCI, NG2 glia acquire a multipotent phenotype. As a result, they differentiated not only to oligodendrocytes but also to astrocytes. Besides the differentiation potential, NG2 glia massively proliferate in acute phases after ischemia and migrate toward the lesion suggesting their important role in glial scar formation (Hypothesis 1, Aim 1).

Furthermore, we examined if NG2 glia differentiation potential into astrocytes is only triggered by FCI compared with other types of CNS injuries. We disclosed that an astrocyte-like NG2 glia subpopulation is only present transiently after FCI and following less severe injury, namely the cortical SW and DEMY in corpus callosum and cortex, subpopulations mirroring different stages of oligodendrocyte maturation markedly prevail. Moreover, we proved that astrocyte-like NG2 glia are a specific transient subpopulation located in the ischemic glial scar, actively involved in the cell cycle displaying a current pattern, which is similar to that identified in cortical astrocytes (Hypothesis 2, Aim 2).

Finally, the transcriptional response to ischemia during adulthood and aging in female mice uncovered age-dependent alterations in processes predominantly associated with inflammation and interferon signaling as well as axonal and synaptic maintenance. Furthermore, our results showed that differential stroke outcome is associated with the overactivation of pro-inflammatory pathways and other potentially detrimental factors in aged mice, rather than activation of the neuroprotective program in young mice (Hypothesis 3, Aim 3).

Taken together, NG2 glia perform multiple functions in both normal and pathological conditions in the brain. They have multipotent properties of self-renewal and repair in many kinds of brain injuries. In response to injury, NG2 glia are not only capable to proliferate and migrate to the lesions but also differentiate into oligodendrocytes or astrocytes. In conclusion, given that NG2 glia are actively involved in fast response to CNS injuries, we

suggest that future studies of NG2 glia may unravel their potential therapies of CNS disorders.

Additionally, our results paint a picture of ischemia as a complex age-related disease and provide insights into the interaction of aging and stroke on a cellular and molecular level. Detailed insights into transcriptional response to ischemia described in this study may contribute to our understanding of the interplay between ischemic pathology and aging, and open avenues for the future search for effective therapeutic approaches.

7 SUMMARY IN CZECH

7.1 Proliferační a diferenciační potenciál NG2 glií po fokální mozkové ischemii

V této práci jsme studovali genetické mapování osudu NG2 glií s využitím genového profilování na úrovni jedné buňky a techniky proteinové exprese. Identifikovali jsme tři subpopulace NG2 glií, které vznikají po FCI: což jsou proliferující NG2 buňky a buňky podobné astrocytům a oligodendrocytům; takové buněčné typy byly dále potvrzeny imunohistochemicky. Souhrnně jsme identifikovali několik dosud neznámých rozdílů mezi expresními profily NG2 glií a charakterizovali specifické geny přispívající k fenotypickým změnám NG2 glií po FCI.

7.2 Výskyt astrocytů odvozených z NG2 glií u různých typu poškození CNS

V této studii jsme porovnávali expresní profily NG2 glií po různých typech poranění CNS (FCI, SW, DEMY). Výsledky odhalily, že subpopulace NG2 glií exprimující GFAP, marker reaktivních astrocytů, byla přítomna pouze po FCI. Po méně závažných poraněních (SW, DEMY) však výrazně převažovala subpopulace odrážející různá stádia zrání oligodendrocytů. Celkově jsme dokázali, že astrocytům podobné NG2 glie jsou specifickou subpopulací NG2 glií objevujících se přechodně pouze po FCI. Tyto buňky, umístěné v post ischemické gliální jizvě, vykazují proudový profil podobný tomu, který byl identifikován v běžných kortikálních astrocytech.

7.3 Vztah mezi mrtvicí a stárnutím na úrovni celého genomu pomocí modelu fokální mozkové ischemie

V těchto experimentech jsme provedli komplexní analýzu RNA sekvenování během stárnutí, po ischemii a v jejich kombinaci u myší ve věku 3 a 18 měsíců. Odhalili jsme sníženou expresi genů zodpovědných za údržbu a stabilitu axonů a synapsí a zvýšenou aktivaci interferonu typu I (IFN-I) po mrtvici u starých myší. Tyto výsledky společně vykreslují obraz ischemické cévní mozkové příhody jako komplexního onemocnění souvisejícího s věkem a poskytují popis vztahu stárnutí a cévní mozkové příhody na buněčné a molekulární úrovni.

8 SUMMARY IN ENGLISH

8.1 Proliferation and differentiation potential of NG2 glia following FCI

In this work, we studied genetic fate-mapping of NG2 glia employing single-cell gene profiling and protein expression techniques. We identified three subpopulations of NG2 glia emerging after FCI: proliferative cells; astrocyte-like and oligodendrocyte-like NG2 cells; such phenotypes were further confirmed by immunohistochemistry. Collectively, here we identified several yet unknown differences between the expression profiles of NG2 glia and characterized specific genes contributing to phenotypical changes of NG2 glia after FCI.

8.2 Appearance of NG2 glia-derived astrocytes between different types of CNS disorders

In this study, we compared NG2 glia expression profiles following different CNS injuries (FCI, SW, DEMY). The results revealed that the subpopulation of NG2 glia expressing GFAP, a marker of reactive astrocytes, is only present after FCI. However, following less severe injuries (SW, DEMY), subpopulations mirroring different stages of oligodendrocyte maturation markedly prevail. Overall, we have proved that astrocyte-like NG2 glia are a specific subpopulation of NG2 glia emerging transiently only following FCI. These cells, located in the post-ischemic glial scar display a current pattern similar to that identified in cortical astrocytes.

8.3 Interaction between stroke and aging at the genome-wide level using a model of FCI

In these experiments, we performed a comprehensive RNA-seq analysis of aging, ischemia, and their interaction in 3- and 18-month-old mice. We uncovered downregulation of axonal and synaptic maintenance genetic program and increased activation of type IFN-I signaling following stroke in aged mice. Together, these results paint a picture of ischemic stroke as a complex age-related disease and provide insights into the interaction of aging and stroke on the cellular and molecular level.

9 LITERATURE REFERENCES

1. ABDULLAH, A., ZHANG, M., FRUGIER, T., BEDOUI, S., TAYLOR, J. M. & CRACK, P. J. 2018. STING-mediated type-I interferons contribute to the neuroinflammatory process and detrimental effects following traumatic brain injury. *Journal of Neuroinflammation,* 15**,** 323.
2. ADAMS, K. L. & GALLO, V. 2018. The diversity and disparity of the glial scar. *Nat Neurosci,* 21**,** 9-15.
3. AGUIRRE, A. & GALLO, V. 2004. Postnatal neurogenesis and gliogenesis in the olfactory bulb from NG2-expressing progenitors of the subventricular zone. *J Neurosci,* 24**,** 10530-41.
4. AGUIRRE, A. A., CHITTAJALLU, R., BELACHEW, S. & GALLO, V. 2004. NG2-expressing cells in the subventricular zone are type C-like cells and contribute to interneuron generation in the postnatal hippocampus. *J Cell Biol,* 165**,** 575-89.
5. AHNSTEDT, H., PATRIZZ, A., CHAUHAN, A., ROY-O'REILLY, M., FURR, J. W., SPYCHALA, M. S., D'AIGLE, J., BLIXT, F. W., ZHU, L., BRAVO ALEGRIA, J. & MCCULLOUGH, L. D. 2020. Sex differences in T cell immune responses, gut permeability and outcome after ischemic stroke in aged mice. *Brain, Behavior, and Immunity,* 87**,** 556-567.
6. AL-IZKI, S., PRYCE, G., O'NEILL, J. K., BUTTER, C., GIOVANNONI, G., AMOR, S. & BAKER, D. 2012. Practical guide to the induction of relapsing progressive experimental autoimmune encephalomyelitis in the Biozzi ABH mouse. *Mult Scler Relat Disord,* 1**,** 29-38.
7. ALBERDI, E., SÁNCHEZ-GÓMEZ, M. V., MARINO, A. & MATUTE, C. 2002. Ca(2+) influx through AMPA or kainate receptors alone is sufficient to initiate excitotoxicity in cultured oligodendrocytes. *Neurobiol Dis,* 9**,** 234-43.
8. ALKAYED, N. J., HARUKUNI, I., KIMES, A. S., LONDON, E. D., TRAYSTMAN, R. J. & HURN, P. D. 1998. Gender-Linked Brain Injury in Experimental Stroke. *Stroke,* 29**,** 159-166.
9. ALLEN, C. L. & BAYRAKTUTAN, U. 2009. Oxidative stress and its role in the pathogenesis of ischaemic stroke. *International journal of stroke,* 4**,** 461-470.
10. AMANI, H., KAZEROONI, H., HASSANPOOR, H., AKBARZADEH, A. & PAZOKI-TOROUDI, H. 2019. Tailoring synthetic polymeric biomaterials towards nerve tissue engineering: a review. *Artificial Cells, Nanomedicine, and Biotechnology,* 47**,** 3524-3539.
11. ANDEROVÁ, M., ANTONOVA, T., PETRÍK, D., NEPRASOVÁ, H., CHVÁTAL, A. & SYKOVÁ, E. 2004. Voltage-dependent potassium currents in hypertrophied rat astrocytes after a cortical stab wound. *Glia,* 48**,** 311-26.
12. ANDEROVÁ, M., KUBINOVÁ, S., JELITAI, M., NEPRASOVÁ, H., GLOGAROVÁ, K., PRAJEROVÁ, I., URDZÍKOVÁ, L., CHVÁTAL, A. & SYKOVÁ, E. 2006. Transplantation of embryonic neuroectodermal progenitor cells into the site of a photochemical lesion: immunohistochemical and electrophysiological analysis. *J Neurobiol,* 66**,** 1084-100.
13. ANDEROVA, M., VORISEK, I., PIVONKOVA, H., BENESOVA, J., VARGOVA, L., CICANIC, M., CHVATAL, A. & SYKOVA, E. 2011. Cell death/proliferation and alterations in glial morphology contribute to changes in diffusivity in the rat hippocampus after hypoxia-ischemia. *J Cereb Blood Flow Metab,* 31**,** 894-907.
14. ANDERS, S., PYL, P. T. & HUBER, W. 2015. HTSeq—a Python framework to work with high-throughput sequencing data. *bioinformatics,* 31**,** 166-169.

15. ANDROVIC, P., KIRDAJOVA, D., TURECKOVA, J., ZUCHA, D., ROHLOVA, E., ABAFFY, P., KRISKA, J., VALNY, M., ANDEROVA, M. & KUBISTA, M. 2020. Decoding the transcriptional response to ischemic stroke in young and aged mouse brain. *Cell reports,* 31**,** 107777.
16. ARUMUGAM, T. V., MANZANERO, S., FURTADO, M., BIGGINS, P. J., HSIEH, Y.-H., GELDERBLOM, M., MACDONALD, K. P., SALIMOVA, E., LI, Y.-I. & KORN, O. 2017. An atypical role for the myeloid receptor Mincle in central nervous system injury. *Journal of Cerebral Blood Flow & Metabolism,* 37**,** 2098-2111.
17. ASANO, S., CHANTLER, P. D. & BARR, T. L. 2016. Gene expression profiling in stroke: relevance of blood–brain interaction. *Current opinion in pharmacology,* 26**,** 80-86.
18. AZAMI TAMEH, A., CLARNER, T., BEYER, C., ATLASI, M. A., HASSANZADEH, G. & NADERIAN, H. 2013. Regional regulation of glutamate signaling during cuprizone-induced demyelination in the brain. *Ann Anat,* 195**,** 415-23.
19. BACK, S. & RIVKEES, S. 2005. Emerging concepts in periventricular white matter injury. *Seminars in perinatology,* 28**,** 405-14.
20. BADAN, I., BUCHHOLD, B., HAMM, A., GRATZ, M., WALKER, L. C., PLATT, D., KESSLER, C. & POPA-WAGNER, A. 2003. Accelerated Glial Reactivity to Stroke in Aged Rats Correlates with Reduced Functional Recovery. *Journal of Cerebral Blood Flow & Metabolism,* 23**,** 845-854.
21. BATTEFELD, A., KLOOSTER, J. & KOLE, M. H. 2016. Myelinating satellite oligodendrocytes are integrated in a glial syncytium constraining neuronal high-frequency activity. *Nat Commun,* 7**,** 11298.
22. BAUER, M., BRAKEBUSCH, C., COISNE, C., SIXT, M., WEKERLE, H., ENGELHARDT, B. & FÄSSLER, R. 2009. Beta1 integrins differentially control extravasation of inflammatory cell subsets into the CNS during autoimmunity. *Proc Natl Acad Sci U S A,* 106**,** 1920-5.
23. BAXI, E. G., DEBRUIN, J., JIN, J., STRASBURGER, H. J., SMITH, M. D., ORTHMANN-MURPHY, J. L., SCHOTT, J. T., FAIRCHILD, A. N., BERGLES, D. E. & CALABRESI, P. A. 2017. Lineage tracing reveals dynamic changes in oligodendrocyte precursor cells following cuprizone-induced demyelination. *Glia,* 65**,** 2087-2098.
24. BEHRENDT, G., BAER, K., BUFFO, A., CURTIS, M. A., FAULL, R. L., REES, M. I., GÖTZ, M. & DIMOU, L. 2013. Dynamic changes in myelin aberrations and oligodendrocyte generation in chronic amyloidosis in mice and men. *Glia,* 61**,** 273-86.
25. BELOV KIRDAJOVA, D., KRISKA, J., TURECKOVA, J. & ANDEROVA, M. 2020. Ischemia-Triggered Glutamate Excitotoxicity From the Perspective of Glial Cells. *Front Cell Neurosci,* 14**,** 51.
26. BENAYOUN, B. A., POLLINA, E. A., SINGH, P. P., MAHMOUDI, S., HAREL, I., CASEY, K. M., DULKEN, B. W., KUNDAJE, A. & BRUNET, A. 2019. Remodeling of epigenome and transcriptome landscapes with aging in mice reveals widespread induction of inflammatory responses. *Genome research,* 29**,** 697-709.
27. BENJAMIN, E. J., VIRANI, S. S., CALLAWAY, C. W., CHAMBERLAIN, A. M., CHANG, A. R., CHENG, S., CHIUVE, S. E., CUSHMAN, M., DELLING, F. N., DEO, R., FERRANTI, S. D. D., FERGUSON, J. F., FORNAGE, M., GILLESPIE, C., ISASI, C. R., JIMÉNEZ, M. C., JORDAN, L. C., JUDD, S. E., LACKLAND, D., LICHTMAN, J. H., LISABETH, L., LIU, S., LONGENECKER, C. T., LUTSEY, P. L., MACKEY, J. S., MATCHAR, D. B., MATSUSHITA, K., MUSSOLINO, M. E., NASIR, K., O'FLAHERTY, M., PALANIAPPAN, L. P., PANDEY, A., PANDEY, D. K., REEVES, M. J., RITCHEY, M. D., RODRIGUEZ, C. J., ROTH, G. A., ROSAMOND, W. D., SAMPSON, U. K. A., SATOU, G. M., SHAH, S. H., SPARTANO, N. L.,

TIRSCHWELL, D. L., TSAO, C. W., VOEKS, J. H., WILLEY, J. Z., WILKINS, J. T., WU, J. H., ALGER, H. M., WONG, S. S. & MUNTNER, P. 2018. Heart Disease and Stroke Statistics-2014;2018 Update: A Report From the American Heart Association. *Circulation,* 137**,** e67-e492.
28. BERGLES, D. E., ROBERTS, J. D., SOMOGYI, P. & JAHR, C. E. 2000. Glutamatergic synapses on oligodendrocyte precursor cells in the hippocampus. *Nature,* 405**,** 187-91.
29. BERNHARDI, R., EUGENÍN-VON BERNHARDI, J., FLORES, B. & EUGENÍN LEÓN, J. 2016. Glial Cells and Integrity of the Nervous System. *Adv Exp Med Biol,* 949**,** 1-24.
30. BLANK, T. & PRINZ, M. 2017. Type I interferon pathway in CNS homeostasis and neurological disorders. *Glia,* 65**,** 1397-1406.
31. BODA, E., DI MARIA, S., ROSA, P., TAYLOR, V., ABBRACCHIO, M. P. & BUFFO, A. 2015. Early phenotypic asymmetry of sister oligodendrocyte progenitor cells after mitosis and its modulation by aging and extrinsic factors. *Glia,* 63**,** 271-286.
32. BODA, E., VIGANÒ, F., ROSA, P., FUMAGALLI, M., LABAT-GEST, V., TEMPIA, F., ABBRACCHIO, M. P., DIMOU, L. & BUFFO, A. 2011. The GPR17 receptor in NG2 expressing cells: focus on in vivo cell maturation and participation in acute trauma and chronic damage. *Glia,* 59**,** 1958-73.
33. BOISVERT, M. M., ERIKSON, G. A., SHOKHIREV, M. N. & ALLEN, N. J. 2018. The aging astrocyte transcriptome from multiple regions of the mouse brain. *Cell reports,* 22**,** 269-285.
34. BOLGER, A. M., LOHSE, M. & USADEL, B. 2014. Trimmomatic: a flexible trimmer for Illumina sequence data. *Bioinformatics,* 30**,** 2114-2120.
35. BONFANTI, E., GELOSA, P., FUMAGALLI, M., DIMOU, L., VIGANÒ, F., TREMOLI, E., CIMINO, M., SIRONI, L. & ABBRACCHIO, M. P. 2017. The role of oligodendrocyte precursor cells expressing the GPR17 receptor in brain remodeling after stroke. *Cell Death Dis,* 8**,** e2871.
36. BOULANGER, J. J. & MESSIER, C. 2017. Doublecortin in Oligodendrocyte Precursor Cells in the Adult Mouse Brain. *Front Neurosci,* 11**,** 143.
37. BOYD, A., ZHANG, H. & WILLIAMS, A. 2013. Insufficient OPC migration into demyelinated lesions is a cause of poor remyelination in MS and mouse models. *Acta Neuropathol,* 125**,** 841-59.
38. BRAMLETT, H. M. & DIETRICH, W. D. 2004. Pathophysiology of Cerebral Ischemia and Brain Trauma: Similarities and Differences. *Journal of Cerebral Blood Flow & Metabolism,* 24**,** 133-150.
39. BRUTTGER, J., KARRAM, K., WÖRTGE, S., REGEN, T., MARINI, F., HOPPMANN, N., KLEIN, M., BLANK, T., YONA, S. & WOLF, Y. 2015. Genetic cell ablation reveals clusters of local self-renewing microglia in the mammalian central nervous system. *Immunity,* 43**,** 92-106.
40. BUFFO, A., VOSKO, M. R., ERTURK, D., HAMANN, G. F., JUCKER, M., ROWITCH, D. & GOTZ, M. 2005. Expression pattern of the transcription factor Olig2 in response to brain injuries: implications for neuronal repair. *Proc Natl Acad Sci U S A,* 102**,** 18183-8.
41. BURKE, S. N. & BARNES, C. A. 2006. Neural plasticity in the ageing brain. *Nat Rev Neurosci,* 7**,** 30-40.
42. BURNS, T. C., VERFAILLIE, C. M. & LOW, W. C. 2009. Stem cells for ischemic brain injury: a critical review. *J Comp Neurol,* 515**,** 125-44.
43. BUTT, A. M., VANZULLI, I., PAPANIKOLAOU, M., DE LA ROCHA, I. C. & HAWKINS, V. E. 2017. Metabotropic Glutamate Receptors Protect Oligodendrocytes from Acute Ischemia in the Mouse Optic Nerve. *Neurochem Res,* 42**,** 2468-2478.

44. CAHOY, J. D., EMERY, B., KAUSHAL, A., FOO, L. C., ZAMANIAN, J. L., CHRISTOPHERSON, K. S., XING, Y., LUBISCHER, J. L., KRIEG, P. A., KRUPENKO, S. A., THOMPSON, W. J. & BARRES, B. A. 2008. A transcriptome database for astrocytes, neurons, and oligodendrocytes: a new resource for understanding brain development and function. *J Neurosci,* 28**,** 264-78.
45. CARMICHAEL, S. T. 2012. Brain excitability in stroke: the yin and yang of stroke progression. *Archives of neurology,* 69**,** 161-167.
46. CEPRIAN, M. & FULTON, D. 2019. Glial Cell AMPA Receptors in Nervous System Health, Injury and Disease. *Int J Mol Sci,* 20.
47. CLARKE, L. E., LIDDELOW, S. A., CHAKRABORTY, C., MÜNCH, A. E., HEIMAN, M. & BARRES, B. A. 2018. Normal aging induces A1-like astrocyte reactivity. *Proceedings of the National Academy of Sciences,* 115**,** E1896-E1905.
48. CLARKE, L. E., YOUNG, K. M., HAMILTON, N. B., LI, H., RICHARDSON, W. D. & ATTWELL, D. 2012. Properties and fate of oligodendrocyte progenitor cells in the corpus callosum, motor cortex, and piriform cortex of the mouse. *J Neurosci,* 32**,** 8173-85.
49. COMI, G. 2009. Shifting the paradigm toward earlier treatment of multiple sclerosis with interferon beta. *Clin Ther,* 31**,** 1142-57.
50. CORPS, K. N., ROTH, T. L. & MCGAVERN, D. B. 2015. Inflammation and Neuroprotection in Traumatic Brain Injury. *JAMA Neurology,* 72**,** 355-362.
51. COX, J. & MANN, M. 2008. MaxQuant enables high peptide identification rates, individualized ppb-range mass accuracies and proteome-wide protein quantification. *Nature biotechnology,* 26**,** 1367-1372.
52. CRIBBS, D. H., BERCHTOLD, N. C., PERREAU, V., COLEMAN, P. D., ROGERS, J., TENNER, A. J. & COTMAN, C. W. 2012. Extensive innate immune gene activation accompanies brain aging, increasing vulnerability to cognitive decline and neurodegeneration: a microarray study. *Journal of neuroinflammation,* 9**,** 1-18.
53. CRUZ, J. C., TSENG, H. C., GOLDMAN, J. A., SHIH, H. & TSAI, L. H. 2003. Aberrant Cdk5 activation by p25 triggers pathological events leading to neurodegeneration and neurofibrillary tangles. *Neuron,* 40**,** 471-83.
54. DAMOISEAUX, J. S. 2017. Effects of aging on functional and structural brain connectivity. *Neuroimage,* 160**,** 32-40.
55. DÁVALOS, A. 2005. Thrombolysis in acute ischemic stroke: successes, failures, and new hopes. *Cerebrovasc Dis,* 20 Suppl 2**,** 135-9.
56. DAVID, F. P. A., LITOVCHENKO, M., DEPLANCKE, B. & GARDEUX, V. 2020. ASAP 2020 update: an open, scalable and interactive web-based portal for (single-cell) omics analyses. *Nucleic Acids Res,* 48**,** W403-w414.
57. DAVIE, K., JANSSENS, J., KOLDERE, D., DE WAEGENEER, M., PECH, U., KREFT, Ł., AIBAR, S., MAKHZAMI, S., CHRISTIAENS, V. & GONZÁLEZ-BLAS, C. B. 2018. A single-cell transcriptome atlas of the aging Drosophila brain. *Cell,* 174**,** 982-998. e20.
58. DAWSON, M. R., LEVINE, J. M. & REYNOLDS, R. 2000. NG2-expressing cells in the central nervous system: are they oligodendroglial progenitors? *J Neurosci Res,* 61**,** 471-9.
59. DAWSON, M. R., POLITO, A., LEVINE, J. M. & REYNOLDS, R. 2003. NG2-expressing glial progenitor cells: an abundant and widespread population of cycling cells in the adult rat CNS. *Mol Cell Neurosci,* 24**,** 476-88.
60. DE BIASE, L. M., NISHIYAMA, A. & BERGLES, D. E. 2010. Excitability and synaptic communication within the oligodendrocyte lineage. *J Neurosci,* 30**,** 3600-11.
61. DE WEERD, N. A., VIVIAN, J. P., NGUYEN, T. K., MANGAN, N. E., GOULD, J. A., BRANIFF, S.-J., ZAKER-TABRIZI, L., FUNG, K. Y., FORSTER, S. C.,

BEDDOE, T., REID, H. H., ROSSJOHN, J. & HERTZOG, P. J. 2013. Structural basis of a unique interferon-β signaling axis mediated via the receptor IFNAR1. *Nature Immunology,* 14**,** 901-907.
62. DEL PINO, I., GARCÍA-FRIGOLA, C., DEHORTER, N., BROTONS-MAS, J. R., ALVAREZ-SALVADO, E., DE LAGRÁN, M. M., CICERI, G., GABALDÓN, M. V., MORATAL, D. & DIERSSEN, M. 2013. Erbb4 deletion from fast-spiking interneurons causes schizophrenia-like phenotypes. *Neuron,* 79**,** 1152-1168.
63. DERGUNOVA, L. V., FILIPPENKOV, I. B., STAVCHANSKY, V. V., DENISOVA, A. E., YUZHAKOV, V. V., MOZEROV, S. A., GUBSKY, L. V. & LIMBORSKA, S. A. 2018. Genome-wide transcriptome analysis using RNA-Seq reveals a large number of differentially expressed genes in a transient MCAO rat model. *BMC Genomics,* 19**,** 655.
64. DESILVA, T. M., KABAKOV, A. Y., GOLDHOFF, P. E., VOLPE, J. J. & ROSENBERG, P. A. 2009. Regulation of glutamate transport in developing rat oligodendrocytes. *J Neurosci,* 29**,** 7898-908.
65. DEWAR, D., UNDERHILL, S. M. & GOLDBERG, M. P. 2003. Oligodendrocytes and ischemic brain injury. *J Cereb Blood Flow Metab,* 23**,** 263-74.
66. DIAS, D. O., KALKITSAS, J., KELAHMETOGLU, Y., ESTRADA, C. P., TATARISHVILI, J., ERNST, A., HUTTNER, H. B., KOKAIA, Z., LINDVALL, O., BRUNDIN, L., FRISÉN, J. & GÖRITZ, C. 2020. Pericyte-derived fibrotic scarring is conserved across diverse central nervous system lesions. *bioRxiv***,** 2020.04.30.068965.
67. DIMOU, L. & GALLO, V. 2015. NG 2-glia and their functions in the central nervous system. *Glia,* 63**,** 1429-1451.
68. DIMOU, L., SIMON, C., KIRCHHOFF, F., TAKEBAYASHI, H. & GOTZ, M. 2008. Progeny of Olig2-expressing progenitors in the gray and white matter of the adult mouse cerebral cortex. *J Neurosci,* 28**,** 10434-42.
69. DIRNAGL, U., IADECOLA, C. & MOSKOWITZ, M. A. 1999. Pathobiology of ischaemic stroke: an integrated view. *Trends Neurosci,* 22**,** 391-7.
70. DOBIN, A., DAVIS, C. A., SCHLESINGER, F., DRENKOW, J., ZALESKI, C., JHA, S., BATUT, P., CHAISSON, M. & GINGERAS, T. R. 2013. STAR: ultrafast universal RNA-seq aligner. *Bioinformatics,* 29**,** 15-21.
71. DOTSON, A. L. & OFFNER, H. 2017. Sex differences in the immune response to experimental stroke: Implications for translational research. *Journal of Neuroscience Research,* 95**,** 437-446.
72. DUGAN, L. L. & CHOI, D. W. 1994. Excitotoxicity, free radicals, and cell membrane changes. *Ann Neurol,* 35 Suppl**,** S17-21.
73. DURÁN-LAFORET, V., FERNÁNDEZ-LÓPEZ, D., GARCÍA-CULEBRAS, A., GONZÁLEZ-HIJÓN, J., MORAGA, A., PALMA-TORTOSA, S., GARCÍA-YÉBENES, I., VEGA-PÉREZ, A., LIZASOAIN, I. & MORO, M. 2019. Delayed Effects of Acute Reperfusion on Vascular Remodeling and Late-Phase Functional Recovery After Stroke. *Front Neurosci,* 13**,** 767.
74. DUSS, S. B., SEILER, A., SCHMIDT, M. H., PACE, M., ADAMANTIDIS, A., MÜRI, R. M. & BASSETTI, C. L. 2017. The role of sleep in recovery following ischemic stroke: a review of human and animal data. *Neurobiology of sleep and circadian rhythms,* 2**,** 94-105.
75. ERECIŃSKA, M. & SILVER, I. A. 2001. Tissue oxygen tension and brain sensitivity to hypoxia. *Respir Physiol,* 128**,** 263-76.
76. ERNY, D., DE ANGELIS, A. L. H., JAITIN, D., WIEGHOFER, P., STASZEWSKI, O., DAVID, E., KEREN-SHAUL, H., MAHLAKOIV, T., JAKOBSHAGEN, K. & BUCH, T. 2015. Host microbiota constantly control maturation and function of microglia in the CNS. *Nature neuroscience,* 18**,** 965-977.

77. ESSERS, J., THEIL, A. F., BALDEYRON, C., VAN CAPPELLEN, W. A., HOUTSMULLER, A. B., KANAAR, R. & VERMEULEN, W. 2005. Nuclear dynamics of PCNA in DNA replication and repair. *Mol Cell Biol,* 25**,** 9350-9.
78. FERENT, J., ZIMMER, C., DURBEC, P., RUAT, M. & TRAIFFORT, E. 2013. Sonic Hedgehog signaling is a positive oligodendrocyte regulator during demyelination. *J Neurosci,* 33**,** 1759-72.
79. FERRAIUOLO, L., MEYER, K., SHERWOOD, T. W., VICK, J., LIKHITE, S., FRAKES, A., MIRANDA, C. J., BRAUN, L., HEATH, P. R., PINEDA, R., BEATTIE, C. E., SHAW, P. J., ASKWITH, C. C., MCTIGUE, D. & KASPAR, B. K. 2016. Oligodendrocytes contribute to motor neuron death in ALS via SOD1-dependent mechanism. *Proc Natl Acad Sci U S A,* 113**,** E6496-e6505.
80. FILICE, F., VÖRCKEL, K. J., SUNGUR, A. Ö., WÖHR, M. & SCHWALLER, B. 2016. Reduction in parvalbumin expression not loss of the parvalbumin-expressing GABA interneuron subpopulation in genetic parvalbumin and shank mouse models of autism. *Molecular brain,* 9**,** 1-17.
81. FRIEDMAN, B. A., SRINIVASAN, K., AYALON, G., MEILANDT, W. J., LIN, H., HUNTLEY, M. A., CAO, Y., LEE, S.-H., HADDICK, P. C. & NGU, H. 2018. Diverse brain myeloid expression profiles reveal distinct microglial activation states and aspects of Alzheimer's disease not evident in mouse models. *Cell reports,* 22**,** 832-847.
82. FRIGERIO, C. S., WOLFS, L., FATTORELLI, N., THRUPP, N., VOYTYUK, I., SCHMIDT, I., MANCUSO, R., CHEN, W.-T., WOODBURY, M. E. & SRIVASTAVA, G. 2019. The major risk factors for Alzheimer's disease: age, sex, and genes modulate the microglia response to Aβ plaques. *Cell reports,* 27**,** 1293-1306. e6.
83. GALICHET, C., CLAYTON, R. W. & LOVELL-BADGE, R. 2021. Novel Tools and Investigative Approaches for the Study of Oligodendrocyte Precursor Cells (NG2-Glia) in CNS Development and Disease. *Frontiers in cellular neuroscience,* 15**,** 673132-673132.
84. GATTRINGER, T., FERRARI, J., KNOFLACH, M., SEYFANG, L., HORNER, S., NIEDERKORN, K., CULEA, V., BEITZKE, M., LANG, W., ENZINGER, C. & FAZEKAS, F. 2014. Sex-Related Differences of Acute Stroke Unit Care. *Stroke,* 45**,** 1632-1638.
85. GODBOUT, J. P., CHEN, J., ABRAHAM, J., RICHWINE, A. F., BERG, B. M., KELLEY, K. W. & JOHNSON, R. W. 2005. Exaggerated neuroinflammation and sickness behavior in aged mice following activation of the peripheral innate immune system. *Faseb j,* 19**,** 1329-31.
86. GOLDMANN, T., ZELLER, N., RAASCH, J., KIERDORF, K., FRENZEL, K., KETSCHER, L., BASTERS, A., STASZEWSKI, O., BRENDECKE, S. M. & SPIESS, A. 2015. USP 18 lack in microglia causes destructive interferonopathy of the mouse brain. *The EMBO journal,* 34**,** 1612-1629.
87. GOLDSCHMIDT, T., ANTEL, J., KÖNIG, F. B., BRÜCK, W. & KUHLMANN, T. 2009. Remyelination capacity of the MS brain decreases with disease chronicity. *Neurology,* 72**,** 1914-21.
88. GORDON, M. N., SCHREIER, W. A., OU, X., HOLCOMB, L. A. & MORGAN, D. G. 1997. Exaggerated astrocyte reactivity after nigrostriatal deafferentation in the aged rat. *Journal of Comparative Neurology,* 388**,** 106-119.
89. GRABERT, K., MICHOEL, T., KARAVOLOS, M. H., CLOHISEY, S., BAILLIE, J. K., STEVENS, M. P., FREEMAN, T. C., SUMMERS, K. M. & MCCOLL, B. W. 2016. Microglial brain region− dependent diversity and selective regional sensitivities to aging. *Nature neuroscience,* 19**,** 504-516.

90. GRACIARENA, M., SEIFFE, A., NAIT-OUMESMAR, B. & DEPINO, A. M. 2018. Hypomyelination and Oligodendroglial Alterations in a Mouse Model of Autism Spectrum Disorder. *Front Cell Neurosci,* 12**,** 517.
91. GRINSPAN, J. B. 2020. Inhibitors of Myelination and Remyelination, Bone Morphogenetic Proteins, are Upregulated in Human Neurological Disease. *Neurochem Res,* 45**,** 656-662.
92. GUDI, V., GINGELE, S., SKRIPULETZ, T. & STANGEL, M. 2014. Glial response during cuprizone-induced de- and remyelination in the CNS: lessons learned. *Front Cell Neurosci,* 8**,** 73.
93. GUO, C. Y., XIONG, T. Q., TAN, B. H., GUI, Y., YE, N., LI, S. L. & LI, Y. C. 2019. The temporal and spatial changes of actin cytoskeleton in the hippocampal CA1 neurons following transient global ischemia. *Brain Res,* 1720**,** 146297.
94. GUO, F., LANG, J., SOHN, J., HAMMOND, E., CHANG, M. & PLEASURE, D. 2015. Canonical Wnt signaling in the oligodendroglial lineage--puzzles remain. *Glia,* 63**,** 1671-93.
95. GUO, F., MA, J., MCCAULEY, E., BANNERMAN, P. & PLEASURE, D. 2009. Early postnatal proteolipid promoter-expressing progenitors produce multilineage cells in vivo. *J Neurosci,* 29**,** 7256-70.
96. GUO, F., MAEDA, Y., MA, J., XU, J., HORIUCHI, M., MIERS, L., VACCARINO, F. & PLEASURE, D. 2010. Pyramidal neurons are generated from oligodendroglial progenitor cells in adult piriform cortex. *J Neurosci,* 30**,** 12036-49.
97. HABERLANDT, C., DEROUICHE, A., WYCZYNSKI, A., HASELEU, J., POHLE, J., KARRAM, K., TROTTER, J., SEIFERT, G., FROTSCHER, M., STEINHÄUSER, C. & JABS, R. 2011. Gray Matter NG2 Cells Display Multiple Ca2+-Signaling Pathways and Highly Motile Processes. *PLOS ONE,* 6**,** e17575.
98. HACKETT, A. R., YAHN, S. L., LYAPICHEV, K., DAJNOKI, A., LEE, D. H., RODRIGUEZ, M., CAMMER, N., PAK, J., MEHTA, S. T., BODAMER, O., LEMMON, V. P. & LEE, J. K. 2018. Injury type-dependent differentiation of NG2 glia into heterogeneous astrocytes. *Exp Neurol,* 308**,** 72-79.
99. HAMMOND, T. R., DUFORT, C., DISSING-OLESEN, L., GIERA, S., YOUNG, A., WYSOKER, A., WALKER, A. J., GERGITS, F., SEGEL, M. & NEMESH, J. 2019. Single-cell RNA sequencing of microglia throughout the mouse lifespan and in the injured brain reveals complex cell-state changes. *Immunity,* 50**,** 253-271. e6.
100. HAMNER, M. A., YE, Z., LEE, R. V., COLMAN, J. R., LE, T., GONG, D. C., RANSOM, B. R. & WEINSTEIN, J. R. 2015. Ischemic Preconditioning in White Matter: Magnitude and Mechanism. *The Journal of Neuroscience,* 35**,** 15599-15611.
101. HANEDA, H., KATABAMI, M., MIYAMOTO, H., ISOBE, H., SHIMIZU, T., ISHIGURO, A., MORIUTI, T., TAKASAKI, Y. & KAWAKAMI, Y. 1991. The relationship of the proliferating cell nuclear antigen protein to cis-diamminedichloroplatinum (II) resistance of a murine leukemia cell line P388/CDDP. *Oncology,* 48**,** 234-8.
102. HANSEN, A. J. 1978. The extracellular potassium concentration in brain cortex following ischemia in hypo- and hyperglycemic rats. *Acta Physiol Scand,* 102**,** 324-9.
103. HARTLEY, M. D., ALTOWAIJRI, G. & BOURDETTE, D. 2014. Remyelination and multiple sclerosis: therapeutic approaches and challenges. *Curr Neurol Neurosci Rep,* 14**,** 485.
104. HARUKUNI, I. & BHARDWAJ, A. 2006. Mechanisms of brain injury after global cerebral ischemia. *Neurol Clin,* 24**,** 1-21.
105. HASSANNEJAD, Z., SHAKOURI-MOTLAGH, A., MOKHATAB, M., ZADEGAN, S. A., SHARIF-ALHOSEINI, M., SHOKRANEH, F. & RAHIMI-MOVAGHAR, V.

2019. Oligodendrogliogenesis and Axon Remyelination after Traumatic Spinal Cord Injuries in Animal Studies: A Systematic Review. *Neuroscience,* 402**,** 37-50.
106. HE, Y., LIU, X. & CHEN, Z. 2020. Glial Scar-a Promising Target for Improving Outcomes After CNS Injury. *J Mol Neurosci,* 70**,** 340-352.
107. HILL, R. A., PATEL, K. D., MEDVED, J., REISS, A. M. & NISHIYAMA, A. 2013. NG2 cells in white matter but not gray matter proliferate in response to PDGF. *J Neurosci,* 33**,** 14558-66.
108. HINZMAN, J. M., DINAPOLI, V. A., MAHONEY, E. J., GERHARDT, G. A. & HARTINGS, J. A. 2015. Spreading depolarizations mediate excitotoxicity in the development of acute cortical lesions. *Exp Neurol,* 267**,** 243-53.
109. HOLTMAN, I. R., RAJ, D. D., MILLER, J. A., SCHAAFSMA, W., YIN, Z., BROUWER, N., WES, P. D., MÖLLER, T., ORRE, M. & KAMPHUIS, W. 2015. Induction of a common microglia gene expression signature by aging and neurodegenerative conditions: a co-expression meta-analysis. *Acta neuropathologica communications,* 3**,** 1-18.
110. HONSA, P., PIVONKOVA, H., DZAMBA, D., FILIPOVA, M. & ANDEROVA, M. 2012. Polydendrocytes display large lineage plasticity following focal cerebral ischemia. *PLoS One,* 7**,** e36816.
111. HONSA, P., VALNY, M., KRISKA, J., MATUSKOVA, H., HARANTOVA, L., KIRDAJOVA, D., VALIHRACH, L., ANDROVIC, P., KUBISTA, M. & ANDEROVA, M. 2016. Generation of reactive astrocytes from NG2 cells is regulated by sonic hedgehog. *Glia,* 64**,** 1518-31.
112. HOYER, S. 1987. Ischemia in aged brain. *Gerontology,* 33**,** 203-6.
113. HU, H., GAN, J. & JONAS, P. 2014. Fast-spiking, parvalbumin+ GABAergic interneurons: From cellular design to microcircuit function. *Science,* 345**,** 1255263.
114. HUANG, J. K., FANCY, S. P., ZHAO, C., ROWITCH, D. H., FFRENCH-CONSTANT, C. & FRANKLIN, R. J. 2011. Myelin regeneration in multiple sclerosis: targeting endogenous stem cells. *Neurotherapeutics,* 8**,** 650-8.
115. HUANG, W., BAI, X., STOPPER, L., CATALIN, B., CARTAROZZI, L. P., SCHELLER, A. & KIRCHHOFF, F. 2018. During Development NG2 Glial Cells of the Spinal Cord are Restricted to the Oligodendrocyte Lineage, but Generate Astrocytes upon Acute Injury. *Neuroscience,* 385**,** 154-165.
116. HUANG, W., GUO, Q., BAI, X., SCHELLER, A. & KIRCHHOFF, F. 2019. Early embryonic NG2 glia are exclusively gliogenic and do not generate neurons in the brain. *Glia,* 67**,** 1094-1103.
117. HUANG, W., ZHAO, N., BAI, X., KARRAM, K., TROTTER, J., GOEBBELS, S., SCHELLER, A. & KIRCHHOFF, F. 2014. Novel NG2-CreERT2 knock-in mice demonstrate heterogeneous differentiation potential of NG2 glia during development. *Glia,* 62**,** 896-913.
118. HUGHES, C. S., MOGGRIDGE, S., MÜLLER, T., SORENSEN, P. H., MORIN, G. B. & KRIJGSVELD, J. 2019. Single-pot, solid-phase-enhanced sample preparation for proteomics experiments. *Nature protocols,* 14**,** 68-85.
119. HUGHES, E. G. & APPEL, B. 2016. The cell biology of CNS myelination. *Current Opinion in Neurobiology,* 39**,** 93-100.
120. HUGHES, E. G., KANG, S. H., FUKAYA, M. & BERGLES, D. E. 2013. Oligodendrocyte progenitors balance growth with self-repulsion to achieve homeostasis in the adult brain. *Nature neuroscience,* 16**,** 668-676.
121. CHAMBERLAIN, K. A., NANESCU, S. E., PSACHOULIA, K. & HUANG, J. K. 2016. Oligodendrocyte regeneration: Its significance in myelin replacement and neuroprotection in multiple sclerosis. *Neuropharmacology,* 110**,** 633-643.

122. CHAMLING, X., KALLMAN, A., BERLINICKE, C., DEVKOTA, P., MERTZ, J. L., CHANG, C., KAUSHIK, A., CHEN, L., CALABRESI, P. A., MAO, H.-Q., WANG, T.-H. & ZACK, D. J. 2020. Single-Cell Transcriptomic Analysis Reveals Molecular Diversity of Human Oligodendrocyte Progenitor Cells. *bioRxiv*, 2020.10.07.328971.
123. CHARI, D. M. 2007. Remyelination in multiple sclerosis. *Int Rev Neurobiol,* 79, 589-620.
124. CHAUHAN, A., HUDOBENKO, J., AL MAMUN, A., KOELLHOFFER, E. C., PATRIZZ, A., RITZEL, R. M., GANESH, B. P. & MCCULLOUGH, L. D. 2018. Myeloid-specific TAK1 deletion results in reduced brain monocyte infiltration and improved outcomes after stroke. *Journal of Neuroinflammation,* 15, 148.
125. CHEN, H.-Z., GUO, S., LI, Z.-Z., LU, Y., JIANG, D.-S., ZHANG, R., LEI, H., GAO, L., ZHANG, X., ZHANG, Y., WANG, L., ZHU, L.-H., XIANG, M., ZHOU, Y., WAN, Q., DONG, H., LIU, D.-P. & LI, H. 2014. A Critical Role for Interferon Regulatory Factor 9 in Cerebral Ischemic Stroke. *The Journal of Neuroscience,* 34, 11897-11912.
126. CHISHOLM, N. C. & SOHRABJI, F. 2016. Astrocytic response to cerebral ischemia is influenced by sex differences and impaired by aging. *Neurobiol Dis,* 85, 245-253.
127. CHITTAJALLU, R., AGUIRRE, A. & GALLO, V. 2004. NG2-positive cells in the mouse white and grey matter display distinct physiological properties. *J Physiol,* 561, 109-22.
128. CHOI, J. W., GARDELL, S. E., HERR, D. R., RIVERA, R., LEE, C. W., NOGUCHI, K., TEO, S. T., YUNG, Y. C., LU, M., KENNEDY, G. & CHUN, J. 2011. FTY720 (fingolimod) efficacy in an animal model of multiple sclerosis requires astrocyte sphingosine 1-phosphate receptor 1 (S1P1) modulation. *Proc Natl Acad Sci U S A,* 108, 751-6.
129. IADECOLA, C. & ROSS, M. E. 1997. Molecular pathology of cerebral ischemia: delayed gene expression and strategies for neuroprotection. *Ann N Y Acad Sci,* 835, 203-17.
130. IHARA, R., VINCENT, B. D., BAXTER, M. R., FRANKLIN, E. E., HASSENSTAB, J. J., XIONG, C., MORRIS, J. C. & CAIRNS, N. J. 2018. Relative neuron loss in hippocampal sclerosis of aging and Alzheimer's disease. *Ann Neurol,* 84, 741-753.
131. IVASHKIV, L. B. & DONLIN, L. T. 2014. Regulation of type I interferon responses. *Nature Reviews Immunology,* 14, 36-49.
132. JEROMIN, A. & BOWSER, R. 2017. Biomarkers in Neurodegenerative Diseases. *In:* BEART, P., ROBINSON, M., RATTRAY, M. & MARAGAKIS, N. J. (eds.) *Neurodegenerative Diseases: Pathology, Mechanisms, and Potential Therapeutic Targets.* Cham: Springer International Publishing.
133. JIA, W., KAMEN, Y., PIVONKOVA, H. & KÁRADÓTTIR, R. T. 2019. Neuronal activity-dependent myelin repair after stroke. *Neurosci Lett,* 703, 139-144.
134. JIN, R., YANG, G. & LI, G. 2010. Inflammatory mechanisms in ischemic stroke: role of inflammatory cells. *Journal of Leukocyte Biology,* 87, 779-789.
135. JUNGBLUT, M., TIVERON, M. C., BARRAL, S., ABRAHAMSEN, B., KNÖBEL, S., PENNARTZ, S., SCHMITZ, J., PERRAUT, M., PFRIEGER, F. W. & STOFFEL, W. 2012. Isolation and characterization of living primary astroglial cells using the new GLAST-specific monoclonal antibody ACSA-1. *Glia,* 60, 894-907.
136. JURÍKOVÁ, M., DANIHEL, Ľ., POLÁK, Š. & VARGA, I. 2016. Ki67, PCNA, and MCM proteins: Markers of proliferation in the diagnosis of breast cancer. *Acta Histochem,* 118, 544-52.
137. KANG, S. H., FUKAYA, M., YANG, J. K., ROTHSTEIN, J. D. & BERGLES, D. E. 2010. NG2+ CNS glial progenitors remain committed to the oligodendrocyte lineage in postnatal life and following neurodegeneration. *Neuron,* 68, 668-81.

138. KANG, S. H., LI, Y., FUKAYA, M., LORENZINI, I., CLEVELAND, D. W., OSTROW, L. W., ROTHSTEIN, J. D. & BERGLES, D. E. 2013. Degeneration and impaired regeneration of gray matter oligodendrocytes in amyotrophic lateral sclerosis. *Nat Neurosci,* 16**,** 571-9.
139. KANTZER, C. G., BOUTIN, C., HERZIG, I. D., WITTWER, C., REIß, S., TIVERON, M. C., DREWES, J., ROCKEL, T. D., OHLIG, S., NINKOVIC, J., CREMER, H., PENNARTZ, S., JUNGBLUT, M. & BOSIO, A. 2017. Anti-ACSA-2 defines a novel monoclonal antibody for prospective isolation of living neonatal and adult astrocytes. *Glia,* 65**,** 990-1004.
140. KÁRADÓTTIR, R., CAVELIER, P., BERGERSEN, L. H. & ATTWELL, D. 2005. NMDA receptors are expressed in oligodendrocytes and activated in ischaemia. *Nature,* 438**,** 1162-6.
141. KÁRADÓTTIR, R., HAMILTON, N. B., BAKIRI, Y. & ATTWELL, D. 2008. Spiking and nonspiking classes of oligodendrocyte precursor glia in CNS white matter. *Nat Neurosci,* 11**,** 450-6.
142. KARVE, I. P., ZHANG, M., HABGOOD, M., FRUGIER, T., BRODY, K. M., SASHINDRANATH, M., EK, C. J., CHAPPAZ, S., KILE, B. T., WRIGHT, D., WANG, H., JOHNSTON, L., DAGLAS, M., ATES, R. C., MEDCALF, R. L., TAYLOR, J. M. & CRACK, P. J. 2016. Ablation of Type-1 IFN Signaling in Hematopoietic Cells Confers Protection Following Traumatic Brain Injury. *eNeuro,* 3**,** ENEURO.0128-15.2016.
143. KAUPPINEN, T. M. & SWANSON, R. A. 2007. The role of poly(ADP-ribose) polymerase-1 in CNS disease. *Neuroscience,* 145**,** 1267-72.
144. KESSARIS, N., FOGARTY, M., IANNARELLI, P., GRIST, M., WEGNER, M. & RICHARDSON, W. D. 2006. Competing waves of oligodendrocytes in the forebrain and postnatal elimination of an embryonic lineage. *Nat Neurosci,* 9**,** 173-9.
145. KESSARIS, N., PRINGLE, N. & RICHARDSON, W. D. 2001. Ventral neurogenesis and the neuron-glial switch. *Neuron,* 31**,** 677-80.
146. KHAWAJA, R. R. A. A., AMIT AND FUKAYA, MASAHIRO AND JEONG, HYE-KYEONG AND GROSS, SCOTT AND GONZALEZ-FERNANDEZ, ESTIBALIZ AND SOBOLOFF, JONATHAN AND BERGLES, DWIGHT AND KANG, SHIN HYEOK 2019. Calcium Influx Through AMPA Receptors Inhibits Oligodendrocyte Regeneration in the Injured Brain *Cell Reports*.
147. KIM, T., CHELLUBOINA, B., CHOKKALLA, A. K. & VEMUGANTI, R. 2019. Age and sex differences in the pathophysiology of acute CNS injury. *Neurochemistry International,* 127**,** 22-28.
148. KIPP, M., HOCHSTRASSER, T., SCHMITZ, C. & BEYER, C. 2016. Female sex steroids and glia cells: Impact on multiple sclerosis lesion formation and fine tuning of the local neurodegenerative cellular network. *Neurosci Biobehav Rev,* 67**,** 125-36.
149. KIPP, M., NYAMOYA, S., HOCHSTRASSER, T. & AMOR, S. 2017. Multiple sclerosis animal models: a clinical and histopathological perspective. *Brain Pathology,* 27**,** 123-137.
150. KIPP, M., VICTOR, M., MARTINO, G. & FRANKLIN, R. J. 2012. Endogeneous remyelination: findings in human studies. *CNS Neurol Disord Drug Targets,* 11**,** 598-609.
151. KIRDAJOVA, D. & ANDEROVA, M. 2020. NG2 cells and their neurogenic potential. *Curr Opin Pharmacol,* 50**,** 53-60.
152. KIRDAJOVA, D., VALIHRACH, L., VALNY, M., KRISKA, J., KROCIANOVA, D., BENESOVA, S., ABAFFY, P., ZUCHA, D., KLASSEN, R., KOLENICOVA, D., HONSA, P., KUBISTA, M. & ANDEROVA, M. 2021. Transient astrocyte-like NG2

glia subpopulation emerges solely following permanent brain ischemia. *Glia,* 69**,** 2658-2681.
153. KOHAMA, S. G., ROSENE, D. L. & SHERMAN, L. S. 2012. Age-related changes in human and non-human primate white matter: from myelination disturbances to cognitive decline. *Age (Dordr),* 34**,** 1093-110.
154. KOMITOVA, M., SERWANSKI, D. R., LU, Q. R. & NISHIYAMA, A. 2011. NG2 cells are not a major source of reactive astrocytes after neocortical stab wound injury. *Glia,* 59**,** 800-9.
155. KOPYLOVA, E., NOÉ, L. & TOUZET, H. 2012. SortMeRNA: fast and accurate filtering of ribosomal RNAs in metatranscriptomic data. *Bioinformatics,* 28**,** 3211-3217.
156. KRISTIÁN, T. & SIESJÖ, B. K. 1998. Calcium in ischemic cell death. *Stroke,* 29**,** 705-18.
157. KUHN, S., GRITTI, L., CROOKS, D. & DOMBROWSKI, Y. 2019. Oligodendrocytes in Development, Myelin Generation and Beyond. *Cells,* 8.
158. KUKLEY, M., CAPETILLO-ZARATE, E. & DIETRICH, D. 2007. Vesicular glutamate release from axons in white matter. *Nat Neurosci,* 10**,** 311-20.
159. KUKLEY, M., KILADZE, M., TOGNATTA, R., HANS, M., SWANDULLA, D., SCHRAMM, J. & DIETRICH, D. 2008. Glial cells are born with synapses. *FASEB J,* 22**,** 2957-69.
160. KUKLEY, M., NISHIYAMA, A. & DIETRICH, D. 2010. The fate of synaptic input to NG2 glial cells: neurons specifically downregulate transmitter release onto differentiating oligodendroglial cells. *J Neurosci,* 30**,** 8320-31.
161. KUZNETSOVA, A., BROCKHOFF, P. & CHRISTENSEN, R. 2017. ImerTest package: tests in linear mixed models. *J. Statist. Softw,* 82**,** 1-26.
162. LECUYER, M.-A., KEBIR, H. & PRAT, A. 2016. Glial influences on BBB functions and molecular players in immune cell trafficking. *Biochimica et Biophysica Acta (BBA)-Molecular Basis of Disease,* 1862**,** 472-482.
163. LEUCHTMANN, E. A., RATNER, A. E., VIJITRUTH, R., QU, Y. & MCDONALD, J. W. 2003. AMPA receptors are the major mediators of excitotoxic death in mature oligodendrocytes. *Neurobiol Dis,* 14**,** 336-48.
164. LEWIS, D. A., HASHIMOTO, T. & VOLK, D. W. 2005. Cortical inhibitory neurons and schizophrenia. *Nature Reviews Neuroscience,* 6**,** 312-324.
165. LI, R., ZHANG, P., ZHANG, M. & YAO, Z. 2020. The roles of neuron-NG2 glia synapses in promoting oligodendrocyte development and remyelination. *Cell Tissue Res,* 381**,** 43-53.
166. LIANG, A. C., MANDEVILLE, E. T., MAKI, T., SHINDO, A., SOM, A. T., EGAWA, N., ITOH, K., CHUANG, T. T., MCNEISH, J. D., HOLDER, J. C., LOK, J., LO, E. H. & ARAI, K. 2016. Effects of Aging on Neural Stem/Progenitor Cells and Oligodendrocyte Precursor Cells after Focal Cerebral Ischemia in Spontaneously Hypertensive Rats. *Cell Transplantation,* 25**,** 705-714.
167. LIDDELOW, S. A., GUTTENPLAN, K. A., CLARKE, L. E., BENNETT, F. C., BOHLEN, C. J., SCHIRMER, L., BENNETT, M. L., MÜNCH, A. E., CHUNG, W.-S., PETERSON, T. C., WILTON, D. K., FROUIN, A., NAPIER, B. A., PANICKER, N., KUMAR, M., BUCKWALTER, M. S., ROWITCH, D. H., DAWSON, V. L., DAWSON, T. M., STEVENS, B. & BARRES, B. A. 2017. Neurotoxic reactive astrocytes are induced by activated microglia. *Nature,* 541**,** 481-487.
168. LIN, S. C. & BERGLES, D. E. 2004. Synaptic signaling between GABAergic interneurons and oligodendrocyte precursor cells in the hippocampus. *Nat Neurosci,* 7**,** 24-32.
169. LIU, F., LI, Z., LI, J., SIEGEL, C., YUAN, R. & MCCULLOUGH, L. D. 2009. Sex differences in caspase activation after stroke. *Stroke,* 40**,** 1842-1848.

170. LIU, H., YANG, Y., XIA, Y., ZHU, W., LEAK, R. K., WEI, Z., WANG, J. & HU, X. 2017. Aging of cerebral white matter. *Ageing Res Rev,* 34**,** 64-76.
171. LOULIER, K., RUAT, M. & TRAIFFORT, E. 2006. Increase of proliferating oligodendroglial progenitors in the adult mouse brain upon Sonic hedgehog delivery in the lateral ventricle. *J Neurochem,* 98**,** 530-42.
172. LOVE, M., ANDERS, S. & HUBER, W. 2014. Differential analysis of count data–the DESeq2 package. *Genome Biol,* 15**,** 10-1186.
173. LUN, A. T. L., RIESENFELD, S., ANDREWS, T., DAO, T. P., GOMES, T. & MARIONI, J. C. 2019. EmptyDrops: distinguishing cells from empty droplets in droplet-based single-cell RNA sequencing data. *Genome Biol,* 20**,** 63.
174. LUOMA, J. I., KELLEY, B. G. & MERMELSTEIN, P. G. 2011. Progesterone inhibition of voltage-gated calcium channels is a potential neuroprotective mechanism against excitotoxicity. *Steroids,* 76**,** 845-55.
175. LUYT, K., VARADI, A. & MOLNAR, E. 2003. Functional metabotropic glutamate receptors are expressed in oligodendrocyte progenitor cells. *Journal of Neurochemistry,* 84**,** 1452-1464.
176. MAGAKI, S. D., WILLIAMS, C. K. & VINTERS, H. V. 2018. Glial function (and dysfunction) in the normal & ischemic brain. *Neuropharmacology,* 134**,** 218-225.
177. MAHER, F. O., MARTIN, D. S. & LYNCH, M. A. 2004. Increased IL-1beta in cortex of aged rats is accompanied by downregulation of ERK and PI-3 kinase. *Neurobiol Aging,* 25**,** 795-806.
178. MAHER, F. O., NOLAN, Y. & LYNCH, M. A. 2005. Downregulation of IL-4-induced signalling in hippocampus contributes to deficits in LTP in the aged rat. *Neurobiol Aging,* 26**,** 717-28.
179. MANCARCI, B. O., TOKER, L., TRIPATHY, S. J., LI, B., ROCCO, B., SIBILLE, E. & PAVLIDIS, P. 2017. Cross-laboratory analysis of brain cell type transcriptomes with applications to interpretation of bulk tissue data. *Eneuro,* 4.
180. MANWANI, B., LIU, F., SCRANTON, V., HAMMOND, M. D., SANSING, L. H. & MCCULLOUGH, L. D. 2013. Differential effects of aging and sex on stroke induced inflammation across the lifespan. *Experimental Neurology,* 249**,** 120-131.
181. MANWANI, B., LIU, F., XU, Y., PERSKY, R., LI, J. & MCCULLOUGH, L. D. 2011. Functional recovery in aging mice after experimental stroke. *Brain, Behavior, and Immunity,* 25**,** 1689-1700.
182. MARQUES, S., VAN BRUGGEN, D. & CASTELO-BRANCO, G. 2019. Single-Cell RNA Sequencing of Oligodendrocyte Lineage Cells from the Mouse Central Nervous System. *Methods Mol Biol,* 1936**,** 1-21.
183. MARQUES, S., VAN BRUGGEN, D., VANICHKINA, D. P., FLORIDDIA, E. M., MUNGUBA, H., VAREMO, L., GIACOMELLO, S., FALCAO, A. M., MEIJER, M., BJORKLUND, A. K., HJERLING-LEFFLER, J., TAFT, R. J. & CASTELO-BRANCO, G. 2018. Transcriptional Convergence of Oligodendrocyte Lineage Progenitors during Development. *Dev Cell,* 46**,** 504-517.e7.
184. MARQUES, S., ZEISEL, A., CODELUPPI, S., VAN BRUGGEN, D., MENDANHA FALCAO, A., XIAO, L., LI, H., HARING, M., HOCHGERNER, H., ROMANOV, R. A., GYLLBORG, D., MUNOZ MANCHADO, A., LA MANNO, G., LONNERBERG, P., FLORIDDIA, E. M., REZAYEE, F., ERNFORS, P., ARENAS, E., HJERLING-LEFFLER, J., HARKANY, T., RICHARDSON, W. D., LINNARSSON, S. & CASTELO-BRANCO, G. 2016. Oligodendrocyte heterogeneity in the mouse juvenile and adult central nervous system. *Science,* 352**,** 1326-1329.
185. MARSH, B., STEVENS, S. L., PACKARD, A. E. B., GOPALAN, B., HUNTER, B., LEUNG, P. Y., HARRINGTON, C. A. & STENZEL-POORE, M. P. 2009. Systemic Lipopolysaccharide Protects the Brain from Ischemic Injury by Reprogramming the

Response of the Brain to Stroke: A Critical Role for IRF3. *The Journal of Neuroscience,* 29**,** 9839-9849.
186. MARTINEZ-LOZADA, Z., WAGGENER, C. T., KIM, K., ZOU, S., KNAPP, P. E., HAYASHI, Y., ORTEGA, A. & FUSS, B. 2014. Activation of sodium-dependent glutamate transporters regulates the morphological aspects of oligodendrocyte maturation via signaling through calcium/calmodulin-dependent kinase IIβ's actin-binding/-stabilizing domain. *Glia,* 62**,** 1543-1558.
187. MATHYS, H., ADAIKKAN, C., GAO, F., YOUNG, J. Z., MANET, E., HEMBERG, M., DE JAGER, P. L., RANSOHOFF, R. M., REGEV, A. & TSAI, L.-H. 2017. Temporal tracking of microglia activation in neurodegeneration at single-cell resolution. *Cell reports,* 21**,** 366-380.
188. MCDONALD, J. W., BHATTACHARYYA, T., SENSI, S. L., LOBNER, D., YING, H. S., CANZONIERO, L. M. & CHOI, D. W. 1998. Extracellular acidity potentiates AMPA receptor-mediated cortical neuronal death. *J Neurosci,* 18**,** 6290-9.
189. MCDONOUGH, A., LEE, R. V., NOOR, S., LEE, C., LE, T., IORGA, M., PHILLIPS, J. L., MURPHY, S., MÖLLER, T. & WEINSTEIN, J. R. 2017a. Ischemia/reperfusion induces interferon-stimulated gene expression in microglia. *Journal of Neuroscience,* 37**,** 8292-8308.
190. MCDONOUGH, A., LEE, R. V. & WEINSTEIN, J. R. 2017b. Microglial Interferon Signaling and White Matter. *Neurochemical Research,* 42**,** 2625-2638.
191. MCTIGUE, D. M. & TRIPATHI, R. B. 2008. The life, death, and replacement of oligodendrocytes in the adult CNS. *J Neurochem,* 107**,** 1-19.
192. MCTIGUE, D. M., WEI, P. & STOKES, B. T. 2001. Proliferation of NG2-positive cells and altered oligodendrocyte numbers in the contused rat spinal cord. *J Neurosci,* 21**,** 3392-400.
193. MENG, Q.-J., LOGUNOVA, L., MAYWOOD, E. S., GALLEGO, M., LEBIECKI, J., BROWN, T. M., SLÁDEK, M., SEMIKHODSKII, A. S., GLOSSOP, N. R. & PIGGINS, H. D. 2008. Setting clock speed in mammals: the CK1ε tau mutation in mice accelerates circadian pacemakers by selectively destabilizing PERIOD proteins. *Neuron,* 58**,** 78-88.
194. MENN, B., GARCIA-VERDUGO, J. M., YASCHINE, C., GONZALEZ-PEREZ, O., ROWITCH, D. & ALVAREZ-BUYLLA, A. 2006. Origin of oligodendrocytes in the subventricular zone of the adult brain. *J Neurosci,* 26**,** 7907-18.
195. MERICO, D., ISSERLIN, R., STUEKER, O., EMILI, A. & BADER, G. D. 2010. Enrichment map: a network-based method for gene-set enrichment visualization and interpretation. *PloS one,* 5**,** e13984.
196. MI, S., PEPINSKY, R. B. & CADAVID, D. 2013. Blocking LINGO-1 as a therapy to promote CNS repair: from concept to the clinic. *CNS Drugs,* 27**,** 493-503.
197. MILOSEVIC, A., LIEBMANN, T., KNUDSEN, M., SCHINTU, N., SVENNINGSSON, P. & GREENGARD, P. 2017. Cell- and region-specific expression of depression-related protein p11 (S100a10) in the brain. *J Comp Neurol,* 525**,** 955-975.
198. MITSIOS, N., SAKA, M., KRUPINSKI, J., PENNUCCI, R., SANFELIU, C., WANG, Q., RUBIO, F., GAFFNEY, J., KUMAR, P. & KUMAR, S. 2007. A microarray study of gene and protein regulation in human and rat brain following middle cerebral artery occlusion. *BMC neuroscience,* 8**,** 1-14.
199. MORI, T., TAN, J., ARENDASH, G. W., KOYAMA, N., NOJIMA, Y. & TOWN, T. 2008. Overexpression of human S100B exacerbates brain damage and periinfarct gliosis after permanent focal ischemia. *Stroke,* 39**,** 2114-21.
200. MORRISON, J. H. & HOF, P. R. 1997. Life and death of neurons in the aging brain. *Science,* 278**,** 412-9.

201. MOSHREFI-RAVASDJANI, B., DUBLIN, P., SEIFERT, G., JENNISSEN, K., STEINHÄUSER, C., KAFITZ, K. W. & ROSE, C. R. 2017. Changes in the proliferative capacity of NG2 cell subpopulations during postnatal development of the mouse hippocampus. *Brain Structure and Function,* 222**,** 831-847.
202. MOSTAFAVI, S., YOSHIDA, H., MOODLEY, D., LEBOITÉ, H., ROTHAMEL, K., RAJ, T., YE, C. J., CHEVRIER, N., ZHANG, S.-Y. & FENG, T. 2016. Parsing the interferon transcriptional network and its disease associations. *Cell,* 164**,** 564-578.
203. MRDJEN, D., PAVLOVIC, A., HARTMANN, F. J., SCHREINER, B., UTZ, S. G., LEUNG, B. P., LELIOS, I., HEPPNER, F. L., KIPNIS, J. & MERKLER, D. 2018. High-dimensional single-cell mapping of central nervous system immune cells reveals distinct myeloid subsets in health, aging, and disease. *Immunity,* 48**,** 380-395. e6.
204. NASRABADY, S. E., RIZVI, B., GOLDMAN, J. E. & BRICKMAN, A. M. 2018. White matter changes in Alzheimer's disease: a focus on myelin and oligodendrocytes. *Acta Neuropathol Commun,* 6**,** 22.
205. NAWASHIRO, H., BRENNER, M., FUKUI, S., SHIMA, K. & HALLENBECK, J. M. 2000. High Susceptibility to Cerebral Ischemia in GFAP-Null Mice. *Journal of Cerebral Blood Flow & Metabolism,* 20**,** 1040-1044.
206. NEDERGAARD, M. & DIRNAGL, U. 2005. Role of glial cells in cerebral ischemia. *Glia,* 50**,** 281-286.
207. NEPRASOVA, H., ANDEROVA, M., PETRIK, D., VARGOVA, L., KUBINOVA, S., CHVATAL, A. & SYKOVA, E. 2007. High extracellular K(+) evokes changes in voltage-dependent K(+) and Na (+) currents and volume regulation in astrocytes. *Pflugers Arch,* 453**,** 839-49.
208. NEWMAN, A. M., LIU, C. L., GREEN, M. R., GENTLES, A. J., FENG, W., XU, Y., HOANG, C. D., DIEHN, M. & ALIZADEH, A. A. 2015. Robust enumeration of cell subsets from tissue expression profiles. *Nature Methods,* 12**,** 453-457.
209. NEWMAN, M. E. 2006. Modularity and community structure in networks. *Proceedings of the national academy of sciences,* 103**,** 8577-8582.
210. NIRAULA, A., SHERIDAN, J. F. & GODBOUT, J. P. 2017. Microglia Priming with Aging and Stress. *Neuropsychopharmacology,* 42**,** 318-333.
211. NISHIYAMA, A., BOSHANS, L., GONCALVES, C. M., WEGRZYN, J. & PATEL, K. D. 2016. Lineage, fate, and fate potential of NG2-glia. *Brain Res,* 1638**,** 116-128.
212. NISHIYAMA, A., KOMITOVA, M., SUZUKI, R. & ZHU, X. 2009. Polydendrocytes (NG2 cells): multifunctional cells with lineage plasticity. *Nat Rev Neurosci,* 10**,** 9-22.
213. NOLTE, C., MATYASH, M., PIVNEVA, T., SCHIPKE, C. G., OHLEMEYER, C., HANISCH, U. K., KIRCHHOFF, F. & KETTENMANN, H. 2001. GFAP promoter-controlled EGFP-expressing transgenic mice: a tool to visualize astrocytes and astrogliosis in living brain tissue. *Glia,* 33**,** 72-86.
214. NOTOMI, T. & SHIGEMOTO, R. 2004. Immunohistochemical localization of Ih channel subunits, HCN1-4, in the rat brain. *J Comp Neurol,* 471**,** 241-76.
215. NOVITCH, B. G., CHEN, A. I. & JESSELL, T. M. 2001. Coordinate regulation of motor neuron subtype identity and pan-neuronal properties by the bHLH repressor Olig2. *Neuron,* 31**,** 773-89.
216. OHTA, K., IWAI, M., SATO, K., OMORI, N., NAGANO, I., SHOJI, M. & ABE, K. 2003. Dissociative increase of oligodendrocyte progenitor cells between young and aged rats after transient cerebral ischemia. *Neuroscience Letters,* 335**,** 159-162.
217. OLIVEIRA-FERREIRA, A. I., MAJOR, S., PRZESDZING, I., KANG, E. J. & DREIER, J. P. 2019. Spreading depolarizations in the rat endothelin-1 model of focal cerebellar ischemia. *J Cereb Blood Flow Metab***,** 271678X19861604.

218. ONTENIENTE, B., COURIAUD, C., BRAUDEAU, J., BENCHOUA, A. & GUEGAN, C. 2003. The mechanisms of cell death in focal cerebral ischemia highlight neuroprotective perspectives by anti-caspase therapy. *Biochem Pharmacol,* 66**,** 1643-9.
219. ORI, A., TOYAMA, B. H., HARRIS, M. S., BOCK, T., ISKAR, M., BORK, P., INGOLIA, N. T., HETZER, M. W. & BECK, M. 2015. Integrated transcriptome and proteome analyses reveal organ-specific proteome deterioration in old rats. *Cell systems,* 1**,** 224-237.
220. OWENS, T., KHOROOSHI, R., WLODARCZYK, A. & ASGARI, N. 2014. Interferons in the central nervous system: a few instruments play many tunes. *Glia,* 62**,** 339-355.
221. PABLO, Y., NILSSON, M., PEKNA, M. & PEKNY, M. 2013. Intermediate filaments are important for astrocyte response to oxidative stress induced by oxygen-glucose deprivation and reperfusion. *Histochem Cell Biol,* 140**,** 81-91.
222. PAKKENBERG, B. & GUNDERSEN, H. J. G. 1997. Neocortical neuron number in humans: Effect of sex and age. *Journal of Comparative Neurology,* 384**,** 312-320.
223. PAN, S., MAYORAL, S. R., CHOI, H. S., CHAN, J. R. & KHEIRBEK, M. A. 2020. Preservation of a remote fear memory requires new myelin formation. *Nat Neurosci,* 23**,** 487-499.
224. PAPAZIAN, I., KYRARGYRI, V., EVANGELIDOU, M., VOULGARI-KOKOTA, A. & PROBERT, L. 2018. Mesenchymal Stem Cell Protection of Neurons against Glutamate Excitotoxicity Involves Reduction of NMDA-Triggered Calcium Responses and Surface GluR1, and Is Partly Mediated by TNF. *Int J Mol Sci,* 19.
225. PAUL, A., CHAKER, Z. & DOETSCH, F. 2017. Hypothalamic regulation of regionally distinct adult neural stem cells and neurogenesis. *Science,* 356**,** 1383-1386.
226. PEKNY, M. & NILSSON, M. 2005. Astrocyte activation and reactive gliosis. *Glia,* 50**,** 427-34.
227. PETERS, A. & SETHARES, C. 2002. Aging and the myelinated fibers in prefrontal cortex and corpus callosum of the monkey. *J Comp Neurol,* 442**,** 277-91.
228. PETRYNIAK, M. A., POTTER, G. B., ROWITCH, D. H. & RUBENSTEIN, J. L. 2007. Dlx1 and Dlx2 control neuronal versus oligodendroglial cell fate acquisition in the developing forebrain. *Neuron,* 55**,** 417-33.
229. PFORTE, C., HENRICH-NOACK, P., BALDAUF, K. & REYMANN, K. G. 2005. Increase in proliferation and gliogenesis but decrease of early neurogenesis in the rat forebrain shortly after transient global ischemia. *Neuroscience,* 136**,** 1133-46.
230. PHILIPS, T., BENTO-ABREU, A., NONNEMAN, A., HAECK, W., STAATS, K., GEELEN, V., HERSMUS, N., KÜSTERS, B., VAN DEN BOSCH, L., VAN DAMME, P., RICHARDSON, W. D. & ROBBERECHT, W. 2013. Oligodendrocyte dysfunction in the pathogenesis of amyotrophic lateral sclerosis. *Brain,* 136**,** 471-82.
231. PIVONKOVA, H., BENESOVA, J., BUTENKO, O., CHVATAL, A. & ANDEROVA, M. 2010. Impact of global cerebral ischemia on K+ channel expression and membrane properties of glial cells in the rat hippocampus. *Neurochemistry International,* 57**,** 783-794.
232. PLEMEL, J. R., LIU, W. Q. & YONG, V. W. 2017. Remyelination therapies: a new direction and challenge in multiple sclerosis. *Nat Rev Drug Discov,* 16**,** 617-634.
233. POLITO, A. & REYNOLDS, R. 2005. NG2-expressing cells as oligodendrocyte progenitors in the normal and demyelinated adult central nervous system. *Journal of anatomy,* 207**,** 707-716.
234. POPA-WAGNER, A., CARMICHAEL, S. T., KOKAIA, Z., KESSLER, C. & WALKER, L. C. 2007. The response of the aged brain to stroke: too much, too soon? *Current Neurovascular Research,* 4**,** 216-227.

235. PRAET, J., GUGLIELMETTI, C., BERNEMAN, Z., VAN DER LINDEN, A. & PONSAERTS, P. 2014. Cellular and molecular neuropathology of the cuprizone mouse model: clinical relevance for multiple sclerosis. *Neurosci Biobehav Rev,* 47**,** 485-505.
236. PRINZ, M. & KNOBELOCH, K.-P. 2012. Type I interferons as ambiguous modulators of chronic inflammation in the central nervous system. *Frontiers in immunology,* 3**,** 67.
237. PSACHOULIA, K., JAMEN, F., YOUNG, K. M. & RICHARDSON, W. D. 2009. Cell cycle dynamics of NG2 cells in the postnatal and ageing brain. *Neuron Glia Biol,* 5**,** 57-67.
238. RAABE, F. J., SLAPAKOVA, L., ROSSNER, M. J., CANTUTI-CASTELVETRI, L., SIMONS, M., FALKAI, P. G. & SCHMITT, A. 2019. Oligodendrocytes as A New Therapeutic Target in Schizophrenia: From Histopathological Findings to Neuron-Oligodendrocyte Interaction. *Cells,* 8.
239. RAMA, R. & GARCÍA, J. C. 2016. Excitotoxicity and Oxidative Stress in Acute Stroke. *Ischemic Stroke - Updates.*
240. RAPPSILBER, J., MANN, M. & ISHIHAMA, Y. 2007. Protocol for micro-purification, enrichment, pre-fractionation and storage of peptides for proteomics using StageTips. *Nature protocols,* 2**,** 1896-1906.
241. RITZEL, R. M., LAI, Y.-J., CRAPSER, J. D., PATEL, A. R., SCHRECENGOST, A., GRENIER, J. M., MANCINI, N. S., PATRIZZ, A., JELLISON, E. R., MORALES-SCHEIHING, D., VENNA, V. R., KOFLER, J. K., LIU, F., VERMA, R. & MCCULLOUGH, L. D. 2018. Aging alters the immunological response to ischemic stroke. *Acta Neuropathologica,* 136**,** 89-110.
242. RIVERS, L. E., YOUNG, K. M., RIZZI, M., JAMEN, F., PSACHOULIA, K., WADE, A., KESSARIS, N. & RICHARDSON, W. D. 2008. PDGFRA/NG2 glia generate myelinating oligodendrocytes and piriform projection neurons in adult mice. *Nat Neurosci,* 11**,** 1392-401.
243. ROBINS, S. C., TRUDEL, E., ROTONDI, O., LIU, X., DJOGO, T., KRYZSKAYA, D., BOURQUE, C. W. & KOKOEVA, M. V. 2013. Evidence for NG2-glia derived, adult-born functional neurons in the hypothalamus. *PLoS One,* 8**,** e78236.
244. ROSELLI, F., CHANDRASEKAR, A. & MORGANTI-KOSSMANN, M. C. 2018. Interferons in traumatic brain and spinal cord injury: current evidence for translational application. *Frontiers in Neurology,* 9**,** 458.
245. ROSSI, D. J., BRADY, J. D. & MOHR, C. 2007. Astrocyte metabolism and signaling during brain ischemia. *Nat Neurosci,* 10**,** 1377-86.
246. ROTH, A., GILL, R. & CERTA, U. 2003. Temporal and spatial gene expression patterns after experimental stroke in a rat model and characterization of PC4, a potential regulator of transcription. *Molecular And Cellular Neuroscience,* 22**,** 353-364.
247. RUSNAKOVA, V., HONSA, P., DZAMBA, D., STÅHLBERG, A., KUBISTA, M. & ANDEROVA, M. 2013. Heterogeneity of astrocytes: from development to injury - single cell gene expression. *PLoS One,* 8**,** e69734.
248. SAAB, A. S., TZVETAVONA, I. D., TREVISIOL, A., BALTAN, S., DIBAJ, P., KUSCH, K., MÖBIUS, W., GOETZE, B., JAHN, H. M., HUANG, W., STEFFENS, H., SCHOMBURG, E. D., PÉREZ-SAMARTÍN, A., PÉREZ-CERDÁ, F., BAKHTIARI, D., MATUTE, C., LÖWEL, S., GRIESINGER, C., HIRRLINGER, J., KIRCHHOFF, F. & NAVE, K. A. 2016. Oligodendroglial NMDA Receptors Regulate Glucose Import and Axonal Energy Metabolism. *Neuron,* 91**,** 119-32.
249. SANCHEZ-GOMEZ, M. V., ALBERDI, E., PEREZ-NAVARRO, E., ALBERCH, J. & MATUTE, C. 2011. Bax and calpain mediate excitotoxic oligodendrocyte death induced by activation of both AMPA and kainate receptors. *J Neurosci,* 31**,** 2996-3006.
250. SATOH, A., IMAI, S. I. & GUARENTE, L. 2017. The brain, sirtuins, and ageing. *Nat Rev Neurosci,* 18**,** 362-374.

251. SAUER, J.-F., STRÜBER, M. & BARTOS, M. 2015. Impaired fast-spiking interneuron function in a genetic mouse model of depression. *Elife,* 4**,** e04979.
252. SAUNDERS, A., MACOSKO, E. Z., WYSOKER, A., GOLDMAN, M., KRIENEN, F. M., DE RIVERA, H., BIEN, E., BAUM, M., BORTOLIN, L. & WANG, S. 2018. Molecular diversity and specializations among the cells of the adult mouse brain. *Cell,* 174**,** 1015-1030. e16.
253. SAVITZ, S. I. 2013. Cell Therapies. *Stroke,* 44**,** S107-S109.
254. SEIB, D. R. & MARTIN-VILLALBA, A. 2015. Neurogenesis in the Normal Ageing Hippocampus: A Mini-Review. *Gerontology,* 61**,** 327-35.
255. SELVAMANI, A., WILLIAMS, MADISON H., MIRANDA, RAJESH C. & SOHRABJI, F. 2014. Circulating miRNA profiles provide a biomarker for severity of stroke outcomes associated with age and sex in a rat model. *Clinical Science,* 127**,** 77-89.
256. SELVARAJ, U. M. & STOWE, A. M. 2017. Long-term T cell responses in the brain after an ischemic stroke. *Discovery medicine,* 24**,** 323-333.
257. SHAO, X., LIAO, J., LU, X., XUE, R., AI, N. & FAN, X. 2020. scCATCH: Automatic Annotation on Cell Types of Clusters from Single-Cell RNA Sequencing Data. *iScience,* 23**,** 100882.
258. SHIVJI, K. K., KENNY, M. K. & WOOD, R. D. 1992. Proliferating cell nuclear antigen is required for DNA excision repair. *Cell,* 69**,** 367-74.
259. SCHOOLS, G. P., ZHOU, M. & KIMELBERG, H. K. 2003. Electrophysiologically "complex" glial cells freshly isolated from the hippocampus are immunopositive for the chondroitin sulfate proteoglycan NG2. *J Neurosci Res,* 73**,** 765-77.
260. SIMON, C., GOTZ, M. & DIMOU, L. 2011. Progenitors in the adult cerebral cortex: cell cycle properties and regulation by physiological stimuli and injury. *Glia,* 59**,** 869-81.
261. SIMONS, M. & NAVE, K. A. 2015. Oligodendrocytes: Myelination and Axonal Support. *Cold Spring Harb Perspect Biol,* 8**,** a020479.
262. SIMPKINS, J. W., RAJAKUMAR, G., ZHANG, Y.-Q., SIMPKINS, C. E., GREENWALD, D., CHUN, J. Y., BODOR, N. & DAY, A. L. 1997. Estrogens may reduce mortality and ischemic damage caused by middle cerebral artery occlusion in the female rat. *Journal of neurosurgery,* 87**,** 724-730.
263. SIRKO, S., BEHRENDT, G., JOHANSSON, P. A., TRIPATHI, P., COSTA, M., BEK, S., HEINRICH, C., TIEDT, S., COLAK, D., DICHGANS, M., FISCHER, I. R., PLESNILA, N., STAUFENBIEL, M., HAASS, C., SNAPYAN, M., SAGHATELYAN, A., TSAI, L. H., FISCHER, A., GROBE, K., DIMOU, L. & GÖTZ, M. 2013. Reactive glia in the injured brain acquire stem cell properties in response to sonic hedgehog. [corrected]. *Cell Stem Cell,* 12**,** 426-39.
264. SKRIPULETZ, T., GUDI, V., HACKSTETTE, D. & STANGEL, M. 2011. De- and remyelination in the CNS white and grey matter induced by cuprizone: The old, the new, and the unexpected. *Histology and Histopathology,* 26**,** 1585-1597.
265. SOFRONIEW, M. V. & VINTERS, H. V. 2010. Astrocytes: biology and pathology. *Acta Neuropathol,* 119**,** 7-35.
266. SOHRABJI, F., BAKE, S. & LEWIS, D. K. 2013. Age-related changes in brain support cells: Implications for stroke severity. *Neurochemistry international,* 63**,** 291-301.
267. SOHRABJI, F., OKOREEH, A. & PANTA, A. 2019. Sex hormones and stroke: Beyond estrogens. *Hormones and Behavior,* 111**,** 87-95.
268. SOLOMON, S. S., SOLOMON, S., MCFALL, A. M., SRIKRISHNAN, A. K., ANAND, S., VERMA, V., VASUDEVAN, C. K., BALAKRISHNAN, P., OGBURN, E. L., MOULTON, L. H., KUMAR, M. S., SACHDEVA, K. S., LAEYENDECKER, O., CELENTANO, D. D., LUCAS, G. M. & MEHTA, S. H. 2019. Integrated HIV

testing, prevention, and treatment intervention for key populations in India: a cluster-randomised trial. *Lancet HIV,* 6**,** e283-e296.
269. SONG, F. E., HUANG, J. L., LIN, S. H., WANG, S., MA, G. F. & TONG, X. P. 2017. Roles of NG2-glia in ischemic stroke. *CNS Neurosci Ther,* 23**,** 547-553.
270. SOREQ, L., ROSE, J., SOREQ, E., HARDY, J., TRABZUNI, D., COOKSON, M. R., SMITH, C., RYTEN, M., PATANI, R. & ULE, J. 2017. Major shifts in glial regional identity are a transcriptional hallmark of human brain aging. *Cell reports,* 18**,** 557-570.
271. SOUSOUNIS, K., BADDOUR, J. A. & TSONIS, P. A. 2014. Aging and regeneration in vertebrates. *Curr Top Dev Biol,* 108**,** 217-46.
272. SPITZER, S., VOLBRACHT, K., LUNDGAARD, I. & KARADOTTIR, R. T. 2016. Glutamate signalling: A multifaceted modulator of oligodendrocyte lineage cells in health and disease. *Neuropharmacology,* 110**,** 574-585.
273. SPITZER, S. O., SITNIKOV, S., KAMEN, Y., EVANS, K. A., KRONENBERG-VERSTEEG, D., DIETMANN, S., DE FARIA, O., JR., AGATHOU, S. & KARADOTTIR, R. T. 2019. Oligodendrocyte Progenitor Cells Become Regionally Diverse and Heterogeneous with Age. *Neuron,* 101**,** 459-471.e5.
274. SRINIVASAN, K., FRIEDMAN, B. A., LARSON, J. L., LAUFFER, B. E., GOLDSTEIN, L. D., APPLING, L. L., BORNEO, J., POON, C., HO, T. & CAI, F. 2016. Untangling the brain's neuroinflammatory and neurodegenerative transcriptional responses. *Nature communications,* 7**,** 1-16.
275. STALLCUP, W. B. & BEASLEY, L. 1987. Bipotential glial precursor cells of the optic nerve express the NG2 proteoglycan. *J Neurosci,* 7**,** 2737-44.
276. STAR, B. J., VOGEL, D. Y., KIPP, M., PUENTES, F., BAKER, D. & AMOR, S. 2012. In vitro and in vivo models of multiple sclerosis. *CNS Neurol Disord Drug Targets,* 11**,** 570-88.
277. STERR, A., KUHN, M., NISSEN, C., ETTINE, D., FUNK, S., FEIGE, B., UMAROVA, R., URBACH, H., WEILLER, C. & RIEMANN, D. 2018. Post-stroke insomnia in community-dwelling patients with chronic motor stroke: Physiological evidence and implications for stroke care. *Scientific Reports,* 8**,** 1-9.
278. STRECKER, J.-K., SCHMIDT, A., SCHÄBITZ, W.-R. & MINNERUP, J. 2017. Neutrophil granulocytes in cerebral ischemia–evolution from killers to key players. *Neurochemistry International,* 107**,** 117-126.
279. STUART, T., BUTLER, A., HOFFMAN, P., HAFEMEISTER, C., PAPALEXI, E., MAUCK, W. M., 3RD, HAO, Y., STOECKIUS, M., SMIBERT, P. & SATIJA, R. 2019. Comprehensive Integration of Single-Cell Data. *Cell,* 177**,** 1888-1902.e21.
280. SUÁREZ-POZOS, E., THOMASON, E. J. & FUSS, B. 2020. Glutamate Transporters: Expression and Function in Oligodendrocytes. *Neurochem Res,* 45**,** 551-560.
281. SUBRAMANIAN, A., TAMAYO, P., MOOTHA, V. K., MUKHERJEE, S., EBERT, B. L., GILLETTE, M. A., PAULOVICH, A., POMEROY, S. L., GOLUB, T. R. & LANDER, E. S. 2005. Gene set enrichment analysis: a knowledge-based approach for interpreting genome-wide expression profiles. *Proceedings of the National Academy of Sciences,* 102**,** 15545-15550.
282. SUN, W., MCCONNELL, E., PARE, J.-F., XU, Q., CHEN, M., PENG, W., LOVATT, D., HAN, X., SMITH, Y. & NEDERGAARD, M. 2013. Glutamate-dependent neuroglial calcium signaling differs between young and adult brain. *Science,* 339**,** 197-200.
283. SZKLARCZYK, D., FRANCESCHINI, A., WYDER, S., FORSLUND, K., HELLER, D., HUERTA-CEPAS, J., SIMONOVIC, M., ROTH, A., SANTOS, A. & TSAFOU, K. P. 2015. STRING v10: protein–protein interaction networks, integrated over the tree of life. *Nucleic acids research,* 43**,** D447-D452.

284. TAKAGI, Y., HARADA, J., CHIARUGI, A. & MOSKOWITZ, M. A. 2002. STAT1 is activated in neurons after ischemia and contributes to ischemic brain injury. *Journal of Cerebral Blood Flow & Metabolism,* 22**,** 1311-1318.
285. TAKANO, T., OBERHEIM, N., COTRINA, M. L. & NEDERGAARD, M. 2009. Astrocytes and Ischemic Injury. *Stroke,* 40**,** S8-S12.
286. TAMURA, Y., KATAOKA, Y., CUI, Y., TAKAMORI, Y., WATANABE, Y. & YAMADA, H. 2007. Multi-directional differentiation of doublecortin- and NG2-immunopositive progenitor cells in the adult rat neocortex in vivo. *Eur J Neurosci,* 25**,** 3489-98.
287. TAN, A. M., ZHANG, W. & LEVINE, J. M. 2005. NG2: a component of the glial scar that inhibits axon growth. *J Anat,* 207**,** 717-25.
288. TANAKA, K., NOGAWA, S., ITO, D., SUZUKI, S., DEMBO, T., KOSAKAI, A. & FUKUUCHI, Y. 2001. Activation of NG2-positive oligodendrocyte progenitor cells during post-ischemic reperfusion in the rat brain. *Neuroreport,* 12**,** 2169-74.
289. TANNER, D. C., CHERRY, J. D. & MAYER-PRÖSCHEL, M. 2011. Oligodendrocyte progenitors reversibly exit the cell cycle and give rise to astrocytes in response to interferon-γ. *J Neurosci,* 31**,** 6235-46.
290. TASIC, B., MENON, V., NGUYEN, T. N., KIM, T. K., JARSKY, T., YAO, Z., LEVI, B., GRAY, L. T., SORENSEN, S. A. & DOLBEARE, T. 2016. Adult mouse cortical cell taxonomy revealed by single cell transcriptomics. *Nature neuroscience,* 19**,** 335-346.
291. TAYLOR, J. M., MINTER, M. R., NEWMAN, A. G., ZHANG, M., ADLARD, P. A. & CRACK, P. J. 2014. Type-1 interferon signaling mediates neuro-inflammatory events in models of Alzheimer's disease. *Neurobiology of aging,* 35**,** 1012-1023.
292. TRAPP, B. D., PETERSON, J., RANSOHOFF, R. M., RUDICK, R., MÖRK, S. & BÖ, L. 1998. Axonal transection in the lesions of multiple sclerosis. *N Engl J Med,* 338**,** 278-85.
293. TRIPATHI, A. 2012. New cellular and molecular approaches to ageing brain. *Ann Neurosci,* 19**,** 177-82.
294. TRIPATHI, R. B., RIVERS, L. E., YOUNG, K. M., JAMEN, F. & RICHARDSON, W. D. 2010. NG2 glia generate new oligodendrocytes but few astrocytes in a murine experimental autoimmune encephalomyelitis model of demyelinating disease. *J Neurosci,* 30**,** 16383-90.
295. TSOA, R. W., COSKUN, V., HO, C. K. & DE VELLIS, J. 2014. Spatiotemporally different origins of NG2 progenitors produce cortical interneurons versus glia in the mammalian forebrain. 111**,** 7444-9.
296. TSUIJI, H., INOUE, I., TAKEUCHI, M., FURUYA, A., YAMAKAGE, Y., WATANABE, S., KOIKE, M., HATTORI, M. & YAMANAKA, K. 2017. TDP-43 accelerates age-dependent degeneration of interneurons. *Scientific reports,* 7**,** 1-13.
297. TURNER, R. J. & SHARP, F. R. 2016. Implications of MMP9 for blood brain barrier disruption and hemorrhagic transformation following ischemic stroke. *Frontiers in cellular neuroscience,* 10**,** 56.
298. TYANOVA, S., TEMU, T., SINITCYN, P., CARLSON, A., HEIN, M. Y., GEIGER, T., MANN, M. & COX, J. 2016. The Perseus computational platform for comprehensive analysis of (prote) omics data. *Nature methods,* 13**,** 731-740.
299. UNAL-CEVIK, I., KILINC, M., CAN, A., GURSOY-OZDEMIR, Y. & DALKARA, T. 2004. Apoptotic and necrotic death mechanisms are concomitantly activated in the same cell after cerebral ischemia. *Stroke,* 35**,** 2189-94.
300. VALNY, M., HONSA, P., KIRDAJOVA, D., KAMENIK, Z. & ANDEROVA, M. 2016. Tamoxifen in the Mouse Brain: Implications for Fate-Mapping Studies Using the Tamoxifen-Inducible Cre-loxP System. *Front Cell Neurosci,* 10**,** 243.

301. VALNY, M., HONSA, P., WALOSCHKOVA, E., MATUSKOVA, H., KRISKA, J., KIRDAJOVA, D., ANDROVIC, P., VALIHRACH, L., KUBISTA, M. & ANDEROVA, M. 2018. A single-cell analysis reveals multiple roles of oligodendroglial lineage cells during post-ischemic regeneration. *Glia,* 66**,** 1068-1081.
302. VANGILDER, R. L., HUBER, J. D., ROSEN, C. L. & BARR, T. L. 2012a. The transcriptome of cerebral ischemia. *Brain Res Bull,* 88**,** 313-9.
303. VANGILDER, R. L., HUBER, J. D., ROSEN, C. L. & BARR, T. L. 2012b. The transcriptome of cerebral ischemia. *Brain research bulletin,* 88**,** 313-319.
304. VEGA-RIQUER, J. M., MENDEZ-VICTORIANO, G., MORALES-LUCKIE, R. A. & GONZALEZ-PEREZ, O. 2019. Five Decades of Cuprizone, an Updated Model to Replicate Demyelinating Diseases. *Curr Neuropharmacol,* 17**,** 129-141.
305. VÉLEZ-FORT, M., MALDONADO, P. P., BUTT, A. M., AUDINAT, E. & ANGULO, M. C. 2010. Postnatal switch from synaptic to extrasynaptic transmission between interneurons and NG2 cells. *J Neurosci,* 30**,** 6921-9.
306. VERMA, M., WILLS, Z. & CHU, C. T. 2018. Excitatory Dendritic Mitochondrial Calcium Toxicity: Implications for Parkinson's and Other Neurodegenerative Diseases. *Front Neurosci,* 12**,** 523.
307. VERRET, L., MANN, E. O., HANG, G. B., BARTH, A. M., COBOS, I., HO, K., DEVIDZE, N., MASLIAH, E., KREITZER, A. C. & MODY, I. 2012. Inhibitory interneuron deficit links altered network activity and cognitive dysfunction in Alzheimer model. *Cell,* 149**,** 708-721.
308. VIGANÒ, F., MÖBIUS, W., GÖTZ, M. & DIMOU, L. 2013. Transplantation reveals regional differences in oligodendrocyte differentiation in the adult brain. *Nat Neurosci,* 16**,** 1370-2.
309. VRENKEN, H., POUWELS, P. J., ROPELE, S., KNOL, D. L., GEURTS, J. J., POLMAN, C. H., BARKHOF, F. & CASTELIJNS, J. A. 2007. Magnetization transfer ratio measurement in multiple sclerosis normal-appearing brain tissue: limited differences with controls but relationships with clinical and MR measures of disease. *Mult Scler,* 13**,** 708-16.
310. WALDMAN, A. T. 2018. Leukodystrophies. *Continuum (Minneap Minn),* 24**,** 130-149.
311. WALLRAFF, A., ODERMATT, B., WILLECKE, K. & STEINHÄUSER, C. 2004. Distinct types of astroglial cells in the hippocampus differ in gap junction coupling. *Glia,* 48**,** 36-43.
312. WANG, H., ZHANG, P., CHEN, W., FENG, D., JIA, Y. & XIE, L.-X. 2012. Evidence for serum miR-15a and miR-16 levels as biomarkers that distinguish sepsis from systemic inflammatory response syndrome in human subjects. *Clinical chemistry and laboratory medicine,* 50**,** 1423-1428.
313. WANG, L. C. & ALMAZAN, G. 2016. Role of Sonic Hedgehog Signaling in Oligodendrocyte Differentiation. *Neurochem Res,* 41**,** 3289-3299.
314. WANG, R., YANG, B. & ZHANG, D. 2011. Activation of interferon signaling pathways in spinal cord astrocytes from an ALS mouse model. *Glia,* 59**,** 946-958.
315. WANNER, I. B., ANDERSON, M. A., SONG, B., LEVINE, J., FERNANDEZ, A., GRAY-THOMPSON, Z., AO, Y. & SOFRONIEW, M. V. 2013. Glial Scar Borders Are Formed by Newly Proliferated, Elongated Astrocytes That Interact to Corral Inflammatory and Fibrotic Cells via STAT3-Dependent Mechanisms after Spinal Cord Injury. *Journal of Neuroscience,* 33**,** 12870-12886.
316. WEI, R., WANG, J., SU, M., JIA, E., CHEN, S., CHEN, T. & NI, Y. 2018. Missing value imputation approach for mass spectrometry-based metabolomics data. *Scientific reports,* 8**,** 1-10.
317. WHEELER, N. A. & FUSS, B. 2016. Extracellular cues influencing oligodendrocyte differentiation and (re)myelination. *Experimental Neurology,* 283**,** 512-530.

318. WON, S. J., KIM, D. Y. & GWAG, B. J. 2002. Cellular and molecular pathways of ischemic neuronal death. *J Biochem Mol Biol,* 35**,** 67-86.
319. WONG, R., RENTON, C., GIBSON, C. L., MURPHY, S. J., KENDALL, D. A. & BATH, P. M. 2013. Progesterone treatment for experimental stroke: an individual animal meta-analysis. *Journal of Cerebral Blood Flow & Metabolism,* 33**,** 1362-1372.
320. WU, G., FENG, X. & STEIN, L. 2010. A human functional protein interaction network and its application to cancer data analysis. *Genome Biology,* 11**,** R53.
321. WU, Y. E., PAN, L., ZUO, Y., LI, X. & HONG, W. 2017. Detecting Activated Cell Populations Using Single-Cell RNA-Seq. *Neuron,* 96**,** 313-329.e6.
322. XIA, W., LIU, Y. & JIAO, J. 2015. GRM7 regulates embryonic neurogenesis via CREB and YAP. *Stem Cell Reports,* 4**,** 795-810.
323. XIN, W., MIRONOVA, Y. A., SHEN, H., MARINO, R. A. M., WAISMAN, A., LAMERS, W. H., BERGLES, D. E. & BONCI, A. 2019. Oligodendrocytes Support Neuronal Glutamatergic Transmission via Expression of Glutamine Synthetase. *Cell Rep,* 27**,** 2262-2271 e5.
324. YANG, Z., SUZUKI, R., DANIELS, S. B., BRUNQUELL, C. B., SALA, C. J. & NISHIYAMA, A. 2006. NG2 glial cells provide a favorable substrate for growing axons. *J Neurosci,* 26**,** 3829-39.
325. YAO, G.-Y., ZHU, Q., XIA, J., CHEN, F.-J., HUANG, M., LIU, J., ZHOU, T.-T., WEI, J.-F., CUI, G.-Y., ZHENG, K.-Y. & HOU, X.-Y. 2018. Ischemic postconditioning confers cerebroprotection by stabilizing VDACs after brain ischemia. *Cell Death & Disease,* 9**,** 1033.
326. YE, J., COULOURIS, G., ZARETSKAYA, I., CUTCUTACHE, I., ROZEN, S. & MADDEN, T. L. 2012. Primer-BLAST: a tool to design target-specific primers for polymerase chain reaction. *BMC Bioinformatics,* 13**,** 134.
327. YE, S. M. & JOHNSON, R. W. 2001. An age-related decline in interleukin-10 may contribute to the increased expression of interleukin-6 in brain of aged mice. *Neuroimmunomodulation,* 9**,** 183-92.
328. YOUNG, K. M., PSACHOULIA, K., TRIPATHI, R. B., DUNN, S. J., COSSELL, L., ATTWELL, D., TOHYAMA, K. & RICHARDSON, W. D. 2013. Oligodendrocyte dynamics in the healthy adult CNS: evidence for myelin remodeling. *Neuron,* 77**,** 873-85.
329. ZAMANIAN, J. L., XU, L., FOO, L. C., NOURI, N., ZHOU, L., GIFFARD, R. G. & BARRES, B. A. 2012. Genomic analysis of reactive astrogliosis. *Journal of neuroscience,* 32**,** 6391-6410.
330. ZAWADZKA, M., RIVERS, L. E., FANCY, S. P., ZHAO, C., TRIPATHI, R., JAMEN, F., YOUNG, K., GONCHAREVICH, A., POHL, H., RIZZI, M., ROWITCH, D. H., KESSARIS, N., SUTER, U., RICHARDSON, W. D. & FRANKLIN, R. J. 2010. CNS-resident glial progenitor/stem cells produce Schwann cells as well as oligodendrocytes during repair of CNS demyelination. *Cell Stem Cell,* 6**,** 578-90.
331. ZEHENDNER, C. M., SEBASTIANI, A., HUGONNET, A., BISCHOFF, F., LUHMANN, H. J. & THAL, S. C. 2015. Traumatic brain injury results in rapid pericyte loss followed by reactive pericytosis in the cerebral cortex. *Scientific reports,* 5**,** 1-9.
332. ZEISEL, A., HOCHGERNER, H., LONNERBERG, P., JOHNSSON, A., MEMIC, F., VAN DER ZWAN, J., HARING, M., BRAUN, E., BORM, L. E., LA MANNO, G., CODELUPPI, S., FURLAN, A., LEE, K., SKENE, N., HARRIS, K. D., HJERLING-LEFFLER, J., ARENAS, E., ERNFORS, P., MARKLUND, U. & LINNARSSON, S. 2018. Molecular Architecture of the Mouse Nervous System. *Cell,* 174**,** 999-1014.e22.
333. ZHAN, J., MANN, T., JOOST, S., BEHRANGI, N., FRANK, M. & KIPP, M. 2020. The Cuprizone Model: Dos and Do Nots. *Cells,* 9**,** 843.

334. ZHANG, L., CHOPP, M., ZHANG, R. L., WANG, L., ZHANG, J., WANG, Y., TOH, Y., SANTRA, M., LU, M. & ZHANG, Z. G. 2010. Erythropoietin amplifies stroke-induced oligodendrogenesis in the rat. *PLoS One,* 5**,** e11016.
335. ZHANG, M., DOWNES, C. E., WONG, C. H., BRODY, K. M., GUIO-AGULAIR, P. L., GOULD, J., ATES, R., HERTZOG, P. J., TAYLOR, J. M. & CRACK, P. J. 2017. Type-I interferon signalling through IFNAR1 plays a deleterious role in the outcome after stroke. *Neurochemistry International,* 108**,** 472-480.
336. ZHANG, R., CHOPP, M. & ZHANG, Z. G. 2013. Oligodendrogenesis after cerebral ischemia. *Front Cell Neurosci,* 7**,** 201.
337. ZHANG, S., ZHU, X., GUI, X., CROTEAU, C., SONG, L., XU, J., WANG, A., BANNERMAN, P. & GUO, F. 2018. Sox2 Is Essential for Oligodendroglial Proliferation and Differentiation during Postnatal Brain Myelination and CNS Remyelination. *The Journal of neuroscience : the official journal of the Society for Neuroscience,* 38**,** 1802-1820.
338. ZHANG, Y., CHEN, K., SLOAN, S. A., BENNETT, M. L., SCHOLZE, A. R., O'KEEFFE, S., PHATNANI, H. P. & GUARNIERI, P. 2014. An RNA-sequencing transcriptome and splicing database of glia, neurons, and vascular cells of the cerebral cortex. 34**,** 11929-47.
339. ZHAO, C., MA, D., ZAWADZKA, M., FANCY, S. P. J., ELIS-WILLIAMS, L., BOUVIER, G., STOCKLEY, J. H., DE CASTRO, G. M., WANG, B., JACOBS, S., CASACCIA, P. & FRANKLIN, R. J. M. 2015. Sox2 Sustains Recruitment of Oligodendrocyte Progenitor Cells following CNS Demyelination and Primes Them for Differentiation during Remyelination. *The Journal of neuroscience : the official journal of the Society for Neuroscience,* 35**,** 11482-11499.
340. ZHOU, M., SCHOOLS, G. P. & KIMELBERG, H. K. 2006. Development of GLAST(+) astrocytes and NG2(+) glia in rat hippocampus CA1: mature astrocytes are electrophysiologically passive. *J Neurophysiol,* 95**,** 134-43.
341. ZHOU, M., XU, G., XIE, M., ZHANG, X., SCHOOLS, G. P., MA, L., KIMELBERG, H. K. & CHEN, H. 2009. TWIK-1 and TREK-1 are potassium channels contributing significantly to astrocyte passive conductance in rat hippocampal slices. *J Neurosci,* 29**,** 8551-64.
342. ZHOU, T., LYNCH, R. M., CHEN, L., ACHARYA, P., WU, X., DORIA-ROSE, N. A., JOYCE, M. G., LINGWOOD, D., SOTO, C., BAILER, R. T., ERNANDES, M. J., KONG, R., LONGO, N. S., LOUDER, M. K., MCKEE, K., O'DELL, S., SCHMIDT, S. D., TRAN, L., YANG, Z., DRUZ, A., LUONGO, T. S., MOQUIN, S., SRIVATSAN, S., YANG, Y., ZHANG, B., ZHENG, A., PANCERA, M., KIRYS, T., GEORGIEV, I. S., GINDIN, T., PENG, H. P., YANG, A. S., MULLIKIN, J. C., GRAY, M. D., STAMATATOS, L., BURTON, D. R., KOFF, W. C., COHEN, M. S., HAYNES, B. F., CASAZZA, J. P., CONNORS, M., CORTI, D., LANZAVECCHIA, A., SATTENTAU, Q. J., WEISS, R. A., WEST, A. P., JR., BJORKMAN, P. J., SCHEID, J. F., NUSSENZWEIG, M. C., SHAPIRO, L., MASCOLA, J. R. & KWONG, P. D. 2015a. Structural Repertoire of HIV-1-Neutralizing Antibodies Targeting the CD4 Supersite in 14 Donors. *Cell,* 161**,** 1280-92.
343. ZHOU, Z., ZHANG, G., LI, X., LIU, X., WANG, N., QIU, L., LIU, W., ZUO, Z. & YANG, J. 2015b. Loss of phenotype of parvalbumin interneurons in rat prefrontal cortex is involved in antidepressant-and propsychotic-like behaviors following acute and repeated ketamine administration. *Molecular neurobiology,* 51**,** 808-819.
344. ZHU, H. & DAHLSTRÖM, A. 2007. Glial fibrillary acidic protein-expressing cells in the neurogenic regions in normal and injured adult brains. *J Neurosci Res,* 85**,** 2783-92.
345. ZHU, X., BERGLES, D. E. & NISHIYAMA, A. 2008. NG2 cells generate both oligodendrocytes and gray matter astrocytes. *Development,* 135**,** 145-57.

346. ZHU, X., HILL, R. A., DIETRICH, D., KOMITOVA, M., SUZUKI, R. & NISHIYAMA, A. 2011. Age-dependent fate and lineage restriction of single NG2 cells. *Development,* 138**,** 745-53.
347. ZISKIN, J. L., NISHIYAMA, A., RUBIO, M., FUKAYA, M. & BERGLES, D. E. 2007. Vesicular release of glutamate from unmyelinated axons in white matter. *Nat Neurosci,* 10**,** 321-30.

10 LIST OF PUBLICATIONS

Publications related to the thesis:

1. **Kirdajova D**, Valihrach L, Valny M, Kriska J, Krocianova D, Benesova S, Abaffy P, Zucha D, Klassen R, Kolenicova D, Honsa P, Kubista M, Anderova M. Transient astrocyte-like NG2 glia subpopulation emerges solely following permanent brain ischemia. Glia. **2021** Nov;69(11):2658-2681. doi: 10.1002/glia.24064. Epub 2021 Jul 27. PMID: 34314531. (IF=7.4520, Q1)

2. Androvic P, **Kirdajova D**, Tureckova J, Zucha D, Rohlova E, Abaffy P, Kriska J,Valny M, Anderova M, Kubista M, Valihrach L. Decoding the Transcriptional Response to Ischemic Stroke in Young and Aged Mouse Brain. Cell Rep. **2020** Jun 16;31(11):107777. doi: 10.1016/j.celrep.2020.107777. PMID: 32553170. (IF=9.423, Q1)

3. Valny M, Honsa P, Waloschkova E, Matuskova H, Kriska J, **Kirdajova D**, Androvic P, Valihrach L, Kubista M, Anderova M. A single-cell analysis reveals multiple roles of oligodendroglial lineage cells during post-ischemic regeneration. Glia. **2018** May;66(5):1068-1081. doi: 10.1002/glia.23301. Epub 2018 Feb 2. PMID: 29393544. (IF=6.200, Q1)

Other publications:

4. Maleninska K, Janikova M, Radostova D, Vojtechova I, Petrasek T, **Kirdajova D**, Anderova M, Svoboda J, Stuchlik A. Selective deficits in attentional set-shifting in mice induced by maternal immune activation with poly(I:C). Behav Brain Res. 2022 Feb 15;419:113678. doi: 10.1016/j.bbr.2021.113678. Epub 2021 Nov 25. PMID: 34838932 (IF=3.332, Q3).

5. Kriska J, Janeckova L, **Kirdajova D**, Honsa P, Knotek T, Dzamba D, Kolenicova D, Butenko O, Vojtechova M, Capek M, Kozmik Z, Taketo MM, Korinek V, Anderova M. Wnt/β-Catenin Signaling Promotes Differentiation of Ischemia-Activated Adult Neural Stem/Progenitor Cells to Neuronal Precursors. Front Neurosci. 2021 Feb 25;15:628983. doi: 10.3389/fnins.2021.628983. PMID: 33716653; PMCID: PMC7947698. (IF=4.677, Q2)

6. **Belov Kirdajova D**, Kriska J, Tureckova J, Anderova M. Ischemia-Triggered Glutamate Excitotoxicity From the Perspective of Glial Cells. Front Cell Neurosci. 2020 Mar 19;14:51. doi: 10.3389/fncel.2020.00051. PMID: 32265656; PMCID: PMC7098326. (IF=5.505, Q1)

7. **Kirdajova D**, Anderova M. NG2 cells and their neurogenic potential. Curr Opin Pharmacol. 2019 Dec 23;50:53-60. doi: 10.1016/j.coph.2019.11.005. [Epub ahead of print] Review. PubMed PMID: 31877531. (IF=5.547, Q1)

8. Kolenicova D, Tureckova J, Pukajova B, Harantova L, Kriska J, **Kirdajova D**, Vorisek I, Kamenicka M, Valihrach L, Androvic P, Kubista M, Vargova L, Anderova M. High potassium exposure reveals the altered ability of astrocytes to regulate their volume in the aged hippocampus of GFAP/EGFP mice. Neurobiol Aging. 2019 Oct 22. pii: S0197-4580(19)30372-0. doi: 10.1016/j.neurobiolaging.2019.10.009. [Epub ahead of print] PubMed PMID: 31757575. (IF=4.347, Q2)

9. Pivonkova H, Hermanova Z, **Kirdajova D**, Awadova T, Malinsky J, Valihrach L, Zucha D, Kubista M, Galisova A, Jirak D, Anderova M. The Contribution of TRPV4 Channels to Astrocyte Volume Regulation and Brain Edema Formation. Neuroscience. 2018 Dec 1;394:127-143. doi: 10.1016/j.neuroscience.2018.10.028. Epub 2018 Oct 24. PubMed PMID: 30367945. (IF=3.244, Q3)

10. Awadová T, Pivoňková H, Heřmanová Z, **Kirdajová D**, Anděrová M, Malínský J. Cell volume changes as revealed by fluorescence microscopy: Global vs local approaches. J Neurosci Methods. 2018 Aug 1;306:38-44. doi: 10.1016/j.jneumeth.2018.05.026. Epub 2018 Jun 7. PubMed PMID: 29885815. (IF=2.785, Q4)

11. Valny M, Honsa P, **Kirdajova D**, Kamenik Z, Anderova M. Tamoxifen in the Mouse Brain: Implications for Fate-Mapping Studies Using the Tamoxifen-Inducible Cre-loxP System. Front Cell Neurosci. 2016 Oct 20;10:243. eCollection 2016. PubMed PMID: 27812322; PubMed Central PMCID: PMC5071318. (IF=4.555, Q1)

12. Honsa P, Valny M, Kriska J, Matuskova H, Harantova L, **Kirdajova D**, Valihrach L, Androvic P, Kubista M, Anderova M. Generation of reactive astrocytes from NG2 cells is regulated by sonic hedgehog. Glia. 2016 Sep;64(9):1518-31. doi: 10.1002/glia.23019. Epub 2016 Jun 24. PubMed PMID: 27340757. (IF=6.200, Q1)

13. Kutová M, Mrzílková J, **Kirdajová D**, Řípová D, Zach P. Simple method for evaluation of planum temporale pyramidal neurons shrinkage in postmortem tissue of Alzheimer disease patients. Biomed Res Int. 2014; 2014:607171. doi:10.1155/2014/607171. Epub 2014 Feb 11. PubMed PMID: 24719875; PubMed Central PMCID: PMC3956417. (IF=1.579, Q3)